Behavior of r.f. Heated Plasmas in a Toroidal Octupole Magnetic Plasma

by

J.C. Sprott

May 1969

PLP 282

University of Wisconsin
Plasma Studies

BEHAVIOR OF R.F. HEATED PLASMAS IN A TOROIDAL OCTUPOLE MAGNETIC FIELD

by

JULIEN CLINTON SPROTT

A thesis submitted in partial fulfillment of the requirements for the degree of

DOCTOR OF PHILOSOPHY

(Physics)

at the

UNIVERSITY OF WISCONSIN

1969

ABSTRACT

BEHAVIOR OF R. F. HEATED PLASMAS IN
A TOROIDAL OCTUPOLE MAGNETIC FIELD

Julien Clinton Sprott
Under the Supervision of Professor D. W. Kerst

Microwave frequencies of 700 - 9000 MHz and powers up to 100 kW have been used to produce and heat plasmas in regions of electron cyclotron resonance in a toroidal octupole magnetic field. A theoretical model has been developed to predict the heating rate of a cold tenuous plasma in an arbitrary non-uniform magnetic field. The model predicts strong heating at places where $\nabla_{//} B = 0$ at resonance. The heating is most efficient when the density is such that the microwave frequency ω lies in the range $\omega_p^2 < \omega^2 < \omega_p^2 Q$ where ω_p is the plasma frequency and Q is the quality factor of the cavity.

Two types of experiments have been performed. In one type, a gun injected plasma with $n \sim 10^9$ cm^{-3}, $kT_e \sim 5$ eV, and $kT_i \sim 40$ eV is heated by a pulse of microwaves with $p \sim 10^{-6}$ torr. Scintillator probes show the predicted localized heating, and indicate that the electron distribution during the heating is non-Maxwellian with an

average energy of 100 eV - 1 keV. After the heating pulse, the energetic electrons are rapidly lost to obstacles in the plasma, so that after ~100 μsec the average energy returns to near its original value.

The other type of experiment consists of raising the background gas pressure to ~ 10^{-4} torr and breaking down the gas by microwaves without preionization. The resulting plasma in the afterglow has $n \sim 10^{9} - 10^{11}$ cm^{-3}, and $kT_i < kT_e \sim 1$ eV. The spatial distribution is a strong function of the position of the resonance zones. Langmuir probe measurements show a temperature decay in agreement with calculations for inelastic electron-neutral collisions. The particle lifetime is ~3 msec, and most(~ 80%) of the plasma is lost to the hoops. Several classes of fluctuations were studied, but it does not appear that they are an important source of plasma loss.

The heating model has been extended to include ion cyclotron heating, and it is shown that the heating rate for ions is the same as for electrons if the electric field has the same strength and if the resonance zones occur in the same places. For low density plasmas ($n \sim 10^{9}$ cm^{-3}) it is shown that low frequency electric fields can penetrate the plasma and that appreciable ion heating should result.

Donald W. Kerst.

ACKNOWLEDGMENTS

I am grateful to Professor D. W. Kerst for his supervision and continued interest in the work reported here. Professor D. M. Meade contributed much discussion and constructive criticism. The sharing of ideas, experimental data, and equipment with Dr. J. A. Schmidt, Dr. D. E. Lencioni, G. W. Kuswa, and A. W. Molvik was especially valuable. The heating systems and other apparatus were capably engineered by P. Nonn. T. Lovell assisted in the development of apparatus.

Financial support was provided by the United States Atomic Energy Commission.

TABLE OF CONTENTS

		Page
I.	INTRODUCTION	1
II.	APPARATUS	8
	A. Toroidal Octupole	8
	B. Microwave Heating Systems	13
	C. Low Frequency R.F. Heating System	19
III.	DIAGNOSTICS	23
	A. Probes	23
	B. Microwave Diagnostics	36
	C. Electrostatic Energy Analyzers	39
	D. Scintillation Detectors	42
IV.	THEORETICAL MODEL FOR ELECTRON CYCLOTRON HEATING	45
	A. Calculation of Heating Rate	45
	B. Additional Calculations	53
	C. Application to Specific Geometries	56
V.	EXPERIMENTS ON ELECTRON CYCLOTRON HEATING	66
	A. General Observations	66
	B. Spatial Distribution	73
	C. Energy Distribution	87
	D. Time Evolution	91

	Page
VI. PROPERTIES OF THE AFTERGLOW PLASMA	96
A. General Behavior	96
B. Plasma Motion and Particle Loss	102
C. Electron Cooling	113
D. Fluctuations	124
VII. ION CYCLOTRON RESONANCE HEATING	133
A. Introduction	133
B. Calculation of Heating Rate	134
C. Experimental Measurements	137
VIII. CONCLUSIONS	142
REFERENCES	144

I. INTRODUCTION

R. F. plasma sources had an early origin in such devices as ion sources for nuclear physics,[1] welding torches,[2] and sources for spectrographic analysis. The absence of the usual discharge electrodes makes possible the production of high purity plasmas and plasmas in which the electrons and neutral gas are nearly in thermal equilibrium.

The electrical breakdown of gases in the absence of a magnetic field has been the subject of several extensive works.[3-5] An electron (charge e) in the absence of a magnetic field obeys an equation of motion of the form

$$m\dot{\vec{v}} = e\vec{E}_o\, e^{i\omega t} - m\vec{v}\nu$$

where ν is the electron-neutral collision frequency (assumed to be velocity independent). The electron therefore oscillates with a frequency ω and a maximum kinetic energy given by

$$W_o = \frac{e^2\,\overline{E^2}}{m(\omega^2 + \nu^2)}$$

where $\overline{E^2}$ is the mean square electric field. Breakdown can occur only if the electric field is sufficiently strong to raise the electron energy W_o to the ionization energy of the neutral gas U_i:

$$\overline{E_B^2} = \frac{m(\omega^2 + \nu^2)}{e^2}\, U_i\ .$$

Note that at high pressures ($\nu >> \omega$), large electric fields are required to induce breakdown. At low pressures ($\nu << \omega$), breakdown occurs more readily, so that, for example, in hydrogen gas at a frequency of 3000 MHz, the breakdown electric field should be about 2 kV/cm. In practice,

the breakdown field at low pressures is higher than that given by[2] this simple estimate, since the electron confinement time or the duration of the r. f. may be less than the ionization time.

Perhaps the earliest interest in the problem of the interaction of electromagnetic waves with a plasma in a magnetic field arose from a desire to understand the behavior of radio waves in the ionosphere. The pioneering work of Appleton[6] and others provided a general dispersion relation (the Appleton equation) from which the reflection and absorption of a wave travelling through the ionosphere can in principle be calculated provided the magnetic field and density of electrons and neutrals along the path of the wave is known. The theoretical predictions along with a wealth of experimental data can be found in a number of textbooks.[7-9]

With the advent of controlled thermonuclear fusion research,[10] it became desirable to develop r. f. techniques for breakdown and heating of large volumes of plasma confined in various magnetic field configurations. The development of high power pulsed radar sources during World War II provided the necessary technology.

The presence of a magnetic field drastically alters the heating process as can be seen in the following example. Consider an electron in a static uniform magnetic field $\vec{B} = B\,\hat{z}$ and a perpendicular oscillating electric field $\vec{E} = E_{\perp o}\,\hat{x}\,e^{i\omega t}$. The equation of motion of the electron is called the Langevin equation and has the form

$$m\dot{\vec{v}} = e\vec{E} + e\vec{v} \times \vec{B} - m\vec{v}\,\nu \ .$$

It is straightforward to show that for $\nu << \omega$ the steady state velocity v_x oscillates with a frequency $\frac{1}{2}(\omega + \omega_c)$ and an amplitude

$$v_{xo} = \frac{2\omega e E_{\perp o}}{m\sqrt{(\omega^2 - \omega_c^2)^2 + 4\omega^2\nu^2}} \cos\left(\frac{\omega - \omega_c}{2} t\right)$$

where ω_c is the electron cyclotron frequency:

$$\omega_c = \frac{eB}{m} .$$

At resonance ($\omega = \omega_c$), the electron executes circular oscillations with a perpendicular energy of

$$W_\perp = \frac{e^2 \overline{E_\perp^2}}{m \nu^2} .$$

The corresponding mean square perpendicular electric field required for breakdown is

$$\overline{E_{\perp B}^2} = m\nu^2 U_i/e^2 .$$

Hence resonance breakdown occurs at electric fields which are ν/ω smaller than those required in the absence of a magnetic field. Furthermore, the electron energy produced by a given electric field is larger by $(\omega/\nu)^2$ if electron cyclotron resonance occurs. For $\omega \neq \omega_c$ the electron energy is smaller and oscillates with the beat frequency $\omega - \omega_c$. In reality, effects such as the energy dependence of ν, the relativistic mass increase, the doppler effect, and radiation complicate this simple picture.

As a further example, we will consider how space charge alters the heating process when the electron density is large. The Langevin equation can be used to determine the polarization field $\vec{P}$ in the plasma by summing the dipole moments of the oscillating charges. If collisions are neglected, the relative dielectric constant for a cold plasma is found to be

$$K = \varepsilon / \varepsilon_o = 1 + P/\varepsilon_o E = 1 - \frac{\omega_p^2}{\omega^2 - \omega_c^2} \qquad (4)$$

where ω_p is the electron plasma frequency,

$$\omega_p = \sqrt{\frac{ne^2}{\varepsilon_o m}} \quad .$$

For $K > 1$, space charge reduces the electric field in the plasma, while for $K < 1$, the electric field is enhanced. At $K = 0$, the electric field becomes infinite, and resonance heating occurs at

$$\omega = \sqrt{\omega_c^2 + \omega_p^2} \quad .$$

This frequency is called the upper hybrid resonance frequency.[11] Note that as the electron density approaches zero, we recover the single particle resonance at the electron cyclotron frequency. For $K < 0$, the electric field is evanescent, which means that waves propagating into the plasma are reflected near the boundary. This condition occurs for

$$\omega_c^2 < \omega^2 < \omega_c^2 + \omega_p^2 \quad .$$

In the absence of a magnetic field ($\omega_c = 0$), we obtain the familiar result that waves cannot propagate in a plasma when their frequency is below the plasma frequency. The magnetic field permits waves with frequencies below the cyclotron frequency to propagate through plasmas of arbitrary density. For propagation parallel to the magnetic field, this is called the whistler mode,[12] and the waves are called electron cyclotron waves.

We could continue discussing increasingly complicated examples of waves in plasmas by taking into account the presence of positive ions,

finite temperatures, and inhomogeneities in density and magnetic field. The result would be to show that there is a wide variety of propagation modes and resonance conditions.[13] Instead, we will mention some particular experiments in which r.f. electric fields have been used to produce or heat plasmas.

It is unfortunately the case that plasma confinement generally requires very non-uniform magnetic fields, and as a result the theory of r.f. heating is quite complicated. Perhaps the simplest geometry and one in which r.f. heating found early application is the magnetic mirror. Linearly or circularly polarized waves can be made to propagate along the mirror axis. In general, the wave frequency is chosen so that the wave passes through two regions of electron cyclotron resonance, and at those places, electron heating is supposed to occur. The earliest such experiments took place at Oak Ridge National Laboratory[14] where it was found that heating was surprisingly efficient in spite of the small size of the region in which cyclotron resonance occurs. These findings encouraged other experiments[15-20] so that now r.f. fields are probably the most common means of heating in mirror machines. Typically these experiments use microwave frequencies from 3 to 10 GHz and power densities of the order of a few watts/cm^3. Background pressures are typically 10^{-5} to 10^{-3} torr, and the plasmas produced consist of a cold (few eV) dense (10^9 to 10^{12} cm^{-3}) component and a more tenuous hot component with an energy as high as a few hundred keV.

Several theories have been developed to explain the heating rate in these mirror machines.[21-23] The theories all involve solving the equation of motion of an electron which is trapped in the mirror and

periodically passes through the resonance region. It is usually assumed that the acceleration is stochastic and that the electrons undergo a random walk in velocity space. None of the theories so far is exact, and the results vary according to the approximations used.

With the development of more complicated geometries such as stellarators and multipoles, it became desirable to extend r.f. heating techniques to these machines. R.F. heating has been successfully employed in the Princeton C Stellarator, in levitrons at Livermore and Culham, in a spherator and linear quadrupole at Princeton, in a levitated toroidal quadrupole at Oak Ridge, and in a toroidal octupole at Wisconsin. A convenient summary of these experiments is included in the papers presented at the Third Conference on Plasma Physics and Controlled Nuclear Fusion Research in Novosibirsk, USSR (1-7 August 1968). The interest in these experiments has been more with the confinement of the plasma than with the heating mechanism. The experimental approach has generally been to inject microwave energy through a hole in the cavity wall and then to look at the behavior of the resulting plasma as it decays.

This thesis is concerned with both the heating mechanism and the properties of the plasmas produced by r.f. electric fields in the Wisconsin toroidal octupole. Chapters II and III deal with the experimental apparatus and diagnostic techniques respectively. In Chapter IV a theoretical model is developed to describe cyclotron heating in an arbitrary non-uniform magnetic field, and the results are applied to the toroidal octupole. Chapters V and VI describe experimental observations of the heating process and of the afterglow plasma respectively, and Chapter VII comments on the extension of these techniques to the problem of

ion cyclotron resonance heating.

All equations are in MKS units, although gauss and centimeters are used frequently in the discussion.

II. APPARATUS

A. Toroidal Octupole

The Wisconsin toroidal octupole has been discussed in detail elsewhere.[24-26] We will review here aspects of the device which are important for understanding the present experiments.

Figure 1 is a diagram of the apparatus. The octupole magnetic field is produced by discharging a 2964 μF capacitor bank into a 60 turn primary winding on the iron core which threads the toroid. Four copper hoops mechanically-supported near the corners of the toroidal vacuum vessel form the transformer secondary. For a typical excitation of 2 kV, a total current of 190 kA flows in the hoops. These currents, along with the image currents in the aluminum walls, produce the octupole field. The magnetic field is pulsed about once a minute with a half cycle of a 100 Hz damped sine wave which can be represented approximately by the function[27]

$$B(t) \propto e^{-t/10} \sin \frac{\pi t}{5} \qquad (0 < t < 5)$$

where t is in msec.

A computer calculated magnetic flux plot in a constant θ plane (where θ is the azimuthal coordinate measured from the plane of gun injection) is shown in fig. 2. The light lines are magnetic field lines (or ψ- lines), and the heavy lines are contours of constant magnetic field strength (arbitrarily normalized to 1 at the outside wall midplane). The magnetic flux is arbitrarily divided into ten equal units (called dorys) and the flux lines are numbered from $\psi = -5$ at

Figure 1. Wisconsin toroidal octupole apparatus.

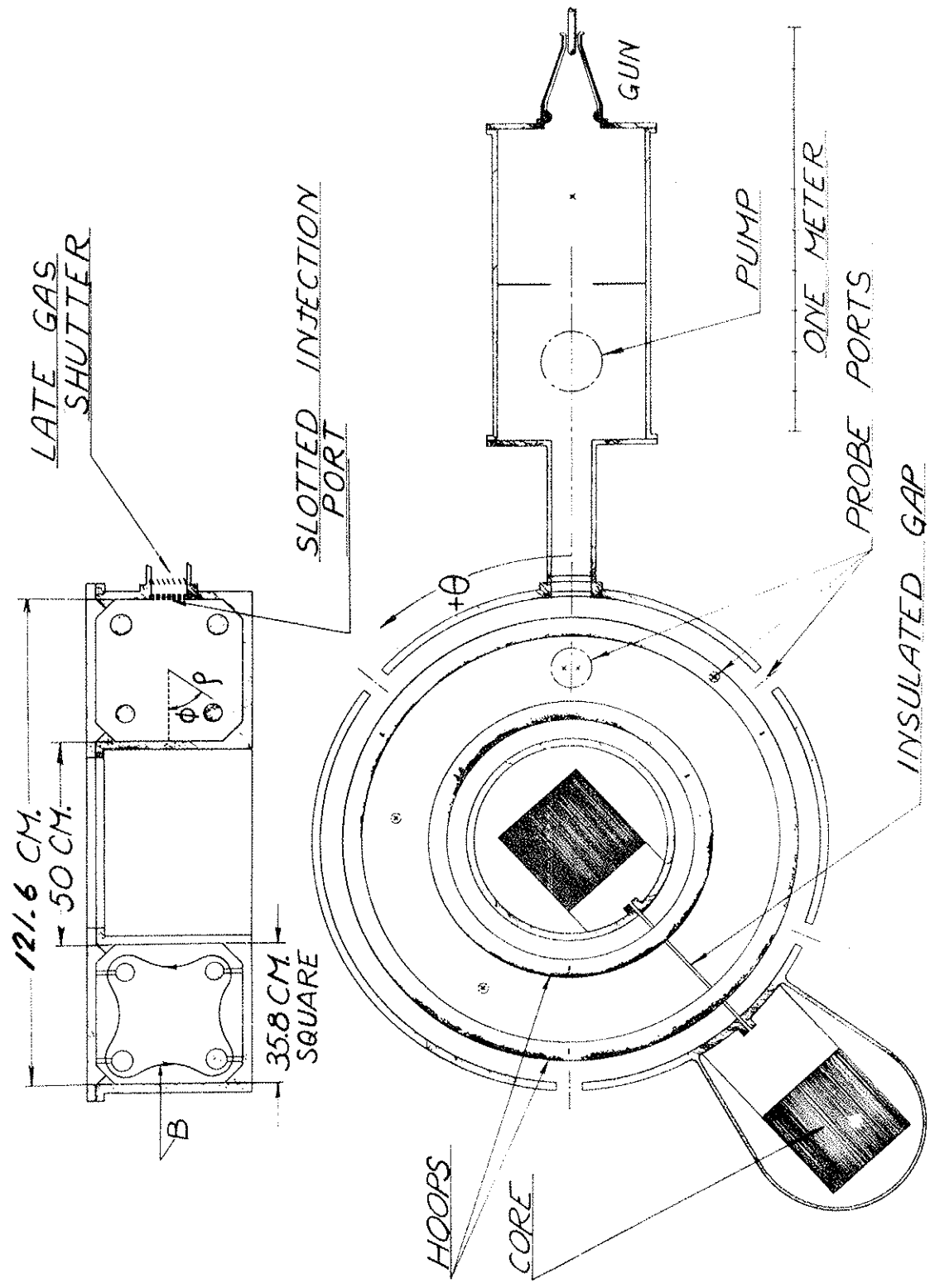
GUN
PUMP
ONE METER
PROBE PORTS
INSULATED GAP
+θ
LATE GAS SHUTTER
SLOTTED INJECTION PORT
121.6 CM.
50 CM.
35.8 CM. SQUARE
B
HOOPS
CORE

Figure 2. Magnetic flux plot of the toroidal octupole showing contours of constant magnetic field strength.

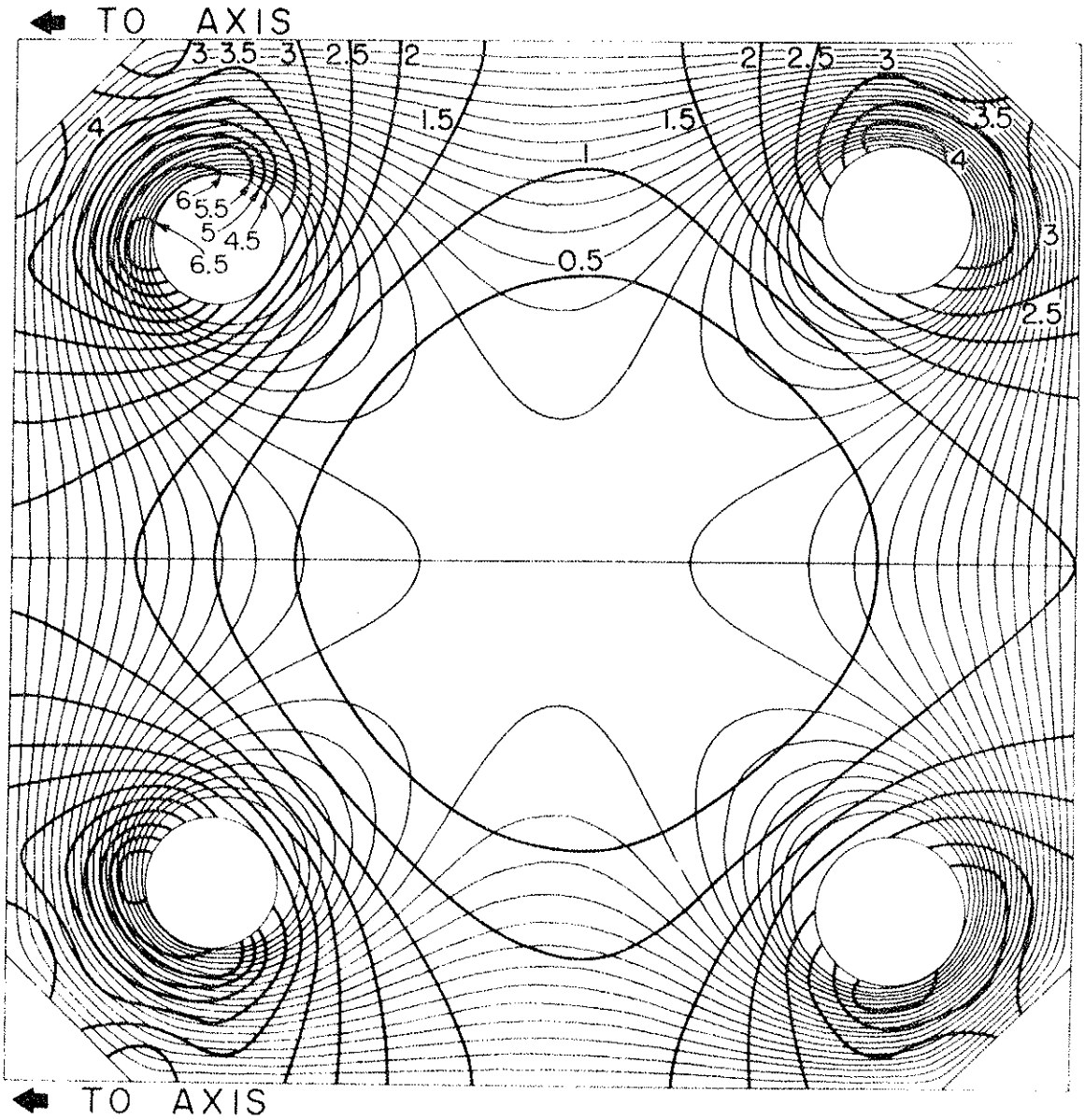
TO AXIS
3
3.5
3
2.5
2
1.5
4
6
5.5
5
4.5
6.5
1
0.5
2
2.5
3
1.5
3.5
4
3
2.5
TO AXIS

at the hoops to $\psi = +5$ at the walls. The separatrix (the field line that passes through the B = 0 axis) is at $\psi = -1.6$, and ψ_{crit} (the field line on which $V'(\psi) = d^2V/d\psi^2 = 0$) is at $\psi = +3$. For 2 kV excitation, the constant B contours in fig. 2 are approximately in units of kG, and one dory is about 4×10^5 gauss-cm^2. The confinement volume is 3×10^5 cm^3.

Plasma from a conical pinch gun similar to that used by Josephson[28] can be injected into the toroid. A pulsed valve admits a puff of gas to the gun just prior to the discharge of a critically damped capacitor bank (9 μF, 18 kV) across the gun electrodes. Un-ionized gas is differentially pumped in a 1.5 meter long drift tank while the plasma enters the octupole field through a slotted port in the wall. Just inside the injection port the density is $\sim 10^{11}$ cm^{-3}, and the ion temperature is ~ 40 eV.

The system is pumped to a base pressure of $\sim 5 \times 10^{-7}$ torr by two 10" oil diffusion pumps. High purity hydrogen can be continuously bled in through a micrometer valve for operation at higher pressures.

B. Microwave Heating Systems

Microwave power for plasma heating is generally produced by pulsed magnetrons.[29] The magnetrons used in this experiment operate at frequencies of 700, 1300, 3250, 5280, and 9000 MHz, with peak output powers ranging up to 100 kW. A summary of the characteristics of the various microwave systems is shown in Table I.

These magnetrons are designed to produce typically 1 μsec pulses

TABLE I. MICROWAVE HEATING SYSTEMS

MICROWAVE BAND	P	L	S	C	X
Magnetron type	700C	5J26	2J38	QK241	6249A
Frequency (MHz)	700	1300	3250	5280	9000
Wavelength (cm)	43	23	9.2	5.6	3.3
Resonant field (G)	250	465	1160	1900	3200
Peak power (kW)	20	40	10	70	100
Ferrite isolator	none	none	20dB	none	13dB
Variable attenuator	none	none	>30dB	30dB	20dB
Directional coupler	none	none	44dB	none	28dB
Output line	coax	coax	WG	WG	WG
Critical density (cm^{-3})	$6x10^{9}$	$2.1x10^{10}$	$1.3x10^{11}$	$3.5x10^{11}$	$1x10^{12}$
Mode number	31	210	3200	14000	68000

of r.f. with a repetition rate of 1 kHz. In our application, considerably longer pulses are desired, but the repetition rate is only about 1 pulse per minute. It was determined that many magnetrons could be run at their rated peak power for these long pulses. In some cases, however, it was necessary to reduce the strength of the magnetron's magnetic field and operate at reduced power. Pulse lengths of 144 μsec are commonly used.

A versatile magnetron pulser was developed to supply filament power and pulsed dc to any of the magnetrons. It is a self-contained unit capable of operating three magnetrons simultaneously. The major components of the pulser are included in fig. 3. Up to 600 J can be stored in a bank of 45 pulse forming networks which are each rated at 15 kV dc, have an impedance of 67 Ω and produce a 16 μsec square pulse when discharged. They can be connected in series to produce pulses up to 720 μsec or in parallel to match impedances down to 1.5 Ω. The networks are discharged with 5C22 thyratrons connected directly to the magnetron cathode or to a 1:6 pulse transformer for magnetrons which require higher voltages. The pulse transformer can be cocked (reverse magnetized with a dc current) to improve its performance on long pulses. A four channel, high stability, calibrated electronic timer is used to trigger the thyratrons and to trigger scopes and perform other functions.

Since the magnetron is called on to supply power to a cavity whose impedance depends critically on frequency, plasma density, and the position of movable probes, it is desirable to use a ferrite isolator in the magnetron output to reduce the VSWR in the line and to insure magnetron stability. A variable attenuator allows the microwave

Figure 3. Typical microwave heating system.

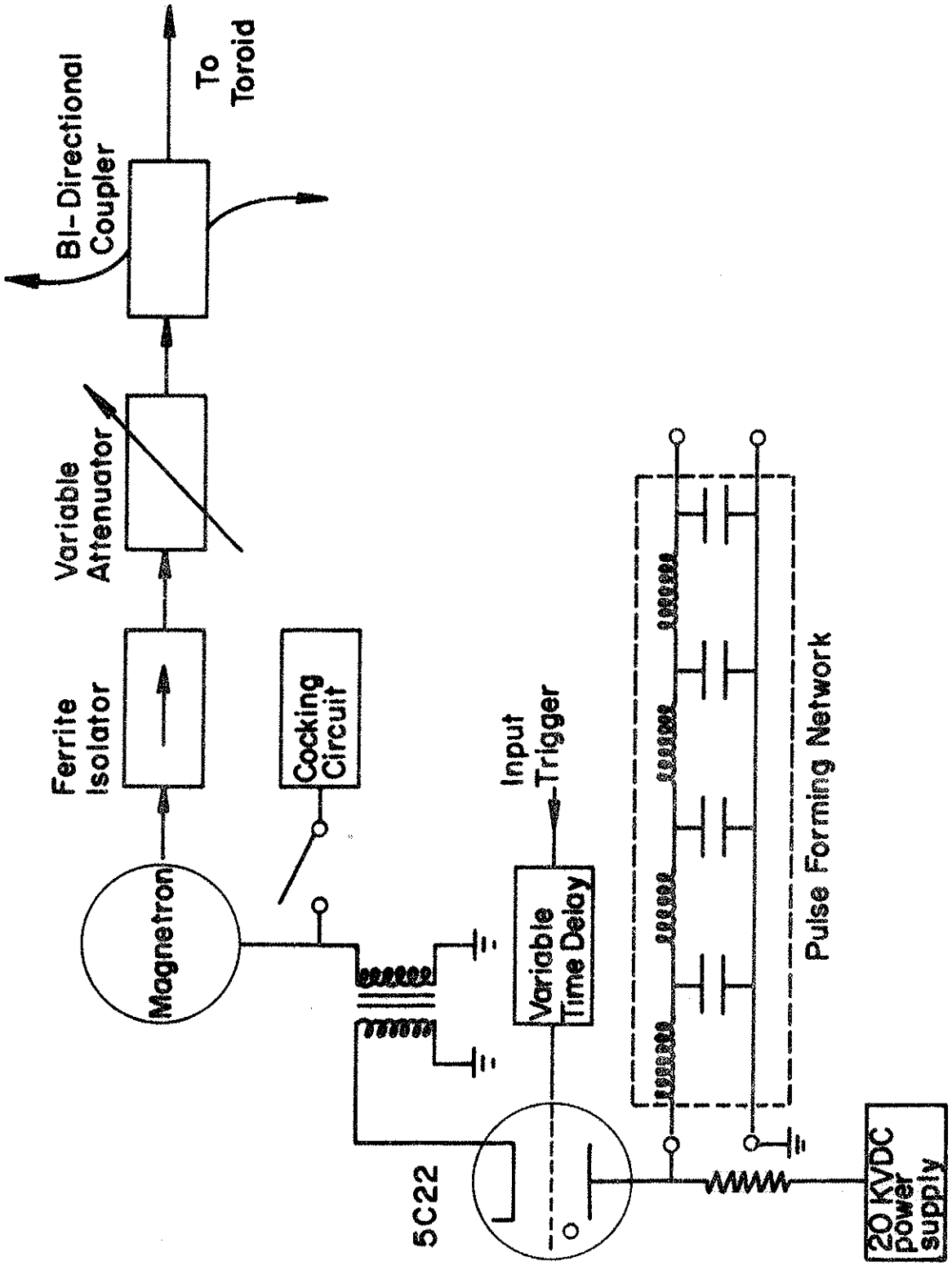
Bi-Directional Coupler
To Toroid
Variable Attenuator
Ferrite Isolator
Cocking Circuit
Input Trigger
Magnetron
Variable Time Delay
Pulse Forming Network
5C22
20 KVDC power supply

power to be adjusted, and a bi-directional coupler samples forward and reflected power in the line. At the higher frequencies, waveguides are used to couple power into the toroidal cavity through a specially contoured hole in the wall covered by a 1/8" lucite vacuum window. At the lower frequencies, evacuated coaxial lines are used which are terminated in 1/4 wave antennas protruding into the cavity. Arcing in the waveguides and at the vacuum windows has sometimes been troublesome at high power levels. The causes and cures of these problems have been discussed in detail by Eason.[30]

Effective microwave heating generally requires large electric fields in the cavity. This is best accomplished by choosing a frequency which corresponds to some resonant mode of the cavity. For a cavity with linear dimensions of many wavelengths, the number of modes between zero frequency and frequency f can be approximated by[31]

$$N = \frac{8\pi}{3} (f/c)^3 V,$$

so that the average mode spacing is

$$\frac{df}{dN} = \frac{c^3}{8\pi f^2 V} \quad . \tag{1}$$

The half width of the modes due to the finite cavity Q is

$$\Delta f = f/Q \quad . \tag{2}$$

The Q of the toroidal cavity without plasma was measured to be about 4000 at 9000 MHz. Measurements at 24 GHz indicate that the Q scales like the square root of the frequency as expected theoretically. Equations (1) and (2) imply that in the present experiment the modes

overlap at frequencies above about 1200 MHz, and the cavity impedance should then be relatively insensitive to frequency. Under these conditions ($\lambda^3 << V/Q$), waves are more likely to be absorbed by the cavity walls than to return to the input waveguide, and so the reflected power is expected to be a small fraction of the incident power, in agreement with observations.

The mean square electric field in the cavity can be determined from the input power P_o by

$$\overline{E^2} = \frac{P_o Q'}{\varepsilon_o \omega V} \qquad (3)$$

where Q' is the perturbed Q of the cavity (in the presence of plasma), and ω is the microwave frequency ($\omega = 2\pi f$). The unperturbed RMS electric field in the cavity is plotted vs P_o in fig. 4 for the highest and lowest frequencies used in the toroidal octupole. Also plotted in fig. 4 is the RMS acceleration of an electron given by

$$a = \frac{e}{m} \sqrt{E^2} .$$

C. Low Frequency R.F. Heating System

Whereas electron cyclotron heating requires microwave frequencies, ion cyclotron heating requires frequencies smaller by the electron/ion mass ratio, m/M. A 1 MHz, 10 kW pulsed r.f. source was developed for ion heating studies. The system consists of a regenerative oscillator that drives a 715B class C amplifier. The oscillator is switched on for times up to 10 msec during which a 16 μF capacitor charged to 6 kV

Figure 4. RMS electric field vs. microwave power in the toroidal octupole (without plasma).

supplies power to the amplifier. The output is single-ended or balanced and will match impedances from 15 to 1000 Ω.

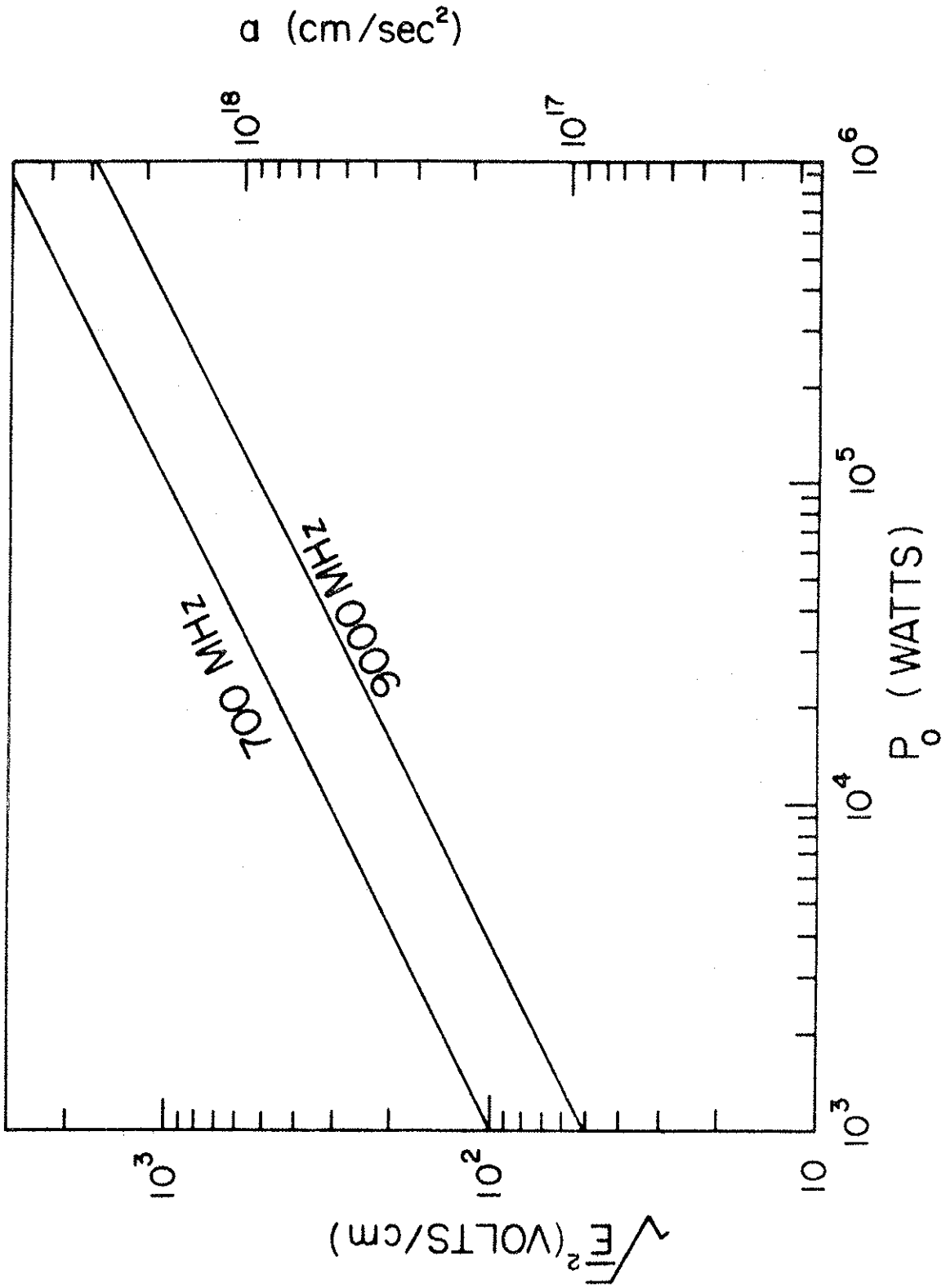
a (cm/sec²)
10¹⁸
10¹⁷
10⁶
10⁵
10⁴
10³
P₀ (WATTS)
900 MHz
700 MHz
10³
10²
10
√E² (VOLTS/cm)

III. DIAGNOSTICS

A. Probes

The most versatile diagnostic tool in this experiment has been the Langmuir probe, discussed almost to the point of exhaustion in several review articles.[32-34] This section contains a review of the basic theory of probes and a discussion of some special probes which have been used in the present experiment.

A conducting electrode placed in a plasma will in general collect a current I given by

$$I = I_{oi} - I_{oe} \exp [e (\Phi - \Phi_p)/kT_e] \tag{4}$$

provided its potential Φ is less than the plasma potential Φ_p. I_{oi} and I_{oe} are the ion and electron saturation currents respectively, and are given approximately by

$$I_{oi} = neA \sqrt{kT^*/2\pi M} \tag{5}$$

and

$$I_{oe} = neA \sqrt{kT_e/2\pi m}.$$

T_e is the electron temperature, n is the plasma density, A is the probe area, and T^* is either the electron or ion temperature, whichever is larger.

1) High impedance probes

In many cases, the bulk motion of a plasma in a magnetic field is determined by the $\vec{E} \times \vec{B}$ drift,

$$\vec{v} = \vec{E} \times \vec{B}/B^2,$$

so that measurements of potential gradients in the plasmas are sufficient to determine plasma motion. A high impedance probe (i.e.: a probe that draws no net current), acquires a potential Φ_f given by equation (1) with I = 0:

$$\Phi_f = \Phi_p - \frac{kT_e}{2e} \ln (MT_e/mT^*). \qquad (6)$$

In the absence of temperature gradients, the electric field can thus be determined from floating potential gradients:

$$\vec{E} = - \nabla\Phi_p = - \nabla\Phi_f \quad .$$

In practice, infinite impedance probes cannot be made, and it is necessary to determine how high an impedance is required for a probe to read floating potential correctly. The plasma behaves like a voltage source Φ_f with some source resistance R_s. This resistance can be estimated by evaluating the slope of $I(\Phi)$ from eq. (4):

$$R_s = - \left.\frac{d\Phi}{dI}\right|_{\Phi_f} = \frac{kT_e}{eI_{oi}} = \frac{kT_e}{ne^2A}\sqrt{\frac{2\pi M}{kT^*}} \quad . \qquad (7)$$

A graph of R_s vs density for various temperatures in a hydrogen plasma is shown in fig. 5.

In order to test eq. (7), a probe in a mercury discharge tube similar to the one described by Burke and Crawford[35] was used to measure R_s. The resistance R_s was first calculated from measured values of I_{oi} and T_e (see next section). R_s was then measured by observing the amplitude of a 150 kHz floating potential fluctuation as external load resistors were added to the circuit. A comparison of the

Figure 5. Probe sheath resistance vs. plasma density for various temperatures in a hydrogen plasma.

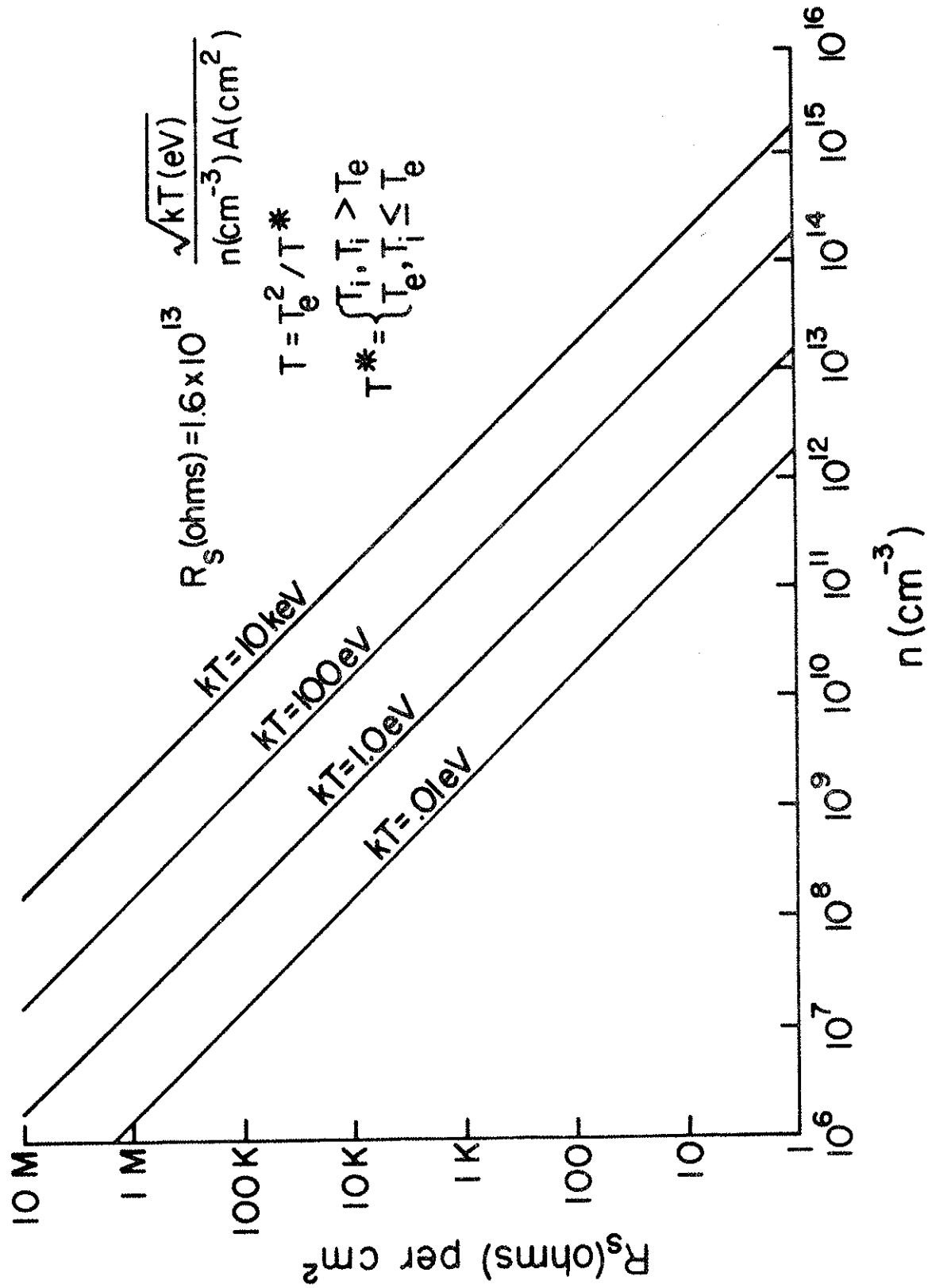
$R_s(\text{ohms}) = 1.6 \times 10^{13} \frac{\sqrt{kT(eV)}}{n(cm^{-3})A(cm^2)}$
$T = T_e^2 / T^*$
$T^* = \begin{cases} T_i, T_i > T_e \\ T_e, T_i \leq T_e \end{cases}$
kT=10keV
kT=100eV
kT=1.0eV
kT=.01eV
10 M
1 M
100 K
10 K
1 K
100
10
R_s(ohms) per cm^2
10^6 10^7 10^8 10^9 10^{10} 10^{11} 10^{12} 10^{13} 10^{14} 10^{15} 10^{16}
n (cm^{-3})

calculated and measured values is shown in fig. 6. The agreement is quite good, confirming the accuracy of eq. (7).

The probe impedance can generally be represented as a parallel RC circuit as shown in fig. 7(a). The high impedance probe will read floating potential correctly only if

$$R_L \gg R_s \quad \text{and} \quad 1/\omega C_L \gg R_s$$

where R_L is the load resistance and C_L is the input capacitance of the measuring circuit and connecting cable. The first condition sets a lower limit on the plasma density in which a particular probe will work, and the second condition determines the maximum frequency response of the probe in a plasma of a given density.

In tenuous, fluctuating plasmas, it is necessary to have a very high probe impedance. R_L can generally be made arbitrarily large, but C_L is limited by the finite length of the probe cable. C_L can be decreased by driving the shield of the probe cable with a signal equal to the floating potential. Alternately, a resistor can be inserted near the probe tip[36] to form a voltage divider with R_L. The probe capacitance can then be reduced to a value equal to the distributed capacitance across the resistor, with a corresponding decrease in voltage gain.

Another type of probe, useful for measuring floating potential, is the capacitance probe, developed by Schmidt.[37] It consists of an electrode sealed in glass which capacitively couples to the plasma. This capacitance, along with the capacitance of the probe cable, forms a voltage divider. Exceedingly high input resistances are achieved

Figure 6. Comparison of calculated and measured values of sheath resistance.

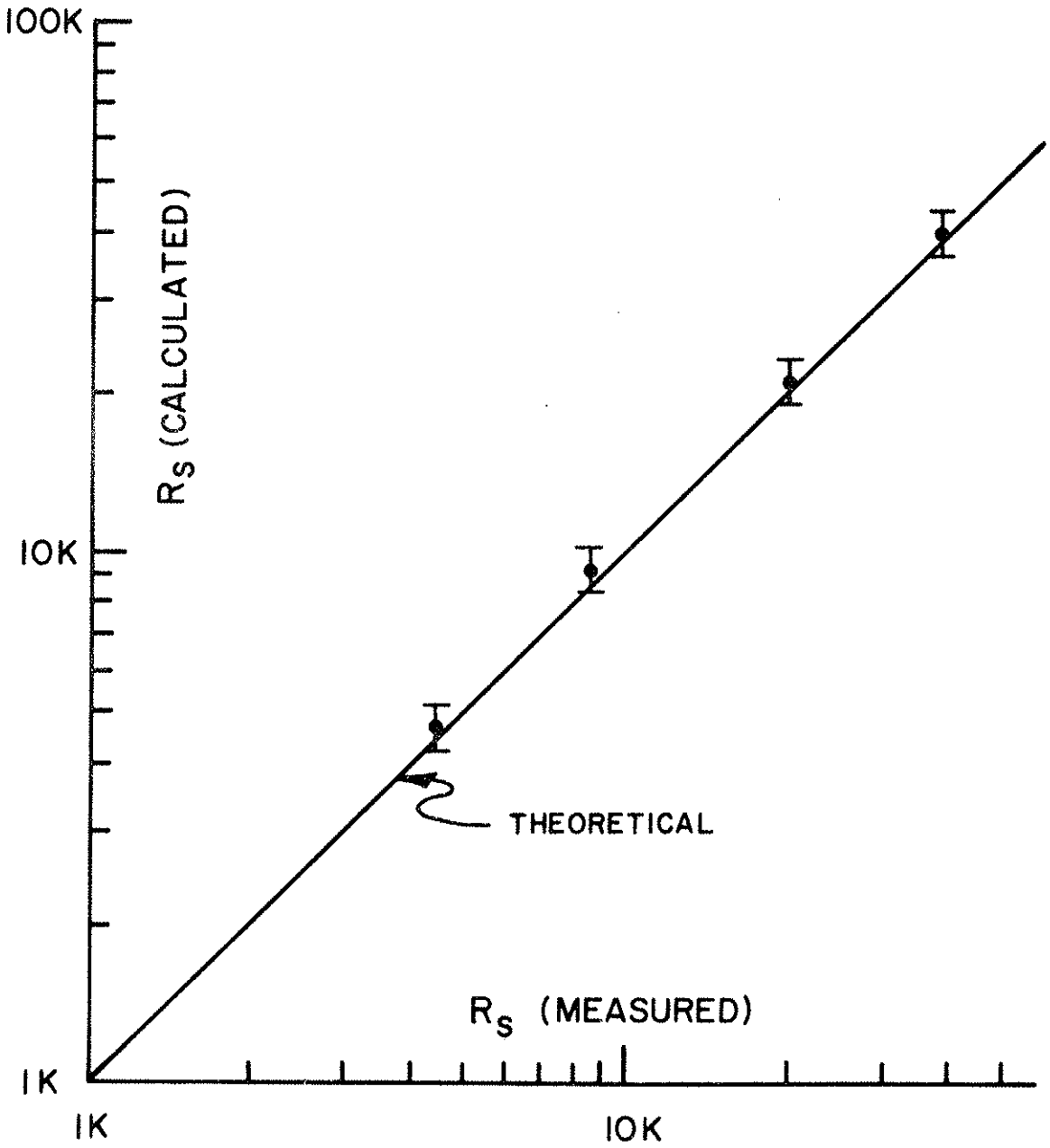
100K
10K
1K
1K
10K
R_S (CALCULATED)
R_S (MEASURED)
THEORETICAL

Figure 7. Electrostatic probe circuits.

(a) HI Z PROBE CIRCUIT

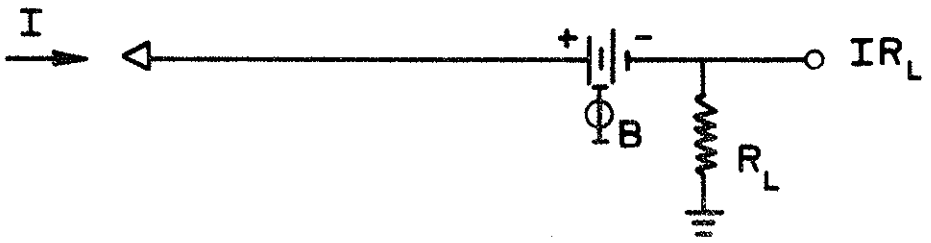

(b) LOW Z PROBE CIRCUIT

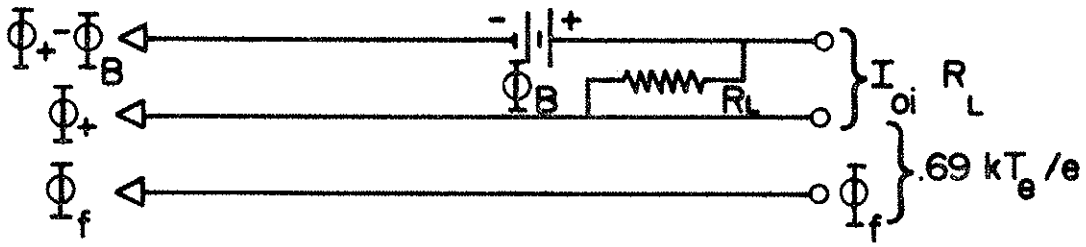

(c) TRIPLE PROBE CIRCUIT

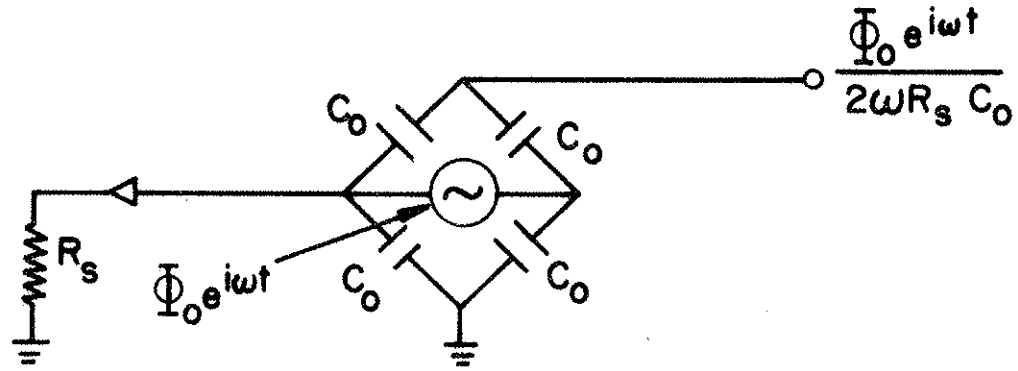

(d) ADMITTANCE PROBE CIRCUIT

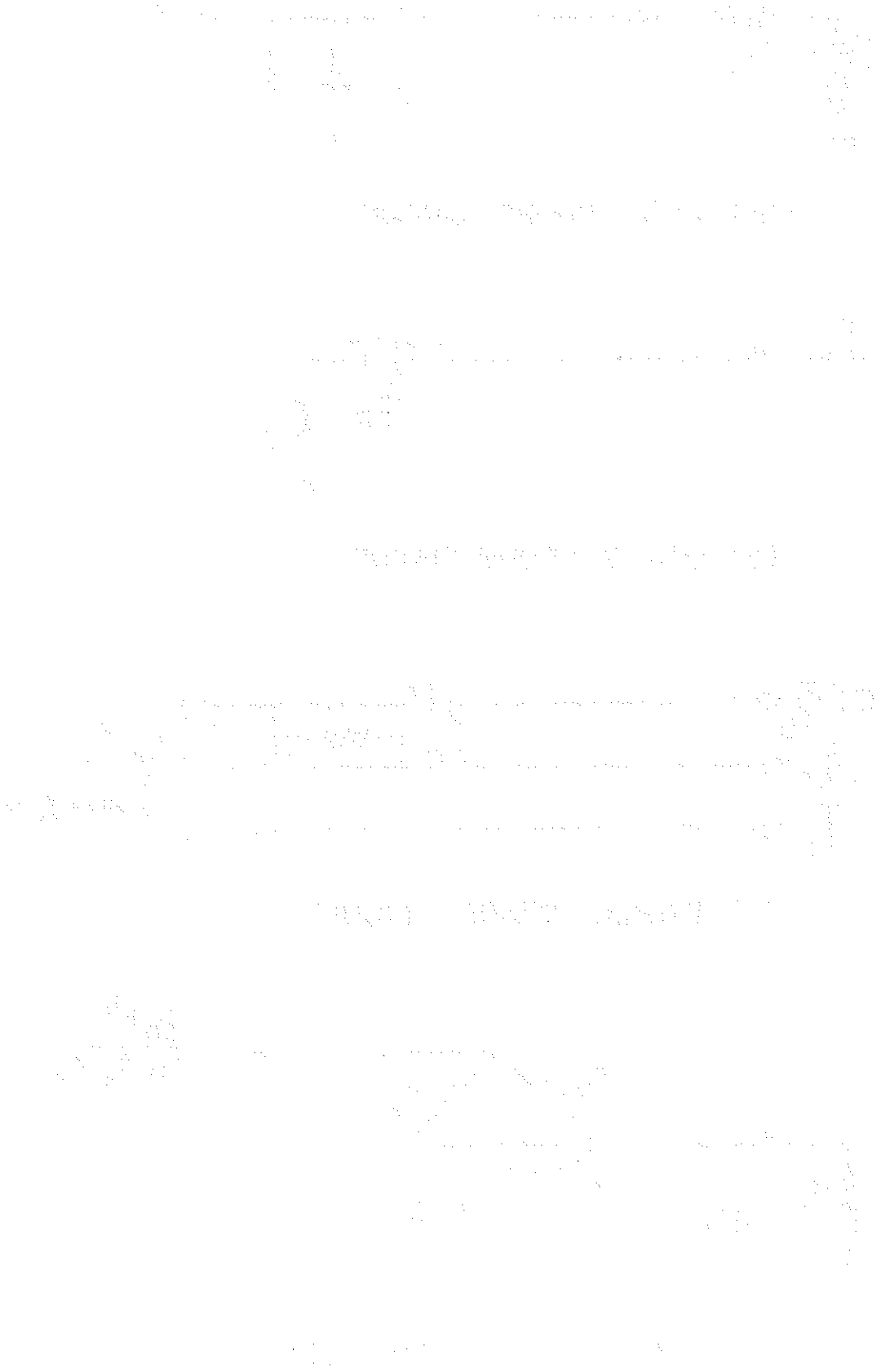

by using a field effect transistor amplifier.

Any of these probes can be used to measure electric fields directly by using two electrodes and a differential amplifier to subtract the floating potentials at two nearby points.

2) Low impedance probes

Langmuir probes can also be used to measure plasma density and electron temperature using the circuit shown in fig. 7(b). It is clear from eq. (4) that by biasing the probe sufficiently negative, all electrons are repelled, and the current to the probe is just equal to the ion saturation current. By measuring this current, one can determine the plasma density from eq. (5) provided the temperature is known.

The electron temperature can be determined by varying the probe bias and measuring the current to the probe. By plotting $\ell n\ (I-I_{oi})$ vs. Φ_B, a straight line should result (if the electron distribution is Maxwellian) whose slope is e/kT_e:

$$\ell n\ (I-I_{oi}) = \frac{e(\Phi_B-\Phi_p)}{kT_e} - \ell n\ I_{oe}$$

The ion temperature cannot, in general, be measured with probes, but in many cases, T_i is less than T_e, so that it is not necessary to know T_i in order to use probe theory.

In cases where the plasma potential is large and fluctuating, the double probe technique of Johnson and Malter[38] is useful. Two adjacent tips are biased with respect to one another, and the impedance to ground is high. Density is determined from the ion saturation current as with a single probe, and the electron

temperature can be determined from the slope of $I(\Phi_B)$ as $\Phi_B \to 0$:

$$kT_e/e = \frac{1}{2} I_{oi} \left.\frac{d\Phi_B}{dI}\right|_{\Phi_B=0} .$$

The frequency response of the double low impedance probe can be improved by placing some of the circuitry near the probe tip.[36]

In order to measure $I(\Phi_B)$ it is necessary either to change Φ_B between each pulse of the magnetic field or to sweep Φ_B in a time short compared with the time during which the plasma properties change appreciably. The first method is hampered by the shot-to-shot irreproducibility of the plasma and by the fact that when large electron currents flow to the probe, the $I(\Phi)$ characteristic is distorted causing the temperature measurement to be incorrect. This distortion occurs during and after a time in which the plasma has a high density or large negative potential. The electron flux apparently causes a contamination of the probe that may last for several minutes. This contamination effect is not well understood, but it appears to be absent in probes which collect less than $\sim 10^{-7}$ coulombs/cm^2. As a result, swept probes are more desirable for measuring T_e since they draw a heavy electron current for a much shorter time.

Low impedance probes should have excellent frequency response since R_L is small (Generally we make $R_L << \Phi_B/I.$). In that case, the response time of the probe is limited by the time required for the sheath to reach equilibrium.[39] This time is given by the transit time of an ion across the sheath and leads to an upper

frequency limit approximately equal to the ion plasma frequency:

$$\omega_{pi} = \sqrt{ne^2/\varepsilon_o M}\ .$$

3) Triple probes

The triple probe is useful because it enables one to simultaneously measure density, electron temperature, and floating potential as a function of time. The triple probe has been discussed by several authors.[40-43] It consists of three nearby electrodes spaced several Debye lengths apart. Two tips are biased as a floating double probe with $\Phi_B >> kT_e/e$ and used to determine density from the ion saturation current by measuring the voltage drop across a small load resistor R_L (see fig. 7(c).). The third tip measures floating potential. The potential difference between the positive tip of the floating double probe and the floating tip can be calculated from eq. (4):

$$\Phi_+ - \Phi_f = \frac{kT_e}{e} \ln 2 \simeq 0.69\ kT_e/e.$$

The triple probe is subject to the usual limitation of density and frequency response, but it could in principle be improved by the same methods[36] used with the single and double probes.

4) Admittance probes

Another method for measuring time resolved electron temperatures uses an admittance probe.[44] The method consists of measuring the ion saturation current with a single Langmuir probe and then measuring the admittance $1/R_s$ by use of a balanced r.f. capacitance bridge. The electron temperature is then determined

from eq. (7): $kT_e/e = I_{oi}R_s$.

The admittance probe circuit is shown in fig. 7(d). A capacitance bridge is required to insure that the probe remain at the d.c. floating potential. The output signal is proportional to $1/R_s$ provided $R_s >> 1/\omega C_o$. The amplitude Φ_o should be large but well below kT_e/e. For best frequency response, ω should be large but well below the ion plasma frequency since the capacitive reactance of the probe sheath becomes comparable to R_s at $\omega = \omega_{pi}$.[45]

The floating double probe, triple probe, and admittance probe are all similar in that they measure both ion saturation current and the slope of the $I(\Phi)$ curve near the floating potential. For hydrogen plasmas with $T_i < T_e$, only the most energetic 2.3% of the electrons in a Maxwellian distribution are sampled, and hence, for a non-Maxwellian distribution, the temperature inferred from these probes may not be representative of the bulk of the electrons. Non-Maxwellian electron distributions are rare in plasmas, and the admittance probe has given agreement with swept single probes and an electrostatic energy analyzer in cases where comparisions have been made. Examples of admittance probe measurements are shown in VI. C.

5) Photoelectric probes

Although not in the same category as Langmuir probes, light sensitive probes have been useful for measuring the time resolved optical light output from the plasma. These probes use a shielded 1N2175 NPN silicon photo duo-diode which is sealed into the end

of a 1/4" o.d. glass tube. The diode is biased to 45 volts, and an oscilloscope is used to measure the current drawn through a 10 kΩ load resistor. The rated sensitivity of the diode is 100 μA for incident radiation of 9 mW/cm^2 in the 7000 to 10,000 Å range. In practice, the diode is about as sensitive as a dark-adapted eye. The response time is < 10 μsec. The diode has a built-in wide angle lens, but collimation can be added to achieve some spatial resolution. Filters can be used if it is desirable to observe a particular wavelength. Examples of photoelectric probe measurements are shown in V. A.

B. Microwave Diagnostics

Microwave diagnostics have the advantage of sampling a large volume with a negligible perturbation to the plasma. Microwave techniques are described a length in several sources.[46,47] All of the methods rely on the fact that the dielectric constant of a plasma at microwave frequencies is a function of the electron density.

In this experiment, K band microwaves (f = 24 GHz) were used for diagnostic purposes. This frequency was chosen so as to be well above the electron cyclotron frequency $\omega >> \omega_c = eB/m$, the electron plasma frequency

$$\omega >> \omega_p = \sqrt{ne^2/\epsilon_o m} ,$$

and the electron collision frequency, ν. When these conditions are satisfied, the local dielectric constant of the plasma is given by

$$K = \varepsilon/\varepsilon_o = 1 - \omega_p^2/\omega^2.$$

The resonant frequency of a cavity mode is therefore shifted by an amount

$$\delta\omega = \omega/\sqrt{K} - \omega \simeq \omega_p^2/2\omega$$

when the cavity is filled uniformly with a plasma. When the plasma density is not constant within the cavity, the mode shift can be determined from Slater's perturbation theorem[48] with the result

$$\frac{\delta\omega}{\omega} = \frac{\int \omega_p^2 E^2 dV}{2\omega^2 \int E^2 dV} .$$

For a plasma with dimensions large compared with the wavelength, as in the present case (λ = 12 mm), the electric fields evenly sample the plasma, and the mode shift is then proportional to the average electron density in the cavity:[25]

$$\frac{\delta\omega}{\omega} = \frac{\bar{n}e^2}{2\varepsilon_o m\omega^2} . \qquad (8)$$

The apparatus consists of a 2K33 klystron oscillator with an output power of about 5 mW. The power is fed through a 1/4" air dielectric coaxial line to a 1/4 wave antenna inside the cavity. A similar antenna on the opposite side of the toroid is connected to a 1N26 diode which detects the received signal. The cavity is resonated in a high order mode ($N \sim 10^6$), and the frequency shift of the mode is observed as a function of time in order to determine $\bar{n}$ (t).

The mode shift can be measured by one of three techniques, depending on the plasma density. For $10^8 \leq \bar{n} \leq 10^9$ cm^{-3}, the klystron is tuned to the side of a cavity mode so that any frequency shift in the mode appears as an amplitude change in the detector. This slope detection method depends on the frequency shift being small so that the amplitude of the detected signal is proportional to frequency. A frequency discriminator at the klystron output is used to feed back a signal to stabilize the klystron.

At higher densities, the frequency shift becomes too large for slope detection. For $5 \times 10^8 \leq \bar{n} \leq 3 \times 10^{10}$ cm^{-3}, the rastered sweep technique is useful. The klystron repeller is swept with a repetitive sawtooth voltage every 30 μsec to sweep through a series of cavity modes. The resulting modes are displayed on a rastered sweep oscilloscope.

At even higher densities ($5 \times 10^9 \leq \bar{n} \leq 10^{12}$ cm^{-3}), the mode counting technique[49] is useful. The klystron frequency is fixed, and the amplitude of the received signal passes through many peaks as the density decays. The average spacing of the observable modes was determined empirically to be $df/dN \simeq 3.0$ MHz/mode, so that each peak represents a density change of $d\bar{n}/dN \simeq 1.8 \times 10^9$ cm^{-3}/mode.

The density obtained from Langmuir probes was compared with the density measured with microwaves using an X-band generated plasma. The density was varied by changing the power level. The average density from the probe was determined from

$$\bar{n} = \frac{\int n(\psi)V'(\psi)d\psi}{\int V'(\psi)d\psi}$$

where $n(\psi)$ was determined from the ion saturation current using eq. (5). The electron temperature was measured with an admittance probe. The density was determined from the microwaves by the mode counting technique. The results are shown in fig. 8. The microwaves indicate a slightly higher density, but the error never exceeds a factor of two.

C. Electrostatic Energy Analyzers

An electrostatic energy analyzer has been used extensively by Erickson[26,50] to measure plasma potential and ion energies for the gun injected plasma in the toroidal octupole. The device consists of a 6 mm i.d. Hipernik tube which provides a field-free duct through which ions can be extracted from the body of a magneto-plasma. The ions then pass through a 127° cylindrical curved plate electrostatic analyzer[51] and are collected on an aluminum target biased to -20 kV. Secondary electrons produced at the target are detected by a plastic scintillator and photomultiplier tube.[52]

Electron energies can be analyzed in a similar way by reversing the bias on the deflector plates and post-accelerating the electrons directly to the scintillator. Such a device has been constructed by Kuswa.[53] Because of the severe shielding required in extracting low energy electrons from a strong magnetic field,

Figure 8. Comparison of average density using Langmuir probes and microwave diagnostics.

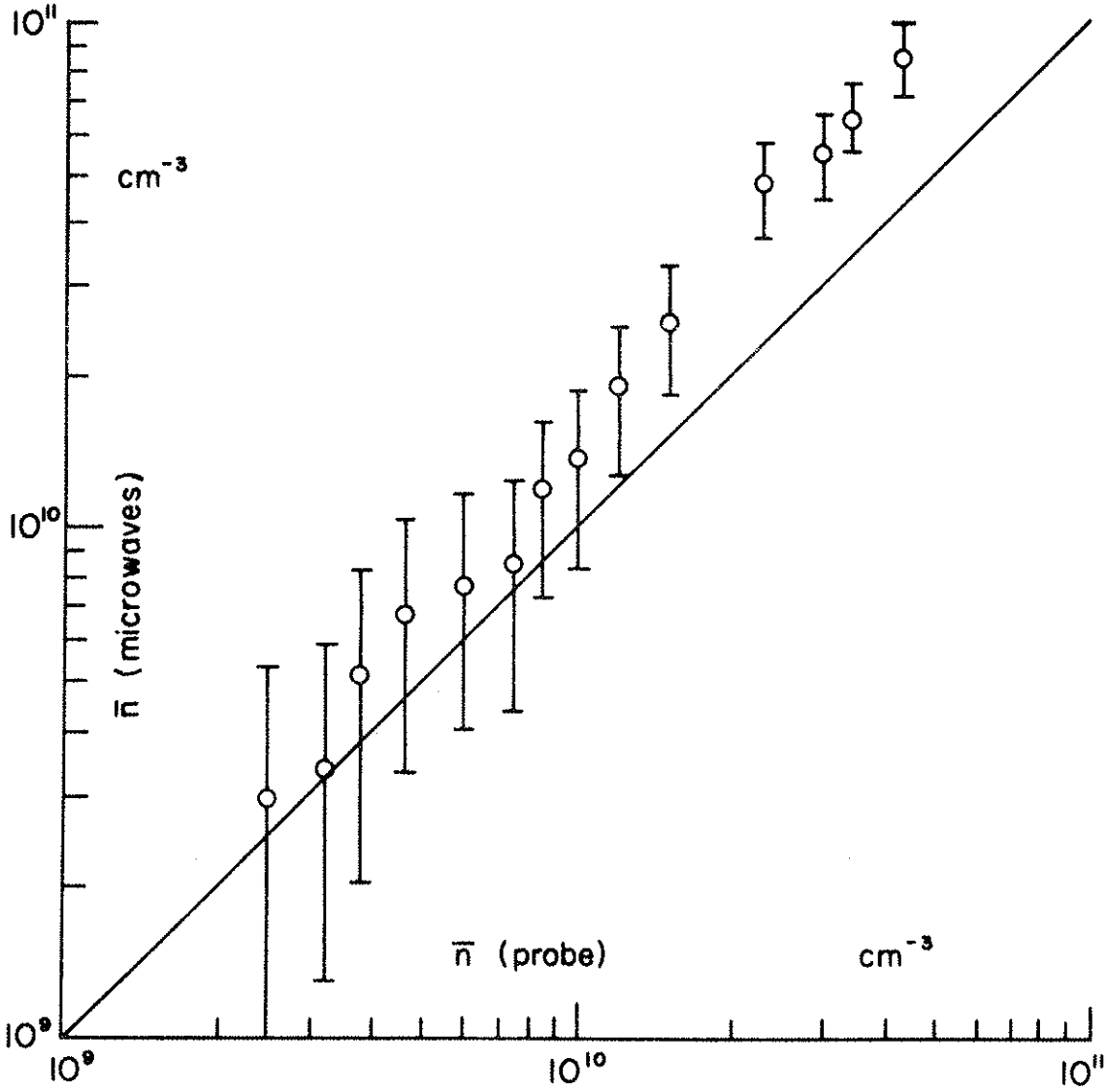
10^{11}
10^{10}
10^{9}
cm^{-3}
$\bar{n}$ (microwaves)
$\bar{n}$ (probe)
cm^{-3}
10^{9}
10^{10}
10^{11}

Kuswa has also developed a modified version of the electron analyzer for use at low energies. It consists of a tiny set of magnetically shielded deflector plates located inside the toroid near the B = 0 axis. Electrons are incident on a biased aluminized scintillator which produces an optical signal that is carried through a light guide to a photomultiplier tube outside the plasma. Alternately, the electron current to an electrode can be amplified with a field effect transistor for direct measurement of either electron or ion distributions.

D. Scintillation Detectors

High energy electrons in a plasma produce X-rays when they strike an object in the plasma or the walls of the vacuum system. These X-rays can be measured using scintillation detectors. A typical detector consists of a 1/2" thick slab of Nuclear Enterprises NE 102 plastic scintillator optically coupled to a 6199 photomultiplier tube. The scintillator is shielded from external light by a .001" copper or aluminum foil.

In its simplest form the scintillation detector is mounted over a hole in the vacuum tank wall and responds to X-rays generated by electrons striking the hoops and walls. Directional information can be obtained by mounting the detector at the end of a long tube which can be pointed at various regions of the plasma.

More precise spatial information can be obtained with scintillator probes. Such a probe consists of a small cylindrical scintillator wrapped in lead foil and sealed into the end of a 1/4"

aluminum tube which can be inserted into the plasma. The face of the scintillator is covered with a thin foil of aluminum or copper. Electrons striking the foil produce X-rays which penetrate the foil and are detected by the scintillator. A flexible light guide carries the optical signal from the scintillator to a photomultiplier tube outside the vacuum.

The usefulness of such a probe can be extended by using foils of various thicknesses allowing one to do crude energy analysis.[54,55] For a Maxwellian electron distribution, the ratio of output signals for two foil thicknesses is given by

$$\frac{I_1}{I_2}(kT_e) = \frac{\int_0^\infty \sqrt{W}\, f(W)\eta_1(W)dW}{\int_0^\infty \sqrt{W}\, f(W)\eta_2(W)dW} = \frac{\int_0^\infty W\eta_1(W)e^{-W/kT_e}dW}{\int_0^\infty W\eta_2(W)e^{-W/kT_e}dW} \qquad (9)$$

where $\eta_1(W)$ and $\eta_2(W)$ are the ratios of photomultiplier current to beam current for the two foils for an incident beam of electrons of energy W. An electron gun can be used to measure $\eta(W)$, and the integrals evaluated numerically to determine $I_1/I_2(kT_e)$. Typically $\eta(W)$ has a threshold of a few keV above which it increases linearly with energy. For distributions which can be represented by a sum of two Maxwellians of different temperatures, the scintillator probe ignores the colder component if its temperature is sufficiently low. Having established the temperature of the hot plasma component, the density of the hot component can be determined from the photomultiplier current I as with a Langmuir probe:

$$I = \frac{1}{4} \, eA \sqrt{\frac{2}{m}} \int_0^\infty \sqrt{W} \, f(W) \eta(W) dW$$

$$= neA \sqrt{\frac{kT_e}{2\pi m}} \int_0^\infty \frac{W}{kT_e} e^{-W/kT_e} \eta(W) dW/kT_e \qquad (10)$$

Several scintillator probes have been constructed. One probe has a set of seven changeable aluminum foils ranging in thickness from .0007" to .0049". It is useful for determining whether the electron distribution is Maxwellian. Another probe has two scintillators covered with .0007" and .0021" thick aluminum foils with separate light guides and photomultiplier tubes. It allows one to simultaneously measure density and temperature of the hot plasma component.

IV. THEORETICAL MODEL FOR ELECTRON CYCLOTRON HEATING

A. Calculation of Heating Rate

The general problem that we would like to solve is to find the time dependent distribution function $f(\vec{r},\vec{v},t)$ of electrons in a cavity of arbitrary size and shape in the presence of a static non-uniform magnetic field $\vec{B}(\vec{r})$, an r.f. electric field $\vec{E}(\vec{r},t)e^{i\omega t}$, a uniform background gas pressure p, and an arbitrary initial distribution function $f_o(\vec{r},\vec{v},t)$. The problem is simplified considerably if we assume that the dimensions of the cavity are large compared with the free space wavelength (or equivalently that the cavity mode number is large) and that the plasma density is sufficiently low that the waves freely penetrate the plasma. These assumptions imply that the electric field is homogeneous and isotropic, so that the mean square electric fields perpendicular and parallel to $\vec{B}$ are related by

$$\overline{E_\perp^2} = 2\overline{E_\parallel^2} = \frac{2}{3}\overline{E^2} \quad .$$

Furthermore, we will assume that the vacuum magnetic field is unperturbed by the plasma (i.e., $\beta = 2\mu_o p/B^2 << 1$).

We define a flux function ψ which is constant on a flux surface and has a value equal to the magnetic flux enclosed by that surface. The magnetic field lines lie in the surfaces and may or may not be confined in the cavity. An orthogonal coordinate system will be used in which $\hat{\psi}$ is a unit vector normal to a flux surface and $\hat{\ell}$ is a unit

vector in the direction of $\vec{B}$. This system is convenient because plasma energy flows readily in the $\hat{\ell}$ direction, and because in many axisymmetric and linear geometries, the coordinate orthogonal to $\hat{\ell}$ and $\hat{\psi}$ is ignorable.

The basic method will be to consider the plasma as a resistive medium and to calculate the power absorbed per unit volume in terms of a real tensor conductivity $\overleftrightarrow{\sigma}$:

$$\frac{dP}{dV} = (\overleftrightarrow{\sigma} \cdot \vec{E}) \cdot \vec{E} = \sigma_{\perp} \overline{E_{\perp}^2} + \sigma_{\parallel} \overline{E_{\parallel}^2} ,$$

or in our coordinates,

$$\frac{dP}{d\psi} = \int (\sigma_{\perp} \overline{E_{\perp}^2} + \sigma_{\parallel} \overline{E_{\parallel}^2}) \frac{d\ell}{B} . \tag{11}$$

The perpendicular and parallel conductivities can be expressed in terms of a collision frequency ν for $\nu << \omega$ as follows:

$$\sigma_{\perp} = \varepsilon_o \omega_p^2 \nu \left[\frac{\omega^2 + \omega_c^2}{(\omega^2 - \omega_c^2)^2 + 4\omega^2\nu^2} \right]$$

$$\sigma_{\parallel} = \varepsilon_o \omega_p^2 \nu / \omega^2 .$$

If $B(\ell)$ is known, the integral in eq. (11) can be evaluated to determine the heating rate. For $\nu << \omega$, the parallel conductivity is small and the perpendicular conductivity is a very sharply peaked function of ℓ, so that we can expand $B(\ell)$ in a Taylor series about its resonance value, retaining only the first order term:

$$B(\ell) = B_o + \ell \left. \frac{dB}{d\ell} \right|_{B_o}$$

where $\ell = 0$ is taken where $B = B_o \equiv m\omega/e$. The integral in eq. (11) can

be evaluated for $-\infty < \ell < +\infty$ to get the result:

$$\frac{dP}{d\psi} = \frac{\pi}{2} \frac{ne\,\overline{E_\perp^2}}{B_o\, dB/d\ell \,|\, B_o}$$

$$= \frac{\pi}{3}\, ne\overline{E^2}\, \frac{d^2V}{dBd\psi}\Big|_{B_o} \qquad (12)$$

Equation (12) is the major theoretical result of this thesis. Note that the power is independent of ν for $\nu << \omega$ and is proportional to the fraction of the volume of the flux shell in which the magnetic field is within dB of the resonance value. The power absorbed by the plasma is proportional to the density in the resonance region and to the square of the electric field.

The same result could have been obtained from a single particle point of view. If the electrons are assumed to have no parallel velocity and no initial perpendicular velocity, the electron energy $W_\perp(\ell,t)$ could be calculated, neglecting collisions, and the power could then be determined by integrating $dW_\perp/dt$ over all the particles along the field line. Alternately, the particles could be allowed to pass through resonance with a constant parallel velocity, and the perpendicular velocity increment could be calculated by integrating the perpendicular acceleration with respect to time along the path of the particles. The flux of particles through resonance could then be used to calculate the power. This approach was used by Kuckes[56] to obtain a result equivalent to eq. (12). The plasma can also be treated as an ensemble of harmonic oscillators with natural frequencies distributed according to the distribution of particles in ω_c space. The total absorption cross section for an isotropic flux of monochromatic photons can be calculated[57] to

get the same result as in eq. (12). Finally, we can calculate the attenuation of waves travelling through a resistive medium by integrating the Appleton equation over all space and over all solid angles and arrive at the same result.

One advantage of the present treatment is that it is not necessary to specify the heating mechanism. In fact, if we interpret the inverse collision frequency ν^{-1} as an effective time during which the phase of an electron remains stationary with respect to the electric field, we can incorporate a variety of heating mechanisms into our model:

$$\nu = \nu_{ei} + \nu_{en} + \frac{1}{T} + \sqrt{v_{\parallel}\ \omega\ \frac{dB/d\ell}{B_o}} + \frac{2\ v_{\parallel}}{\lambda} \quad .$$

The first two terms represent collisions with ions and neutrals. The third term arises from the fact that the electrons can only stay in phase for the duration of the r.f. pulse (T), or in the case of stochastic electric fields,[58,59] for a time equal to the autocorrelation time. The fourth term is the non-adiabatic effect considered by Kuckes[56] and results from the finite parallel velocity that takes the particle through the resonance. The fifth term arises from the fact that on the average the electric field reverses direction every half wavelength in a multimode cavity. Seidl[60] has shown that in the absence of any randomizing effect ($\nu = 0$), there can be no heating in a non-uniform field. The fact that the heating rate is independent of ν is consistent with the fact that the same result is obtained independent of the heating mechanism.

It is important to note that the power absorbed by the plasma may not go directly into electron heating. For example, with electron-neutral

collisions, the electrons reach an equilibrium energy given by

$$W_\perp = \sigma_\perp \overline{E_\perp^2}/n\nu$$

in a time of $\sim\nu^{-1}$, whereupon the power goes into heating the neutral gas which is usually rapidly lost to the walls of the vacuum system. Similarly, for electron-ion collisions the ions are heated causing a decrease in ν which in turn raises the electron energy, so that an equilibrium is maintained while both species are heated.

The requirement that $\nu \ll \omega$ places an upper limit on the parallel velocity for which eq. (12) is valid:

$$v_\parallel \ll \omega \frac{B_o}{dB/d\ell} \quad .$$

In addition, relativity and the doppler effect can be neglected only if

$$v_\parallel \ll c \ .$$

The assumption that resonance occurs at the cyclotron frequency puts an upper limit on the plasma density:

$$\omega_p^2 \ll \omega^2 \ .$$

Furthermore, the assumption that the electric field is unperturbed by the plasma near resonance places a limit on the density by requiring that the width of the resonance be much less than the skin depth, or

$$\omega_p^2 \ll \omega c \, |\nabla B| \, / B_o \quad .$$

Hence the model is valid only for low temperatures and low densities, although the limitations are not too restrictive.

Although the power absorbed by the plasma is independent of the randomizing mechanism, the energy distribution function is different for the $\nu_{//} = 0$ and the large $\nu_{//}$ cases. For $\nu_{//} = 0$, only a small fraction of the particles are heated, and $W_\perp(\ell)$ is proportional to $\sigma_\perp(\ell)$. At intermediate energies, the distribution function can be shown to have the form

$$f(W_\perp, W_{//}) \propto W_\perp^{-1.5}\, \delta(W_{//})$$

where the δ function at $W_{//} = 0$ arises from the requirement that $\nu_{//} = 0$.

It is interesting to note that a power law spectrum has been observed for primary cosmic ray protons incident on the earth's atmosphere, and a similar spectrum for interstellar relativistic electrons has been deduced from observations of cosmic synchrotron radiation,[61] although the power is typically 2.5 - 3.5 rather than 1.5. Fermi[62] also predicted a power law spectrum by considering the stochastic acceleration of cosmic rays by collisions with moving clouds of magnetic field.

When $\nu_{//}$ effects dominate, the heating is more uniform, and Lichtenberg[22] has shown that the resulting distribution is Gaussian:

$$f(W_\perp) = n \sqrt{\frac{2}{\pi\, \overline{W_\perp^2}}}\; \exp\left(-\, W_\perp^2 / 2\, \overline{W_\perp^2}\right)$$

where

$$\overline{W_\perp^2} = \frac{1}{n} \int_0^\infty W_\perp^2\, f(W_\perp)\, dW_\perp$$

is the mean square perpendicular energy. In reality, we expect electron-electron collisions and other thermalizing effects to cause a relaxation

toward a Maxwell-Boltzmann distribution:

$$f(W) = \frac{2n}{kT_e}\sqrt{\frac{W}{\pi kT_e}}\exp(-W/kT_e) \quad .$$

Equation (12) predicts an infinite heating rate whenever $dB/d\ell = 0$ in the resonance region. This condition can occur at either a local maximum or a local minimum in $B(\ell)$. For $B(\ell)$ maximum, the ∇B force tends to repel the particles from resonance, whereas at a minimum the particles tend to be trapped in resonance because of the large $v_\perp/v_\parallel$ produced by the heating. The heating rate is never infinite, of course, and at places where $dB/d\ell = 0$, we ought to include the next higher term in the Taylor series:

$$B(\ell) = B_o + \frac{1}{2}\,\ell^2\,\left.\frac{d^2B}{d\ell^2}\right|_{B_o} \quad .$$

By substituting this form of B into the perpendicular conductivity in eq. (11) and neglecting the parallel conductivity, the integral can be evaluated for $-\infty < \ell < +\infty$ in a manner identical to that used to obtain eq. (12) to get a heating rate given by

$$\frac{dP}{d\psi} = \frac{\pi}{2}\,\frac{ne\,\overline{E_\perp^2}}{B_o^2}\sqrt{\frac{\omega B_o}{\nu\left.d^2B/d\ell^2\right|_{B_o}}} \quad . \tag{13}$$

There are three effects which limit the perpendicular energy to which a particle trapped in resonance can be accelerated. 1) The finite duration of the heating pulse T limits the electron gyroradius to the value obtained for the case of pure resonance acceleration:

$$\rho_e = E_\perp T/B_o$$

2) The relativistic mass increase causes a particle that is intially in resonance to reach an equilibrium energy which can be calculated by finding the steady state solution to the one dimensional equation of motion of a slightly relativistic electron:

$$\ddot{x} + \omega^2\left(1 - \frac{v^2}{c^2}\right) x = \frac{eE_\perp}{m} e^{i\omega t} \quad .$$

By substituting

$$x = \rho_e e^{i\omega t} \ ,$$

the limiting gyroradius is found to be

$$\rho_e{}^3 = \frac{eE_\perp}{m\omega^2} \lambda^2$$

where λ is $1/2\pi$ times the free space wavelength of the r.f. 3) Perpendicular magnetic field gradients also cause a shift in the particle gyrofrequency when the energy increases. For $\nabla_\perp B$ in the x-direction, the equation of motion is

$$\ddot{x} + \omega^2\left(1 + \frac{3}{2}x \frac{\nabla_\perp B}{B}\right)x = \frac{eE_\perp}{m} \cos \omega t.$$

The steady state solution is determined by substituting

$$x = \rho_e \cos \omega t + x_o,$$

neglecting harmonic terms ($\cos 2\omega t$) and terms of order $x^2\left(\frac{\nabla_\perp B}{B}\right)^2$, and assuming that the acceleration is sufficiently gentle that it takes many cyclotron periods for the limiting energy to be reached

$(E_\perp/\rho_e \omega B << 1)$. The result is

$$\rho_e^3 = \frac{4eE_\perp}{9m\omega^2} \left(\frac{B}{\nabla_\perp B}\right)^2 \quad . \tag{14}$$

In most heating experiments the last two non-linear effects are dominant and are of the same order. The electron energies observed in many experiments including those in Chapter V are comparable with these limitations, indicating that the simple linear theory is probably inadequate for explaining the heating rate.

B. Additional Calculations

The total power absorbed by the plasma can be determined by integrating eq. (12) over all ψ:

$$P = \frac{\pi}{3} e \overline{E^2} \int n \left.\frac{d^2V}{dBd\psi}\right|_{B_o} d\psi \ ,$$

which for the special case of n = const gives

$$P = \frac{\pi}{3} n e \overline{E^2} \left.\frac{dV}{dB}\right|_{B_o} \quad . \tag{15}$$

The heating efficiency η can be calculated by dividing the absorbed power by the input r.f. power given by eq. (3):

$$\eta = \frac{P}{P_o} = \frac{\pi}{3} \frac{\omega_p^2}{\omega^2} Q' \frac{B_o}{V} \left.\frac{dV}{dB}\right|_{B_o} \quad . \tag{16}$$

The quantity $\frac{B_o}{V} \left.\frac{dV}{dB}\right|_{B_o}$ is a geometrical factor that measures the effectiveness of cyclotron heating at a given frequency in a particular magnetic field configuration. Typically this factor is of order unity.

It is clear then that the efficiency approaches 100% when the density exceeds a value such that

$$\omega_p^2 = \omega^2/Q \quad .$$

The model for cyclotron heating can easily be extended to the case of resistive r.f. heating by substituting the appropriate conductivity for $\omega >> \omega_c$:

$$\sigma = \varepsilon_o \frac{\omega_p^2 \nu}{\omega^2 + \nu^2} \quad .$$

For $\nu << \omega$ and $\omega_p << \omega$ the absorbed power is given by

$$\frac{dP}{d\psi} = \nu \frac{ne^2}{m\omega^2} \overline{E^2} \frac{dV}{d\psi} \quad .$$

The mass dependence indicates that the power is absorbed primarily by electrons rather than ions. For n = const, the efficiency of resistive heating is given by

$$\eta = \frac{\omega_p^2}{\omega^2} Q' \frac{\nu}{\omega} \quad ,$$

which is the order of ν/ω smaller than in the resonance case.

For $n = n(\psi)$, the average increase in perpendicular energy caused by the heating is found from

$$nV' \Delta\overline{W}_\perp = t \frac{dP}{d\psi}$$

or for the case of resonance heating,

$$k \Delta\overline{W}_\perp(\psi,t) = \frac{\pi}{3} e\overline{E^2} t \frac{1}{V'} \frac{d^2V}{dBd\psi}\Big|_{B_o} \quad . \qquad (17)$$

If ionization of the background gas is taken into account, the power absorbed by the plasma can be written as

$$\frac{dP}{d\psi} = V' (\overline{W}_\perp + U_i) \frac{dn}{dt} + V' n \frac{d}{dt} \overline{W}_\perp \tag{18}$$

where U_i is the ionization energy. dn/dt can be written in terms of the ionization time τ_i as

$$\frac{dn}{dt} = \frac{n}{\tau_i} \quad . \tag{19}$$

Substituting eqs. (12) and (19) into (18) gives a differential equation for the electron energy:

$$\frac{d}{dt} \overline{W}_\perp + \frac{\overline{W}_\perp + U_i}{\tau_i} = \frac{\pi}{3} e\overline{E^2} \frac{1}{V'} \frac{d^2V}{dBd\psi}\Big|_{B_o} \quad . \tag{20}$$

If the duration of the r.f. pulse is short compared with τ_i, the second term in eq. (20) can be neglected, and the energy increases linearly with time according to eq. (17) while the density remains constant. If the r.f. pulse duration is long compared with τ_i, the energy initially increases linearly, but after $\sim \tau_i$ it reaches an equilibrium value of

$$\overline{W}_\perp (\psi,t) = \frac{\pi}{3} e\overline{E^2} \tau_i \frac{1}{V'} \frac{d^2V}{dBd\psi}\Big|_{B_o} - U_i \ , \tag{21}$$

and the density then increases exponentially:

$$n(\psi,t) = n_o(\psi) \, e^{t/\tau_i} \quad . \tag{22}$$

When the r.f. is turned off, the energy decays according to the

equation

$$\frac{d}{dt}\ \overline{W}_\perp + \frac{\overline{W}_\perp + U_i}{\tau_i} = 0. \qquad (23)$$

The ionization time τ_i is given in terms of the ionization cross section $\sigma_i(v)$, the neutral density n_n, and the electron velocity distribution function $f(v)$ by

$$\frac{1}{n_n \tau_i} = \int_o^\infty \sigma_i(v)\ vf(v)\ dv.$$

Numerical tables of this integral for various $\sigma_i(v)$ have been prepared by Drawin[63] for a Maxwellian $f(v)$. These tables were used to calculate the ionization time of electrons in hydrogen gas as a function kT_e, with the result shown in fig. 9. Note that for $kT_e > U_i$, τ_i is a weak function of temperature, so that for 13 eV < kT_e < 30 keV, $p\tau_i \approx 10^{-9}$ torr-sec within a factor of two. Furthermore, we expect $p\tau_i$ to be fairly independent of the exact form of the distribution function for energies in this range.

C. Application to Specific Geometries

1. Magnetic mirror

The magnetic field along the axis of a mirror machine can be approximated by

$$B(Z) = B(0)(1 + \beta Z^2).$$

The heating rate predicted by our model in such a magnetic field can be calculated from

$$\frac{dW_\perp}{dt} = \frac{1}{nV'}\frac{dP}{d\psi} = \frac{\pi}{2} e\ \overline{E_\perp^2}\ \frac{1}{V'}\ \frac{d^2V}{dBd\psi}\Big|_{B_o}$$

Figure 9. Ionization time for a Maxwellian distribution of electrons with temperature T_e in hydrogen gas with a density n_n.

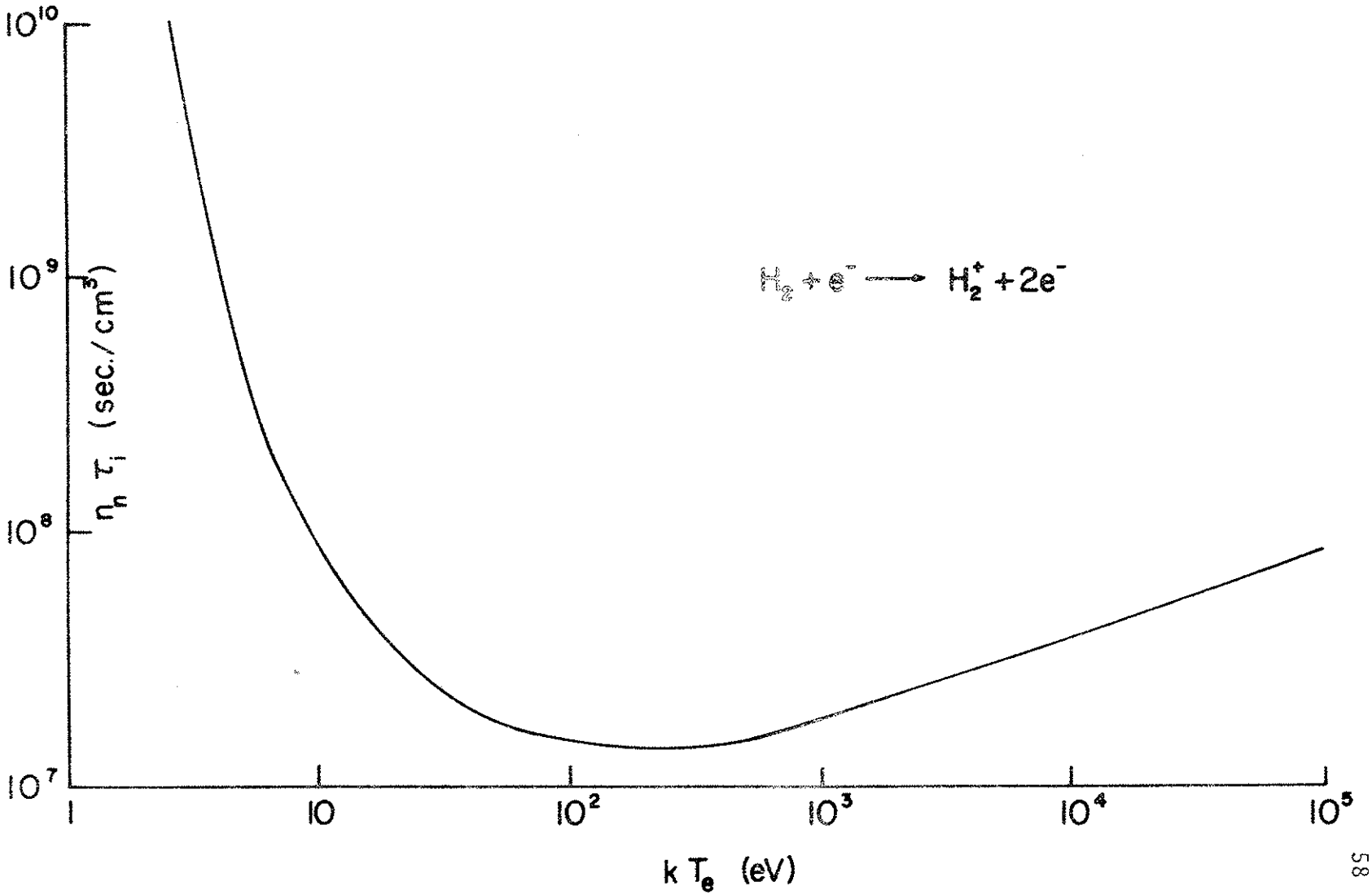
10^{10}
10^{9}
10^{8}
10^{7}
$n_n \tau_i$ (sec./cm^3)
$H_2 + e^- \longrightarrow H_2^+ + 2e^-$
1
10
10^2
10^3
10^4
10^5
k T_e (eV)

where

$$V' = \int \frac{d\ell}{B} = \frac{1}{B(0)} \int_{-\infty}^{\infty} \frac{dZ}{1 + \beta Z^2}$$

with the result that

$$\frac{dW_\perp}{dt} = \frac{e\overline{E_\perp^2}}{2B_o\sqrt{r-1}}$$

where $r = B_o/B(0)$.

In addition to the cylotron heating, there is an additional heating caused by the axial compression of the plasma which occurs because $v_\perp/v_{||}$ increases until the particles mirror at the resonance zones. This effect can be included in V' by evaluating the integral from $-Z_o$ to $+Z_o$ to get the result

$$\frac{dW_\perp}{dt} = \frac{\pi e\overline{E_\perp^2}}{4B_o} \frac{1}{\sqrt{r-1}\ \tan\sqrt{r-1}} \tag{24}$$

The result of eq. (24) is somewhat larger than that of Kawamura and Terashima,[23]

$$\frac{dW_\perp}{dt} = \frac{e\overline{E_\perp^2}}{32\ B_o} \frac{r}{r-1} ,$$

but smaller than the result of the stochastic treatment by Guest:[21]

$$\frac{dW_\perp}{dt} = \frac{e\overline{E_\perp^2}}{B_o} \left[\frac{Z_o\ c}{\lambda v_\perp(0)}\right]^{1/3} \left[\frac{r}{\sqrt{r-1}}\right]^{5/3} .$$

All of these results have the common feature of predicting an infinite heating rate at the midplane ($r = 1$). The special case of $r = 1$ has been discussed by Fessenden.[15]

2. Symmetric linear multipole

For a symmetric linear multipole in which $n = n(\psi)$, the heating rate is given by

$$\frac{dW_\perp}{dt} = \frac{\pi}{3} e\overline{E^2} \frac{1}{V'} \left. \frac{d^2V}{dBd\psi} \right|_{B_o} .$$

The quantity $V'(\psi)$ is infinite on the flux surface (called the separatrix) that passes through the $B = 0$ axis, and hence heating is expected to be small there. At low frequencies, there is a flux surface on each side of the separatrix at which the heating rate is infinite. Beyond these surfaces the heating should be zero. As the frequency is increased, the infinities move farther from the separatrix until they disappear at the surface of the current conductors.

Near the center of a multipole, the magnetic field strength is given by

$$B = \alpha r^{\ell-1}$$

where 2ℓ is the multipole number, and α is a constant. The resonance contours are concentric cylinders. Near the center, $n = \text{const}$ is often a good approximation, and eq. (15) gives for the absorbed power,

$$P = \frac{2\pi^2 L\, ne\overline{E^2}}{3\alpha\,(\ell-1)} \left(\frac{B_o}{\alpha} \right)^{(3-\ell)/(\ell-1)} \qquad (25)$$

where L is the length of the system. Near the heating peaks, the perpendicular field gradient is given by

$$\nabla_\perp B = (\ell-1)\,\alpha \left(\frac{B_o}{\alpha} \right)^{(\ell-2)/(\ell-1)} .$$

By substituting this result into eq. (14) we can calculate the maximum electron energy for which the linear theory applies. Note that a multipole, unlike a mirror, has no point at which $\nabla B = 0$ for $B \neq 0$. For this and other reasons, we expect cyclotron heating to be somewhat less effective in a multipole than in a magnetic mirror.

3. Wisconsin toroidal octupole

A flux plot of the Wisconsin toroidal octupole has been shown in fig. 2. The toroidal geometry causes the peak in $d^2V/dBd\psi$ between the separatrix ($\psi = -1.6$) and the wall to split into three peaks, while the peak between the separatrix and the hoops occurs at a different value of ψ for the inner and outer hoops. The calculations for near the center of a linear multipole should be applicable to the toroidal octupole if we take $\ell = 4$ and $L = 2\pi R_o$ where R_o is the distance from the major axis of the toroid to the $B = 0$ circle.

The function $\frac{1}{V'} \left.\frac{d^2V}{dBd\psi}\right|_{B_o}$ has been evaluated by computer for the values of B_o shown in fig. 2. One typical curve (for the line $B_o = 1$) is shown in fig. 10. For $kT_e > U_i$, profiles of T_e in ψ space should approximately follow this function. By integrating over space we obtain the function $\frac{B_o}{V'} \left.\frac{dV}{dB}\right|_{B_o}$ which is a measure of the effectiveness of cyclotron heating in the toroidal octupole, and this quantity is plotted vs B_o in fig. 11. For typical conditions using S-band heating at a pressure of 10^{-4} torr, eq. (21) predicts a mean initial equilibrium energy of the order of a few keV.

Figure 10. Graph of the function $\frac{1}{V'} \frac{d^2V}{dBd\psi}\Big|_{B_o}$ which describes the power absorbed per unit ψ vs. ψ in the toroidal octupole for a typical resonance zone at $B_o = 1$.

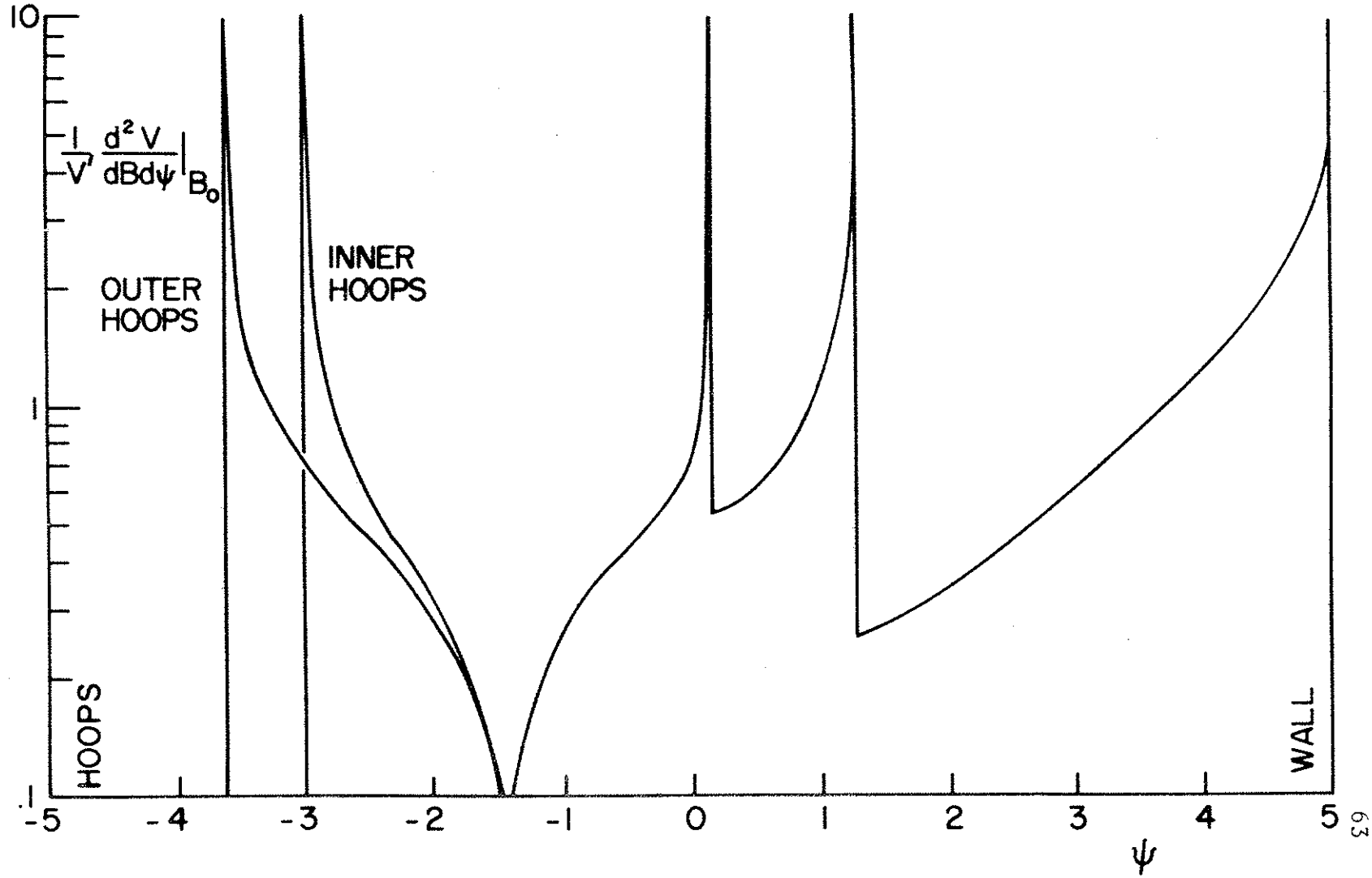
10
1
.1
$\frac{1}{V'}\frac{d^2V}{dBd\psi}\Big|_{B_o}$
OUTER HOOPS
INNER HOOPS
HOOPS
WALL
-5
-4
-3
-2
-1
0
1
2
3
4
5
ψ

Figure 11. Graph of the function $\frac{B_o}{V}\frac{dV}{dB}\Big|_{B_o}$ which describes the total power absorbed by a plasma of uniform density for resonance at B_o in the toroidal octupole.

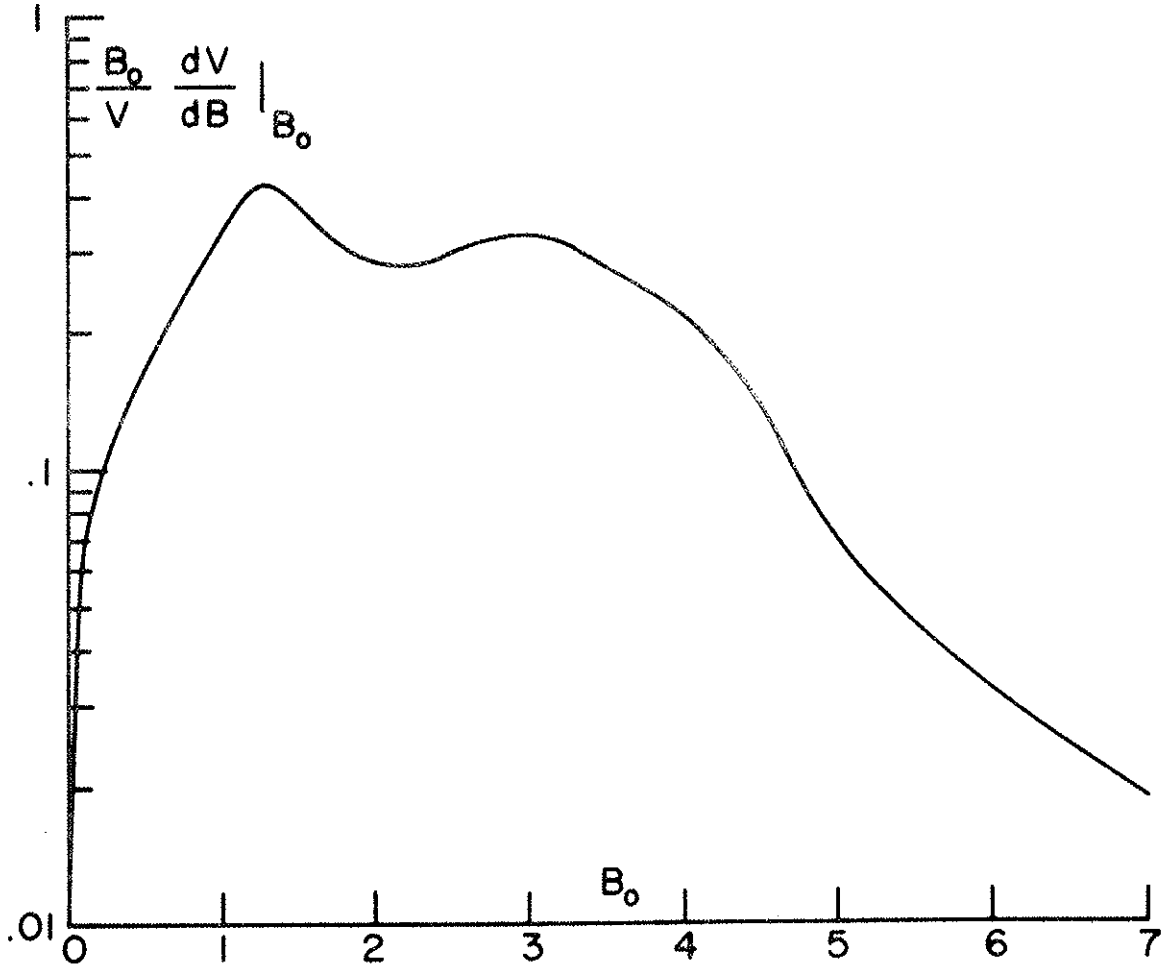
1
.1
.01
$\frac{B_o}{V}\frac{dV}{dB}\Big|_{B_o}$
B_o
0
1
2
3
4
5
6
7

V. EXPERIMENTS ON ELECTRON CYCLOTRON HEATING

A. General Observations

There are two distinct and widely different types of plasmas produced by r.f. heating in the toroidal octupole. The plasma present during the heating pulse is energetic, anisotropic, and non-Maxwellian, and it is highly localized in space. After the microwaves disappear, there is a brief transition period during which the plasma cools, thermalizes, and spreads out to fill the machine. After this transition, an afterglow plasma resembling that produced by gun injection is observed to slowly decay. This chapter describes the plasma present during the r.f. heating and transition periods, while Chapter VI deals with the afterglow plasma.

If microwave power is injected into the toroidal cavity with low background pressure ($p \lesssim 10^{-6}$ torr) and no preionization, negligible power is absorbed by the gas. This is not unexpected since eq. (12) predicts that the power absorbed is proportional to the free electron density in the resonance region. The electron density can be raised by two means: 1) Preionization can be provided by a hot filament or with a gun injected plasma, or 2) the background gas pressure can be increased until the ionization time is short compared with the r.f. pulse length, so that the electron density can build up during the heating pulse.

The plasmas produced during the heating pulse and in the afterglow are somewhat different for the two cases. For low background pressure ($p \lesssim 10^{-6}$ torr) and preionization, the electron density

is nearly constant before, during, and after the heating, but the average electron energy rises to a high value (~1 keV) during the heating pulse, and then rapidly returns to near its original value after the microwaves are off. At high background pressures ($p \gtrsim 10^{-4}$ torr), preionization makes little difference, and the density rapidly climbs to a high value ($\sim 10^{11}$ cm^{-3}) during the heating pulse while the electrons remain relatively cool ($\lesssim$ 100 eV). The afterglow plasma at high pressure is denser ($\sim 10^{10}$ cm^{-3}) and cooler ($\sim$ 1 eV) than that produced at low pressure. Figure 12 summarizes these observations. Note the large X-ray signal during the heating pulse at low pressures, and the large ion saturation current in the afterglow at high pressures. These observations are in qualitative agreement with the predictions of eq. (20).

In order to test the influence of r.f. pulse length on the heating process, the average density 500 μsec after the end of the microwave pulse was measured vs. pulse length using probe and microwave diagnostics. Figure 13 shows that for a pressure of 10^{-4} torr the density builds up exponentially until a saturation is reached. A floating double probe on the B = 0 axis shows a similar exponential rise during the heating pulse. The saturation value varies approximately like f^2 for the various microwave systems, suggesting a cutoff associated with the plasma frequency, although the density in the afterglow is typically one to two orders of magnitude below that for which $\omega_p = \omega$. The initial rise is exponential, as predicted, with a growth time in agreement with the simple relation, $p\tau_i \simeq 10^{-9}$ torr-sec. The rise time is observed to vary inversely

Figure 12. Oscilloscope traces showing the effects of preionization and background pressure on the properties of the plasma.

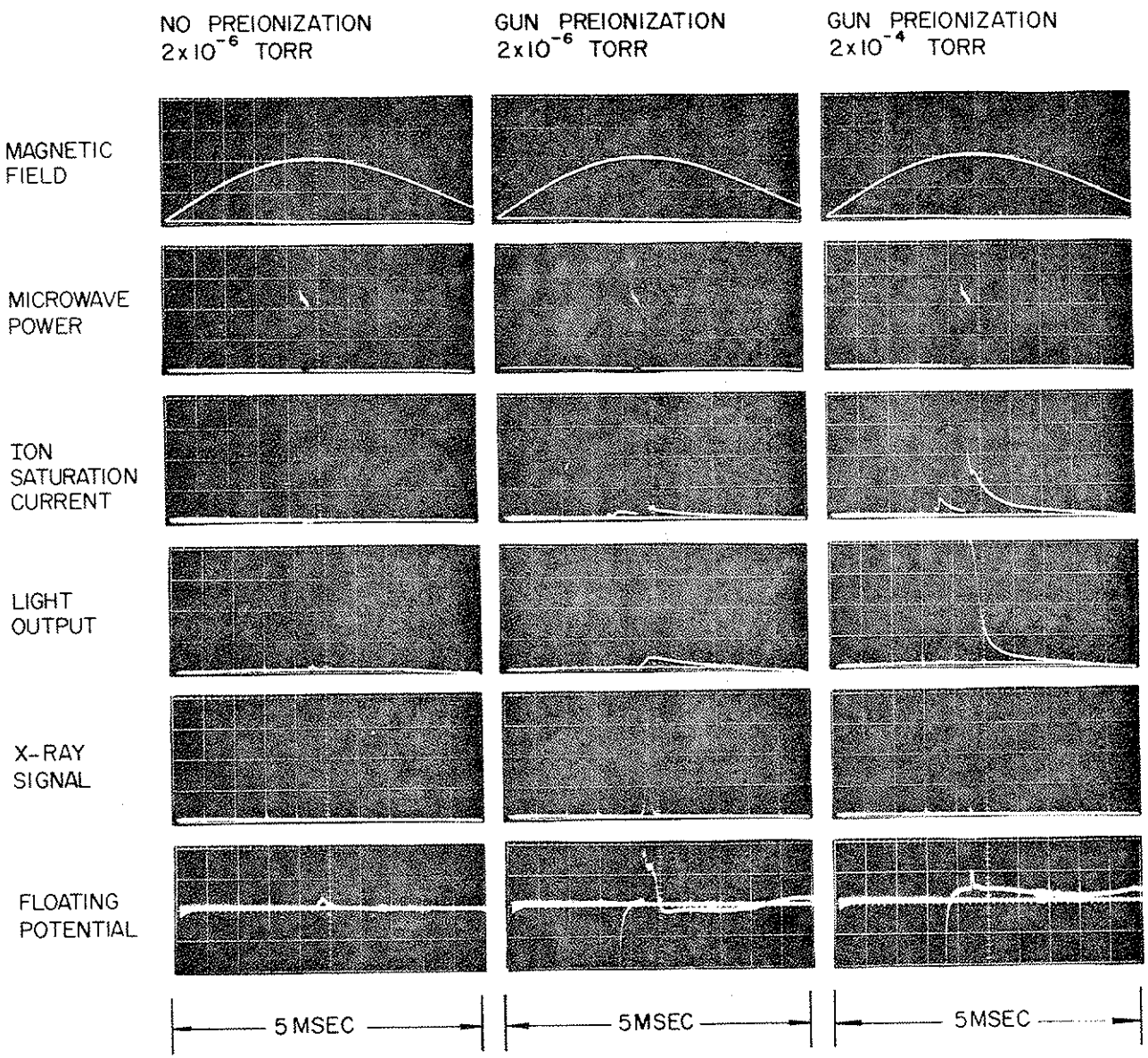
NO PREIONIZATION
2x10⁻⁶ TORR
GUN PREIONIZATION
2x10⁻⁶ TORR
GUN PREIONIZATION
2x10⁻⁴ TORR
MAGNETIC FIELD
MICROWAVE POWER
ION SATURATION CURRENT
LIGHT OUTPUT
X-RAY SIGNAL
FLOATING POTENTIAL
5 MSEC
5MSEC
5MSEC

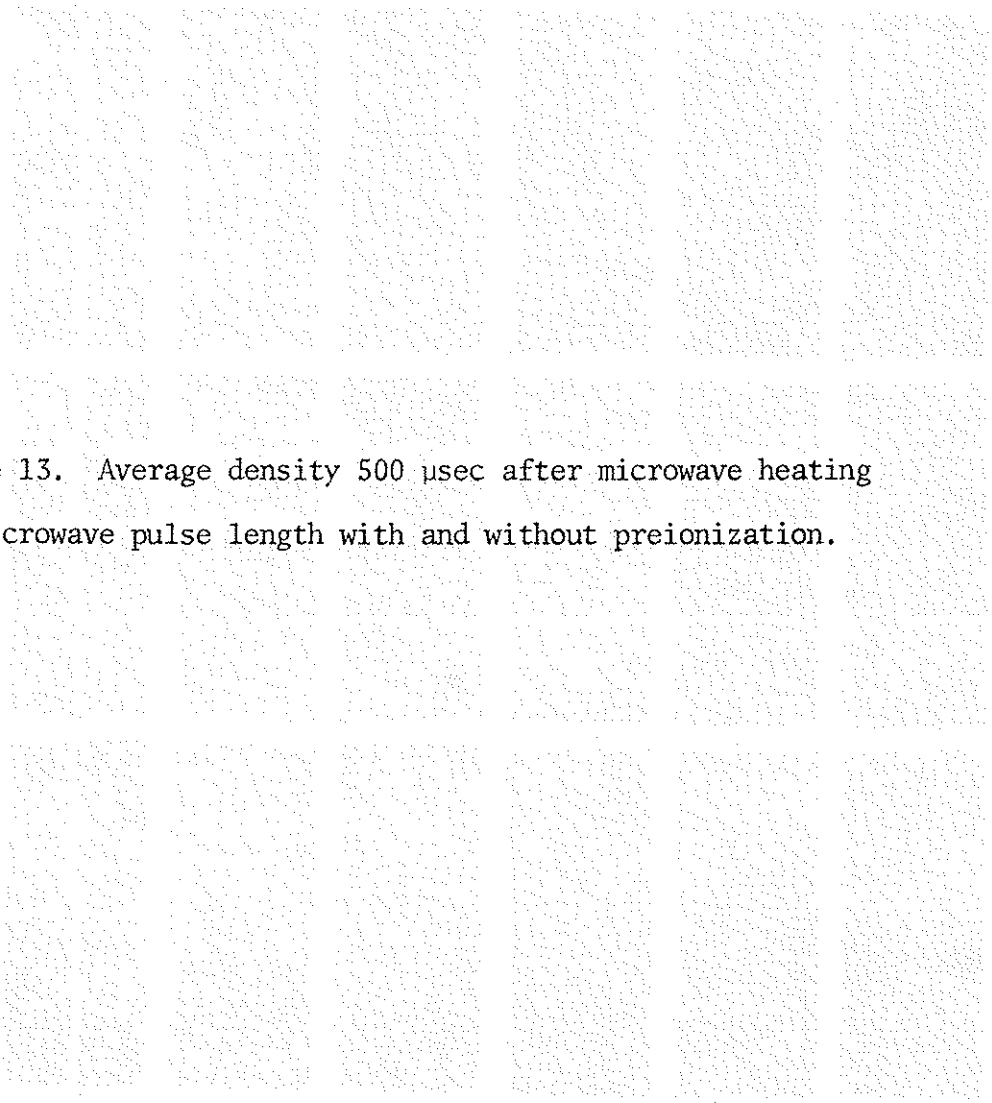

Figure 13. Average density 500 μsec after microwave heating vs. microwave pulse length with and without preionization.

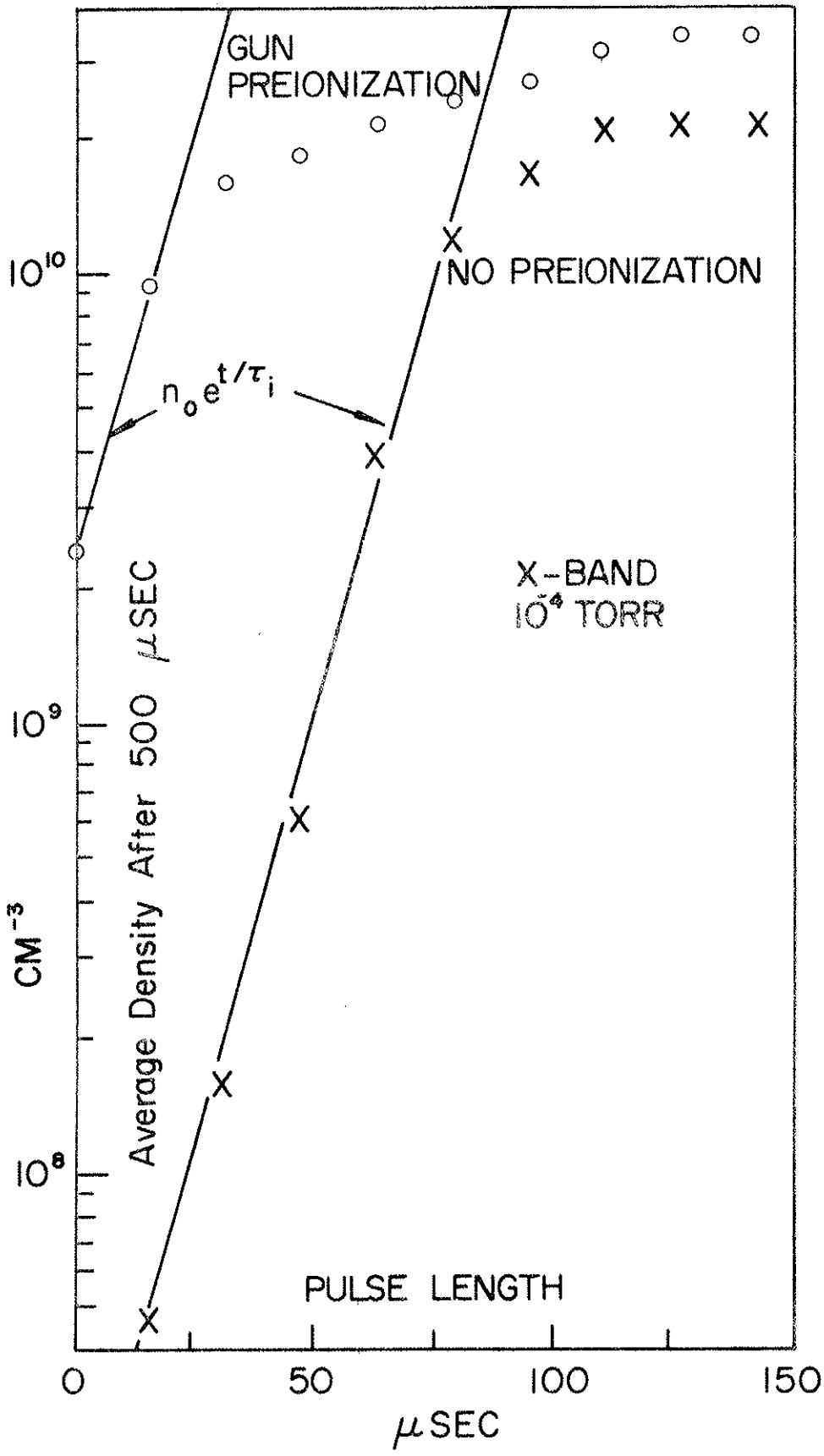
GUN
PREIONIZATION
NO PREIONIZATION
$n_o e^{t/\tau_i}$
X-BAND
10^{-4} TORR
10^{10}
10^{9}
10^{8}
CM^{-3}
Average Density After 500 μSEC
PULSE LENGTH
0
50
100
150
μSEC

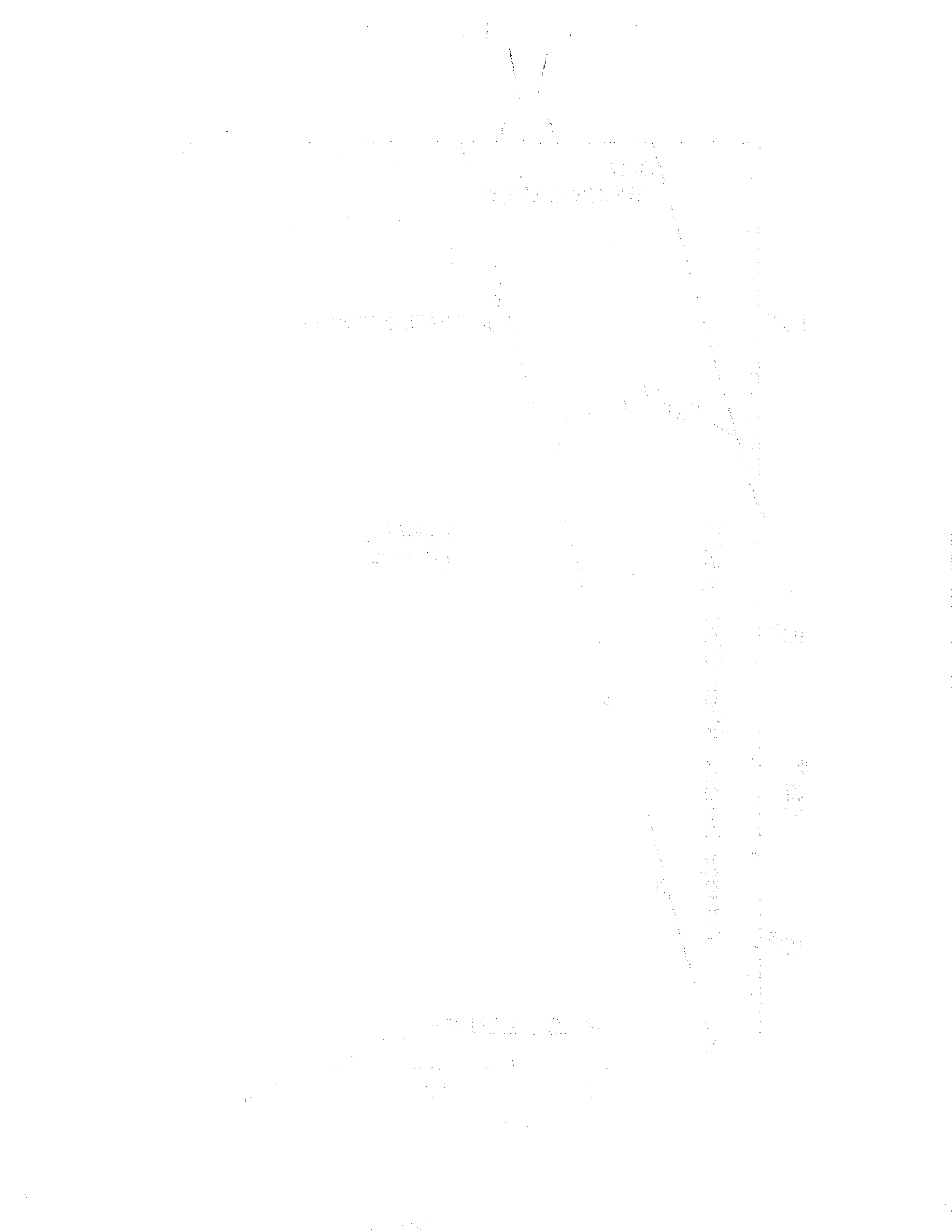

with background pressure as expected. For a typical pulse length of 144 μsec, it is therefore difficult to produce a dense plasma without preionization for pressures below about 5×10^{-5} torr.

The reproducibility of the plasma is very much better at the higher pressures, and the density traces seldom vary by more than a few percent in the afterglow. This reproducibility is apparently caused by the fact that the local density in the resonance region builds up until $\omega_p = \omega$, whereupon the electric field is excluded from the plasma, and the heating stops. The density is thus self-limiting at a value determined solely by the microwave frequency. After the pulse is over, the plasma spreads out to fill the toroid with a resulting density in the afterglow that is considerably smaller than the cut-off density.

In this high pressure regime, preionization has little effect as indicated by fig. 13. The properties of the afterglow plasma are nearly independent of microwave power, for powers above about 1 kW, although the X-ray flux from the plasma during heating decreases sharply when the power is reduced. These observations are consistent with an average electron energy during heating that is proportional to power as predicted by eq. (21), but an ionization time τ_i that is independent of electron energy.

As the magnetic field strength is increased, no observable plasma is produced until resonance occurs within the machine. The average density then rises sharply and becomes relatively independent of field strength as suggested by fig. 11. The spatial distribution of the afterglow plasma and the X-ray flux depend strongly on the

with background pressure as expected. For a typical pulse length of 144 μsec, it is therefore difficult to produce a dense plasma without preionization for pressures below about 5×10^{-5} torr.

The reproducibility of the plasma is very much better at the higher pressures, and the density traces seldom vary by more than a few percent in the afterglow. This reproducibility is apparently caused by the fact that the local density in the resonance region builds up until $\omega_p \approx \omega$, whereupon the electric field is excluded from the plasma, and the heating stops. The density is thus self-limiting at a value determined solely by the microwave frequency. After the pulse is over, the plasma spreads out to fill the toroid with a resulting density in the afterglow that is considerably smaller than the cut-off density.

In this high pressure regime, preionization has little effect as indicated by Fig. 13. The properties of the afterglow plasma are nearly independent of microwave power, for powers above about 1 kW, although the X-ray flux from the plasma during heating decreases sharply when the power is reduced. These observations are consistent with an average electron energy during heating that is proportional to power as predicted by eq. (23), but an ionization time τ_i that is independent of electron energy.

As the magnetic field strength is increased, no observable plasma is produced until resonance occurs within the machine. The average density then rises sharply and becomes relatively independent of field strength as suggested by Fig. 14. The spatial distribution of the afterglow plasma and the X-ray flux depend strongly on the

position of the resonance zones, however.

B. Spatial Distribution.

Perhaps the most striking feature of the heating model in Chapter IV is that the heating rate in ψ-space should vary like the function

$$\frac{1}{V'} \left.\frac{d^2V}{dBd\psi}\right|_{B_o} (\psi).$$

This function is zero on the separatrix and infinite on the ψ-surfaces that are tangent to the surface $B = B_o$. This prediction was tested under a variety of heating conditions using floating double probes and scintillator probes.

Using S-band microwaves and a pressure of 10^{-4} torr with no preionization, the spatial distribution of ion saturation current was measured with a floating double probe. It was determined that the ion saturation current is nearly constant along a field line, and has large gradients perpendicular to $\vec{B}$. Figure 14 shows a profile of I_{oi} for a scan along the midplane from the inner wall to the center and then diagonally up to an inner hoop (see fig.2) The current was measured 60 μsec after the beginning of the r.f. pulse, just before the current saturated in the resonance regions. Note that the peaks approximately coincide with infinite values of

$$\left.\frac{d^2V}{dBd\psi}\right|_{B_o},$$

and that there is a pronounced dip at the separatrix ($\psi = -1.6$).

A similar experiment was performed under the same conditions except the pressure was reduced to 10^{-6} torr and a gun plasma with

Figure 14. Ion saturation current vs. ψ during S-band heating at 10^{-4} torr.

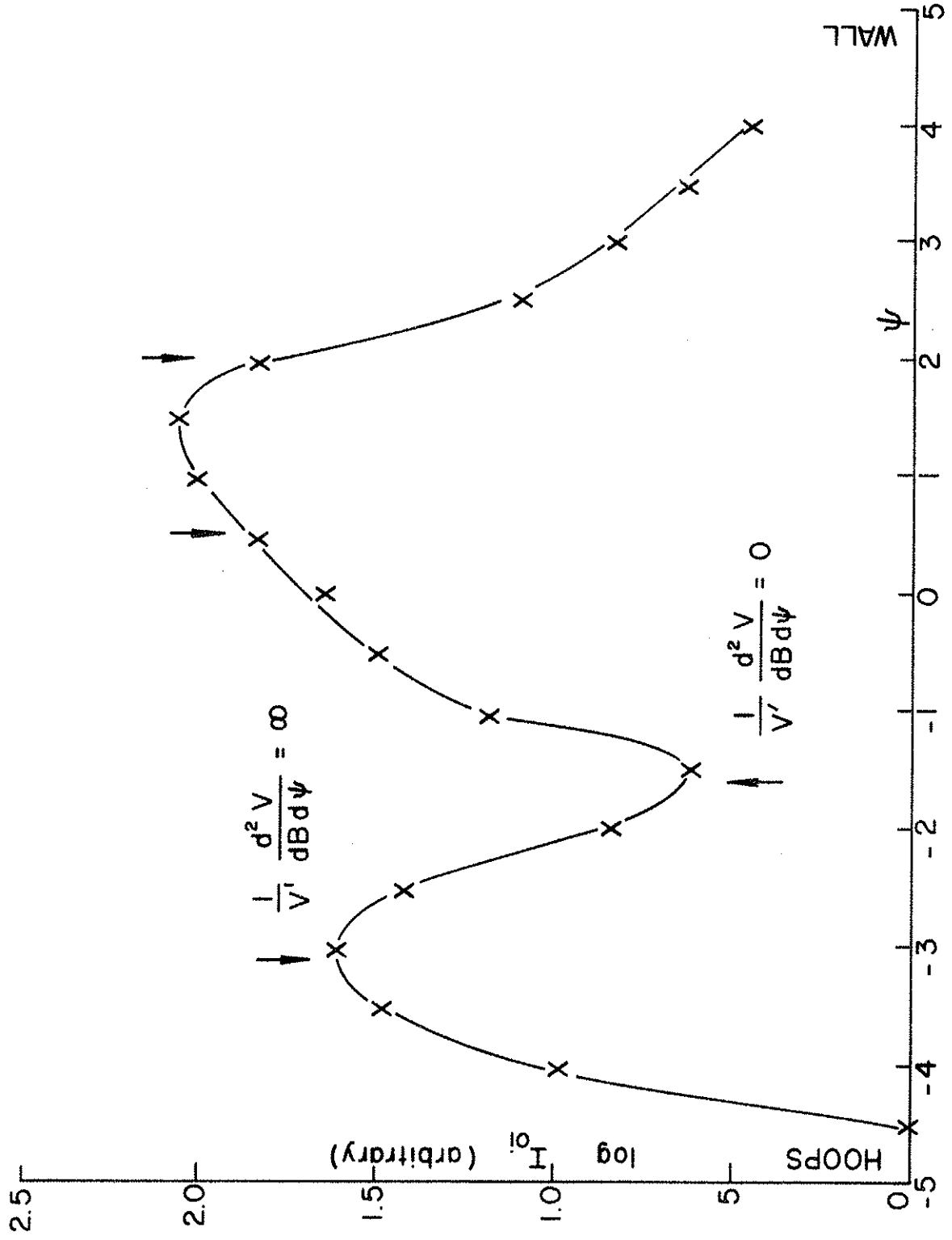
HOOPS
WALL
log I_{oi} (arbitrary)
ψ
$\frac{1}{V'}\frac{d^2V}{dB\,d\psi} = 0$
$\frac{1}{V'}\frac{d^2V}{dB\,d\psi} = \infty$

ABUNDANCE
MASS (AMU)

$n \sim 10^9$ cm^{-3} was injected 500 μsec before the microwave pulse. The integrated output signal from a scintillator probe (see III. D.) with a .001" copper foil having a threshold energy of ~ 8 keV was measured vs. ψ during the heating pulse along the same scan as in fig. 14. The result is shown in fig. 15. Again, the energy appears to be high in the resonance regions and low at the separatrix. The scintillator probe signal is a strong function of microwave power and background gas pressure. The points in fig. 15 and in the following figures represent the average of three shots of the plasma, and the error bars show the highest and lowest of the three shots.

A spatial scan was made of the upper inside quadrant of the field using the same scintillator probe. Figure 16 shows the result. The diagonal lines are the lines along which the probe scans were made. The dotted lines are magnetic field lines. Note that energy tends to flow along the magnetic field, but that most of the energetic particles are trapped near the local field minimum, suggesting a velocity anisotropy.

A probe scan across the midplane crosses the same field lines on which resonance occurs at a place away from resonance. No peak is observed there for the probe with a threshold of 8 keV, but a probe with a thinner aluminum foil having a threshold of about 3 keV does show a small broad peak. This observation is consistent with the fact that ion saturation current is constant along a field line and indicates that the velocity anisotropy is greater at high energies.

Figure 15. Scintillator probe output signal vs. ψ during S-band heating at 10^{-6} torr with gun preionization.

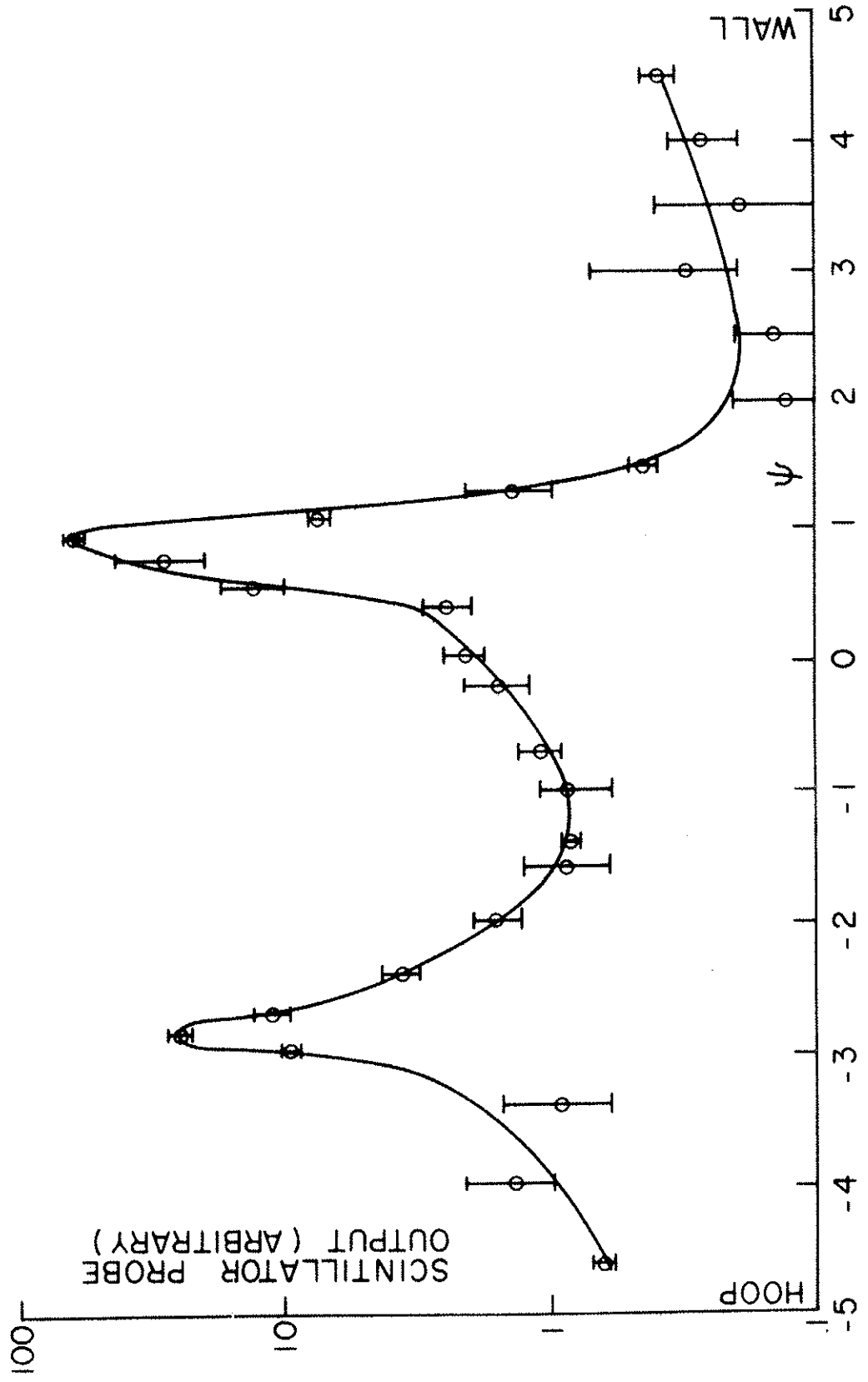
SCINTILLATOR PROBE
OUTPUT (ARBITRARY)
100
10
1
HOOP
WALL
-5
-4
-3
-2
-1
0
1
2
3
4
5
ψ

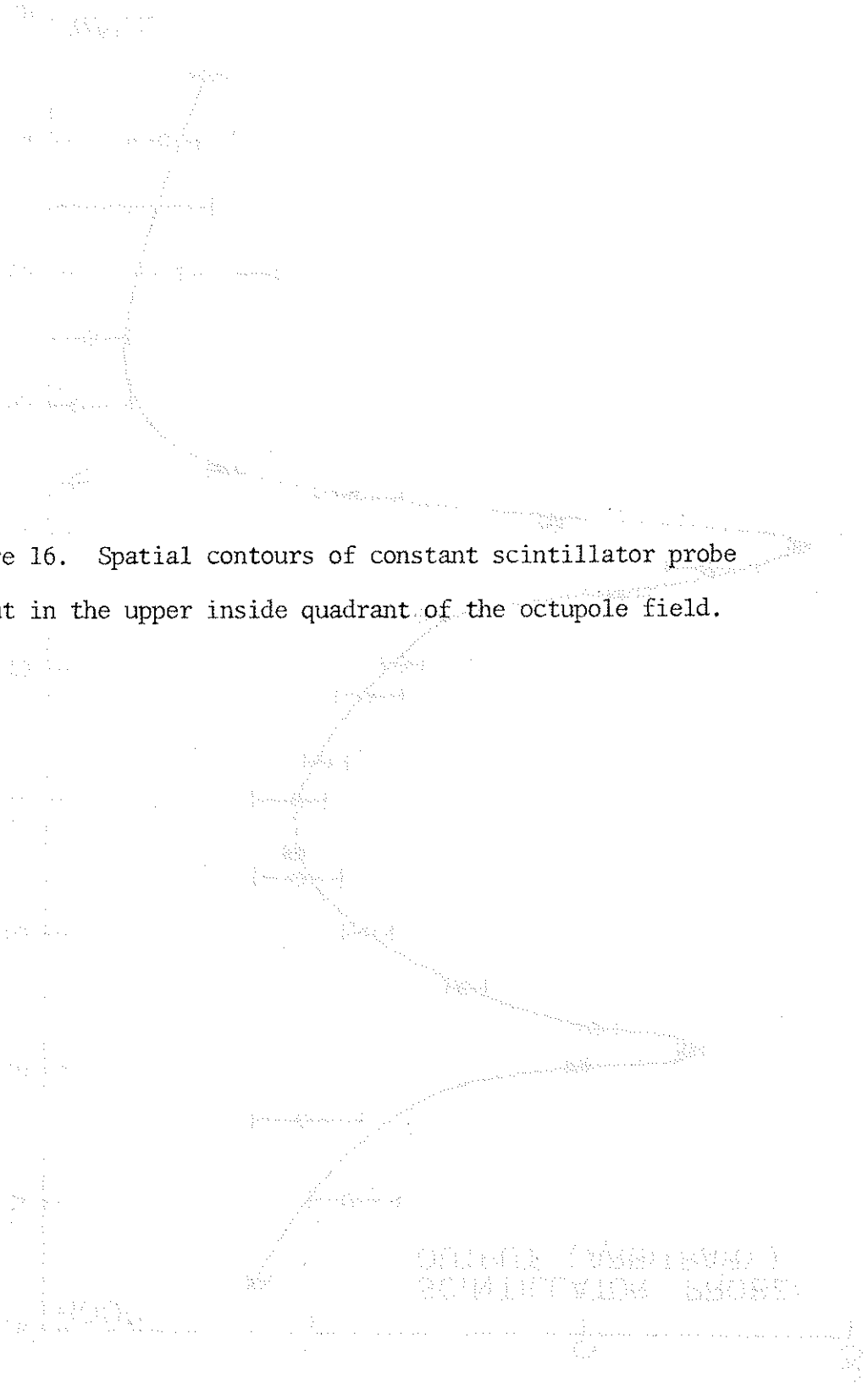

Figure 16. Spatial contours of constant scintillator probe output in the upper inside quadrant of the octupole field.

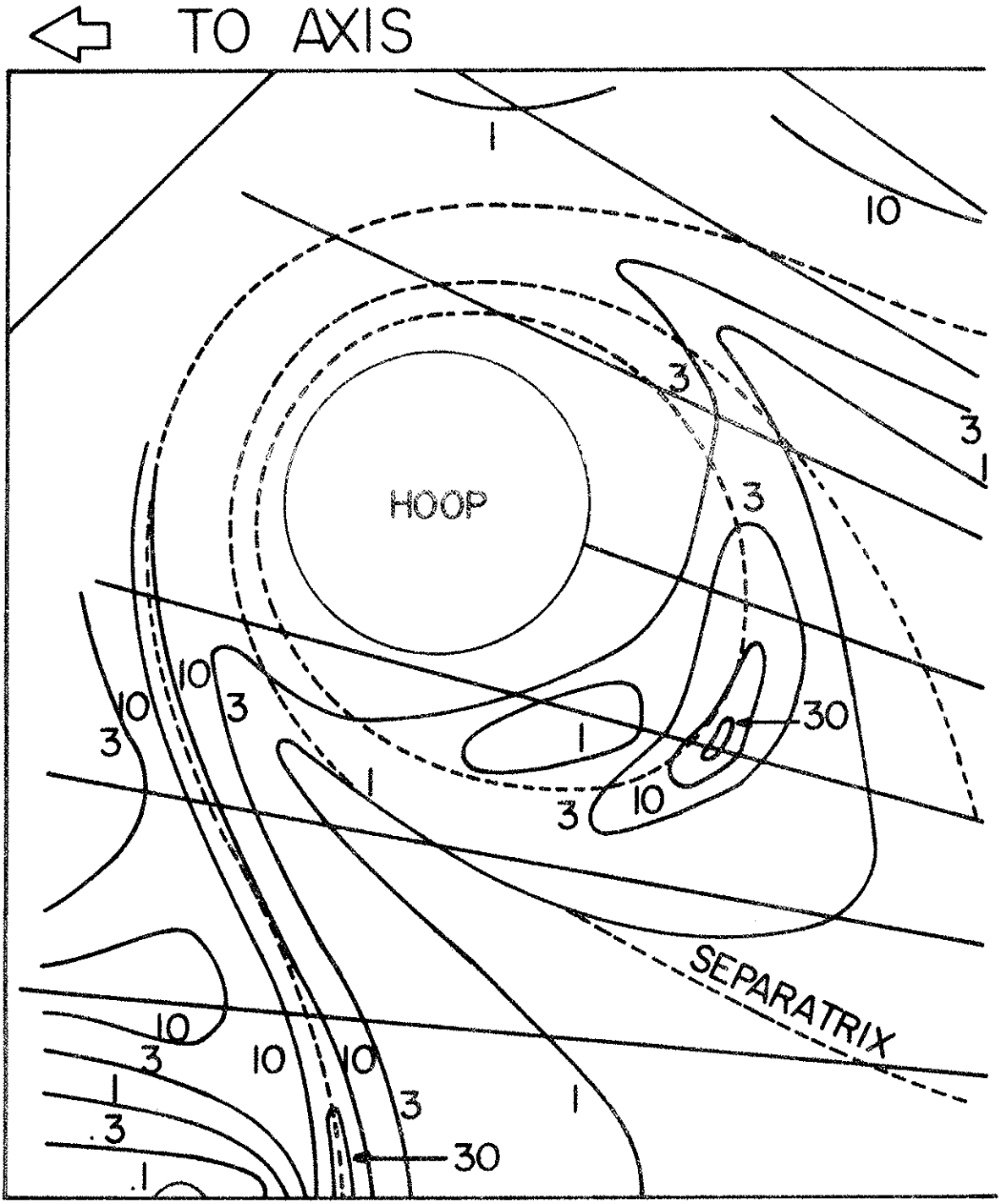
TO AXIS
HOOP
SEPARATRIX
1
10
3
30
.3
.1

The low signals obtained on the midplane between the inner wall and the resonance peak result from the fact that the probe traverses the resonance and obstructs the heating. This effect can be demonstrated by observing the scintillator probe signal at the resonance peak at one port while another 1/4" probe is inserted along the midplane at some other port. As the second probe is pushed across the resonance region, the scintillator probe signal falls more than two orders of magnitude. This observation indicates that energy flows readily in the azimuthal direction as would be expected since 10 keV electrons in the resonance region ∇B drift around the machine about once per μsec.

By changing the current in the hoops, the position of the resonance zones can be changed. By resonating on the line $B_o = 2$ in fig. 2, the resonance zone outside the separatrix can be made to disappear while resonance still occurs near the inner hoops. As the resonance zones are moved near the walls and near the hoops, we expect to see X-rays produced by energetic electrons striking the walls and hoops. A collimated scintillation detector with an acceptance cone of 5^o located outside of the field was pointed at the walls and hoops, and it was established that large X-ray fluxes do come from these regions when the field strength is appropriately adjusted.

Figure 17 shows a plot of the output signal from an uncollimated scintillation detector located at a port on top of the machine in the vertical midplane. The lower hoops and bottom wall are in the field of view of the detector but not the side walls at the midplane. As

Figure 17. X-ray signal from the plasma vs. capacitor bank voltage for two different microwave frequencies.

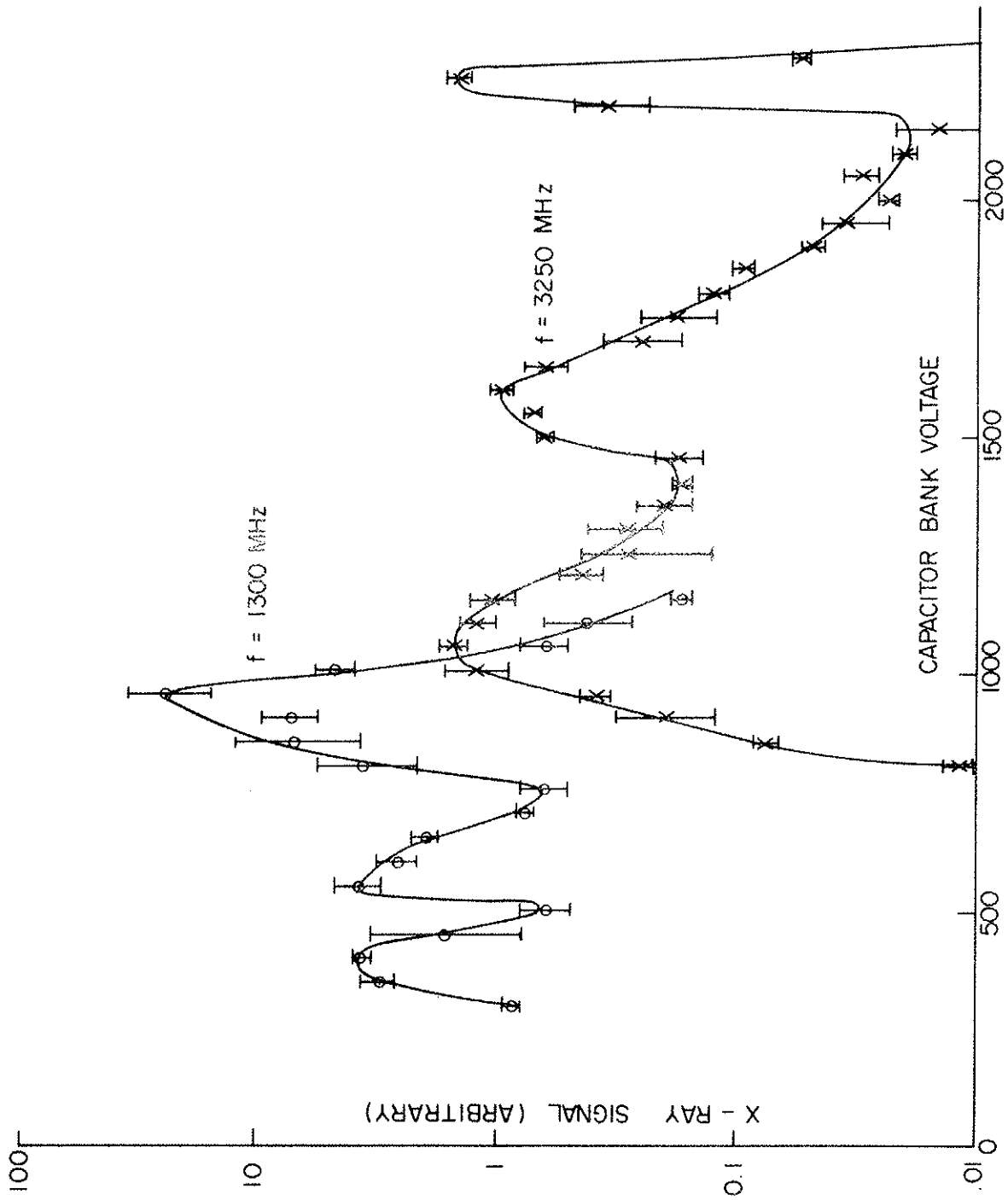
f = 1300 MHz
f = 3250 MHz
CAPACITOR BANK VOLTAGE
0
500
1000
1500
2000
X - RAY SIGNAL (ARBITRARY)
.01
0.1
1
10
100

the capacitor bank voltage used to excite the hoops is raised, three prominant peaks are observed. The first two correspond to resonance zones near the inner and outer hoops respectively, while the third peak is caused by electrons in the resonance zone near the wall striking the scintillator foil. The position of the peaks scales with frequency in the proper way for the two cases in fig. 17. The L-band (1300 MHz) signals are larger than the S-band (3250 MHz) signals probably as a result of the higher power of the L-band system. The fact that additional peaks are not observed indicates that absorption at harmonics of the cyclotron frequency[64,65] is negligible.

In order to determine the optimum magnetic field strength for cyclotron heating at a particular microwave frequency, a scintillator probe with a .0007" aluminum foil was placed on the B = 0 axis, and the capacitor bank voltage was varied. Figure 18 shows the result for heating at 1300 MHz. The probe signal shows a peak at 1600 volts, corresponding to resonance at $B_o = 0.6$ in fig. 2. It was shown in eq. (15) that the power absorbed by the plasma for $n \neq n(\psi)$ should be proportional to the function $dV/dB\big|_{B_o}$, which according to fig. 11 has a maximum at $B_o = 1.2$. The observed maximum could be lower than the predicted value for several reasons. 1) The density $n(\psi)$ is not constant, but is peaked near the separatrix. 2) The trapping efficiency of the energetic electrons may be greater for resonance deeper in the magnetic well. 3) The resulting density profile of energetic electrons may be more sharply peaked about the separatrix for resonance deeper in the well.

Figure 18. Scintillator probe signal on the B = 0 axis vs. capacitor bank voltage for heating at 1300 MHz.

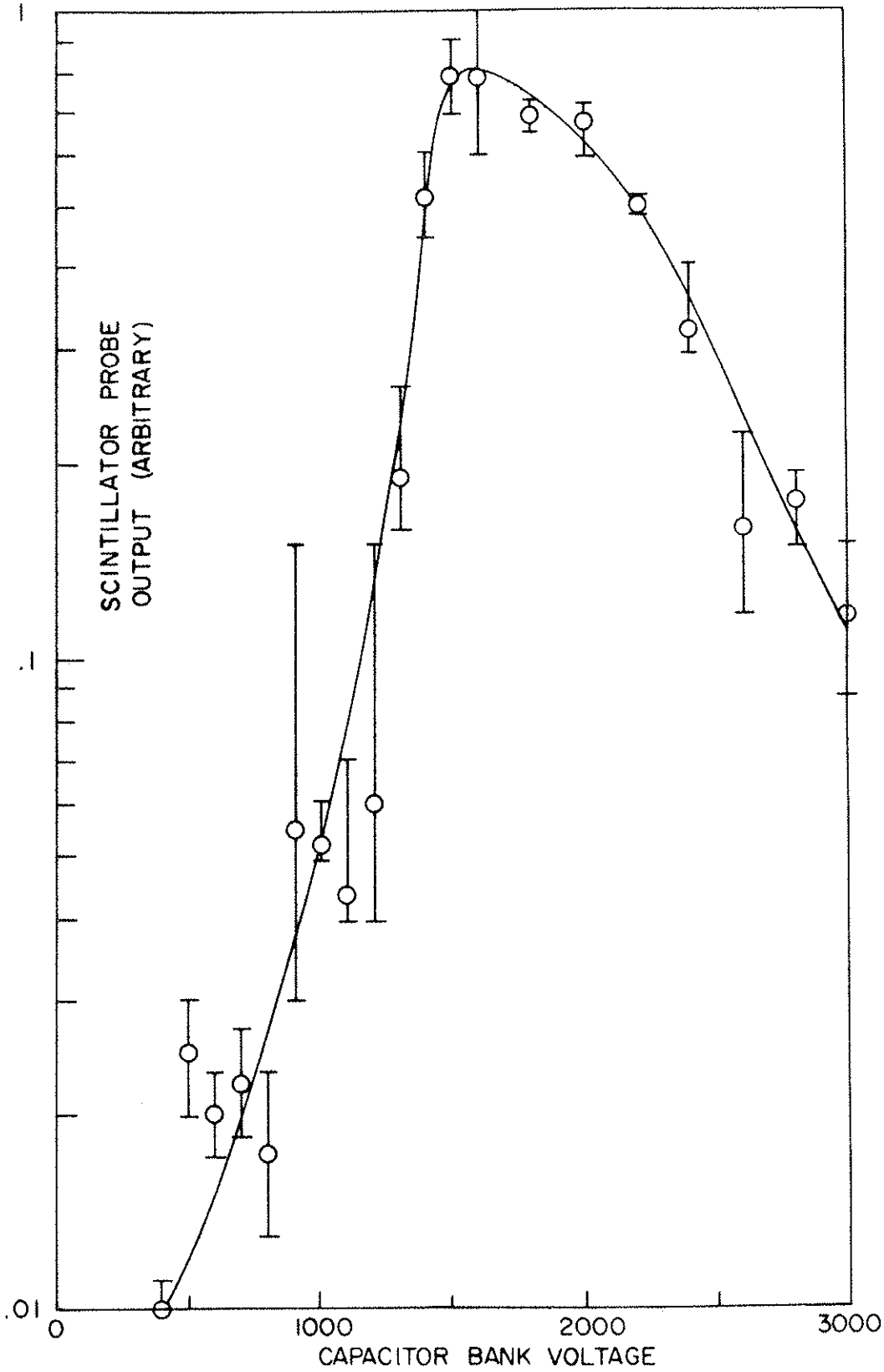
1
.1
.01
SCINTILLATOR PROBE
OUTPUT (ARBITRARY)
0
1000
2000
3000
CAPACITOR BANK VOLTAGE

C. Energy Distribution

Extensive measurements of the electron distribution function on the B = 0 axis during the r.f. heating have been made by Kuswa[66] using electrostatic energy analyzers (see III. C.). Although the energy density on the B = 0 axis is smaller than in the resonance regions, the volume of the resonance zones is so small that the total electron distribution is closely approximated by the distribution on the B = 0 axis. Since the heating rate at the separatrix is expected to be small (see fig. 10), the high energy electrons observed on the zero field axis are presumably formed in the resonance regions and diffuse to the center by some process not well understood.

Kuswa has shown that, for a variety of conditions, the electron distribution at intermediate energies can be approximated by the function

$$f(W) = \frac{3n}{\overline{W}} e^{-\sqrt{6W/\overline{W}}} \qquad (26)$$

where $\overline{W}$ is the average electron energy:

$$\overline{W} = \frac{1}{n}\int_0^\infty W f(W) dW.$$

At low energies (< 100 eV), the distribution looks Maxwellian, but problems of magnetic fields penetrating the detector, secondary emission, and the measurement of plasma potential complicate the interpretation. The average energy $\overline{W}$ is typically 100 eV - 1 keV. The tail of the distribution (W > 10 keV) can be fit by a Maxwellian with a temperature of 1 - 10 keV. Densities measured with analyzers are typically 10^9 - 10^{10} cm^{-3}. These non-Maxwellian distributions

can exist at high energies because the electron-electron collision time as calculated by Spitzer[67] is many orders of magnitude longer than the duration of the experiment.

It is interesting to note, that if energetic electrons are lost primarily by thermal flow to obstacles in the plasma, a distribution function $f_o(W)$ at $t = 0$ would evolve into a distribution of the form

$$f(W,t) = f_o(W)e^{-t/\tau(W)} = f_o(W)e^{-\frac{At}{V}\sqrt{\frac{W}{8m}}} \qquad (27)$$

if heating and other loss processes are neglected. For large t, the exponential term dominates, and a distribution function of the form of eq. (26) results. The measured distribution function during the heating does not evolve in time according to eq. (27), however, and a complete understanding of eq. (26) would involve details of both the heating process and the mechanism by which plasma diffuses out of the resonance regions.

Scintillator probes have also been used to estimate the energy and density of the plasma on the $B = 0$ axis. Probes with variable foil thickness show that the distribution is not Maxwellian. A double scintillator probe with aluminum foils of .0007" and .0021" was used to measure the density and "temperature" (actually the slope of the distribution function at energies of a few keV). Figure 19 shows a case in which the X-band system was used to heat the gun plasma with various background gas pressures. At 10^{-6} torr, the density and temperature as measured by the probe are $1.5 \times 10^{10} cm^{-3}$ and 1.4 keV respectively. Since the distribution is not Maxwellian,

Figure 19. Scintillator probe measurement of density and temperature on the B = 0 axis for X-band heating of a gun plasma vs. background gas pressure.

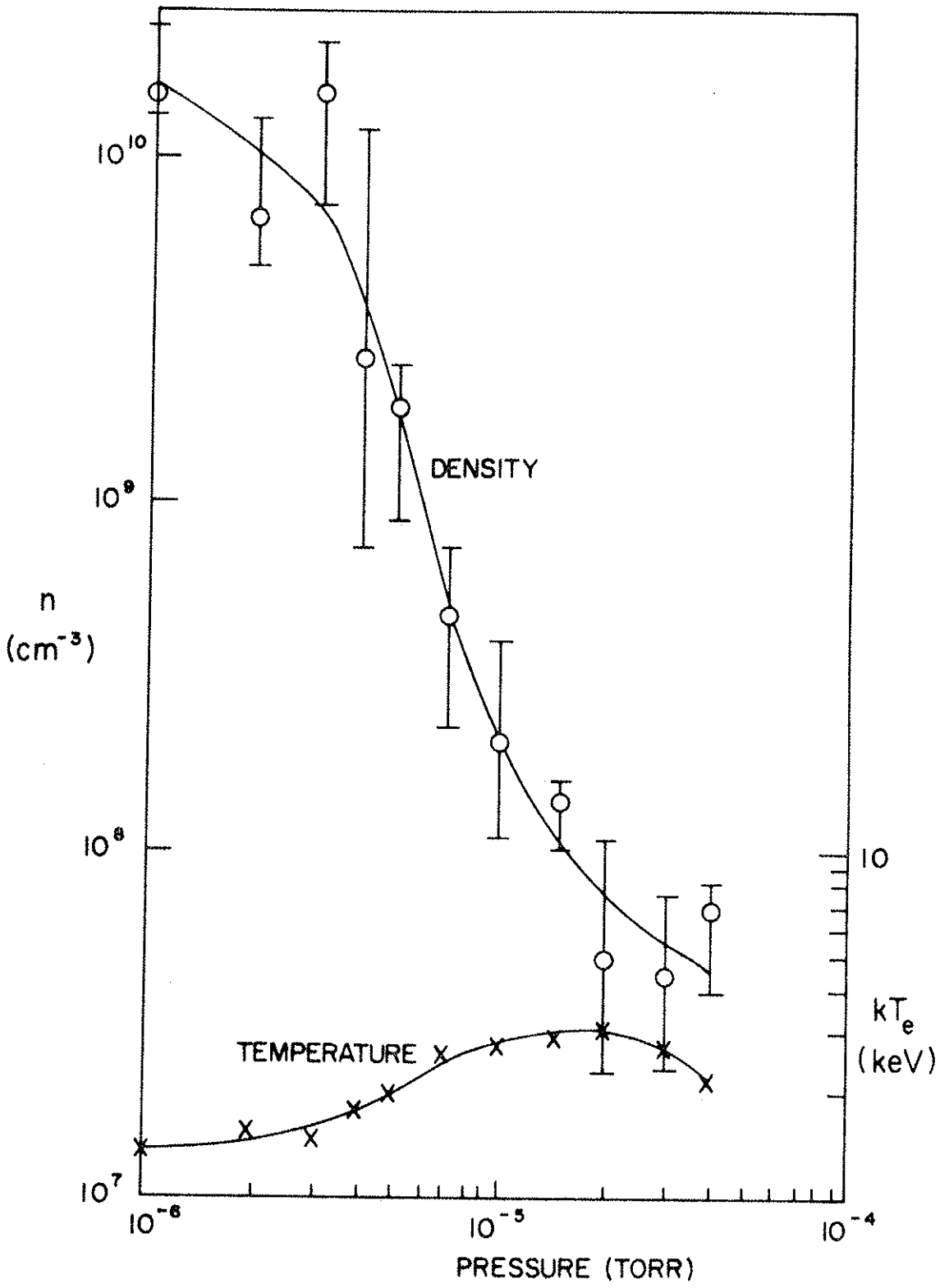
10^{10}
10^{9}
10^{8}
10^{7}
n
(cm^{-3})
DENSITY
TEMPERATURE
10
kT_e
(keV)
10^{-6}
10^{-5}
10^{-4}
PRESSURE (TORR)

the numerical values should not be taken too seriously. The energy analyzer gives for this case a density of 6×10^9 cm^{-3} and an average energy of 700 eV. Figure 19 shows that the density of energetic electrons drops sharply with increasing pressure, although the total electron density is known to increase.

If the scintillator probe is recalibrated by substituting a distribution function of the form of eq. (26) into Eqs. (9) and (10), the average energy measured by the probe at 10^{-6} torr is about 300 eV. This discrepancy is believed to be caused by very high energy electrons (> 40 keV) which penetrate the foil and produce large light signals in the scintillator, or by ultraviolet light produced by ion bombardment of the foil. If the analyzer measurement of 700 eV is accepted, the scintillator probe gives a density of 4×10^9 cm^{-3}, in reasonable agreement with the analyzer.

D. Time Evolution

Electrostatic analyzers and scintillator probes both show that the energetic electron density builds up rapidly in a few μsec after the r.f. pulse is turned on, and then reaches a saturation, or even decreases. This behavior suggests the presence of a strong loss mechanism that balances the r.f. heating after an initial transient period. Figure 20 shows an example of the time evolution of the energetic electron density and temperature (assumed Maxwellian) on the B = 0 axis as measured by a scintillator probe. The gun plasma was heated by a 30 μsec pulse of X-band microwaves with a background pressure of 10^{-6} torr.

Figure 20. Scintillator probe measurement of the time evolution of density and temperature on the B = 0 axis for X-band heating of a gun plasma at a pressure of 10^{-6} torr.

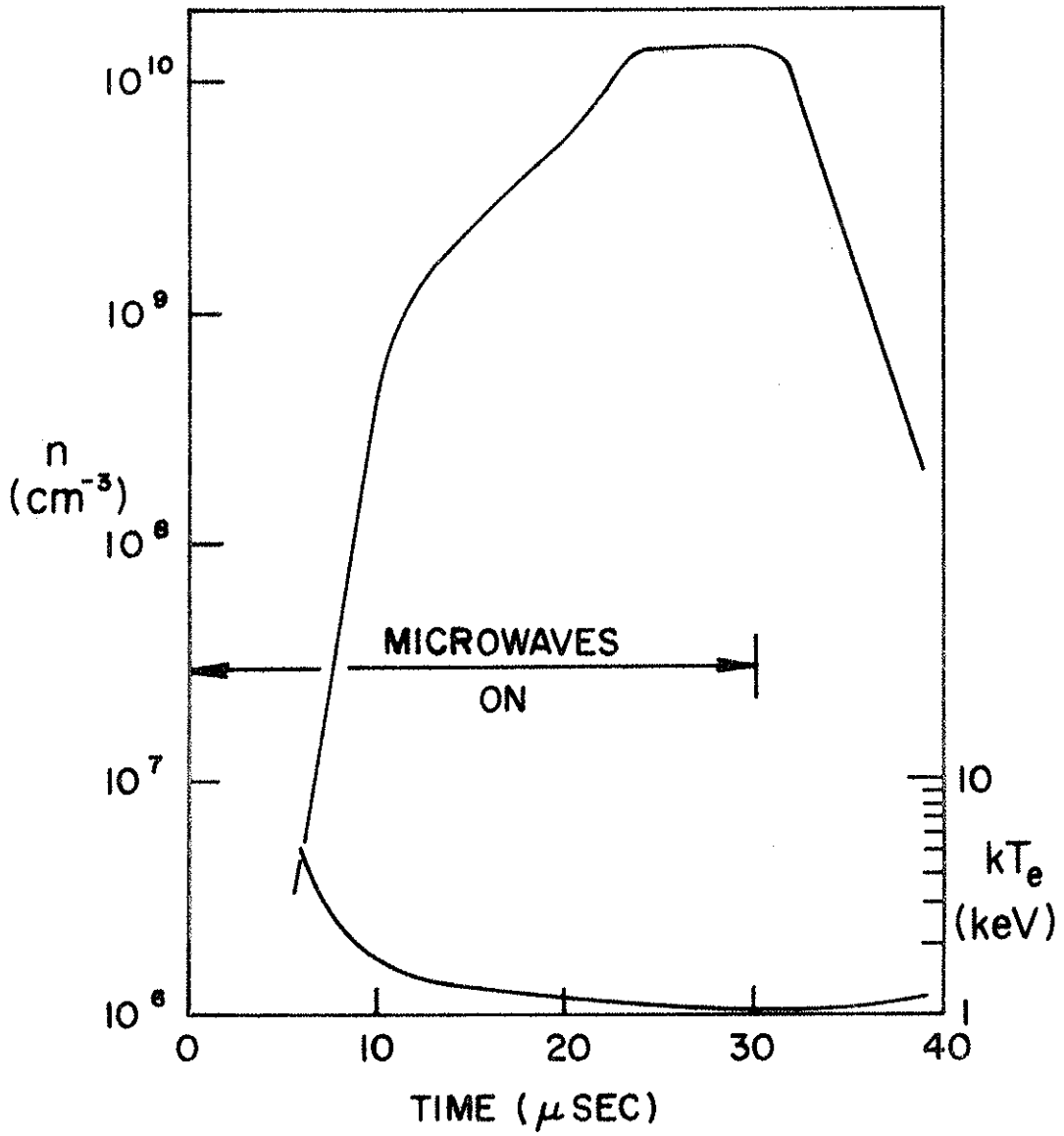
10^{10}
10^{9}
n
(cm^{-3})
10^{8}
10^{7}
10^{6}
MICROWAVES
ON
10
kT_e
(keV)
1
0
10
20
30
40
TIME (μSEC)

At early times during the r.f. pulse, the measured energy density in the plasma is comparable to the r.f. energy density, suggesting that the heating efficiency is close to 100% in agreement with the fact that eq. (16) predicts high efficiency for densities above about 10^8 cm^{-3}. This result is to be compared with the energy density in the afterglow of a microwave produced plasma that gives an efficiency of about 0.1%.

Theoretical estimates (see fig. 26.) indicate that at these low background pressures the dominant cooling mechanism for energetic electrons is thermal flow to obstacles in the plasma (hoop supports and probes). To test this prediction, the decay of the energetic electron density during the transition period after the end of the r.f. pulse was examined. Figure 20 shows the rapid decay of density after the microwaves go off. Kuswa[66] has shown using an electrostatic analyzer that the lifetime of electrons of a given energy is proportional to $W^{-0.5}$ as expected for obstacle loss. The cross section calculated from these data is about 90 cm^2 in reasonable agreement with the geometrical area of the probes, analyzers, and hoop supports. Additional obstacles inserted into the plasma increase the decay rate.

The evolution of the energy distribution after the r.f. pulse is off should follow eq. (27). As t increases, the average energy decreases until electron-electron collisions become important. Within 100 μsec after the end of the microwave pulse, the distribution function returns to a Maxwellian with an electron temperature only slightly greater than that of the initial gun injected plasma

(~ 5 eV). The temperature then continues to decrease (see fig. 27.) at a rate that is consistent with obstacle losses.

VI. PROPERTIES OF THE AFTERGLOW PLASMA

A. General Behavior

When the microwave pulse is over, the energetic component of the plasma decays quickly as discussed in the previous section, and a lower temperature Maxwellian remains which decays with a much longer lifetime. With low background pressure and gun preionization, the resulting plasma in the afterglow is practically indistinguishable from the usual gun injected plasma except for a slightly higher density and electron temperature. The plasma produced at high background pressure with no preionization is somewhat different from the gun injected plasma, and it is this case that will be examined in some detail in this chapter.

The most important difference between the microwave produced plasma and the gun injected plasma is the ion temperature. The microwaves do not appreciably heat the ions, and at the densities in the present experiment, energy transfer from the electrons should be small, and so we expect the ions to be in thermal equilibrium with the background neutral gas. Energy analyzer measurements place an upper limit of $\sim$1 eV on the ion temperature.

As mentioned previously, the electron heating is strongly localized in the resonance zones. Because of the high order mode, the perpendicular component of the r.f. field in the resonance region varies with azimuth, and hence it is not surprising that azimuthal density variations of about a factor of two are observed in the after-

glow. These variations are smallest on the separatrix and persist throughout the life of the plasma. The cold plasma component quickly flows along the field, so that in the afterglow we can to a good approximation take the density to be constant on a magnetic field line: $n = n(\psi)$.

In general, the heating zones appear on either side of the separatrix (as in fig. 14), so that large density gradients opposite to those required for MHD stability exist near the separatrix. Such an inverted gradient can be stable provided[68]

$$pV'' \frac{d}{d\psi} \ell n \, (pV'^{5/3}) > 0 \, . \tag{28}$$

For $T_e \neq T_e(\psi)$, this condition is equivalent to requiring that the slope of the ion saturation current on a log scale be less than the slope of the function $V'^{-5/3}$:

$$\left| \frac{d \ \ell n \ I_{oi}}{d\psi} \right| < \left| \frac{d \ \ell n \ V'^{5/3}}{d\psi} \right| \, .$$

Figure 21 shows a case in which the initial ion saturation current distribution (at 60 μsec) exceeds the stability limit. This kind of situation is accompanied by large fluctuating electric fields which allow the plasma to rapidly collapse toward the separatrix producing a relatively flat density distribution within a hundred μsec. The ion saturation current thereafter decays slowly with relatively little change in spatial distribution.

Oscillographs summarizing the gross behavior of the plasma are shown in fig. 22. Figure 22(a) and (b) show the large ion saturation current, floating potential, and azimuthal electric field in the

Figure 21. Ion saturation current distribution in ψ-space for various times after the beginning of a 100 μsec pulse of S-band microwaves.

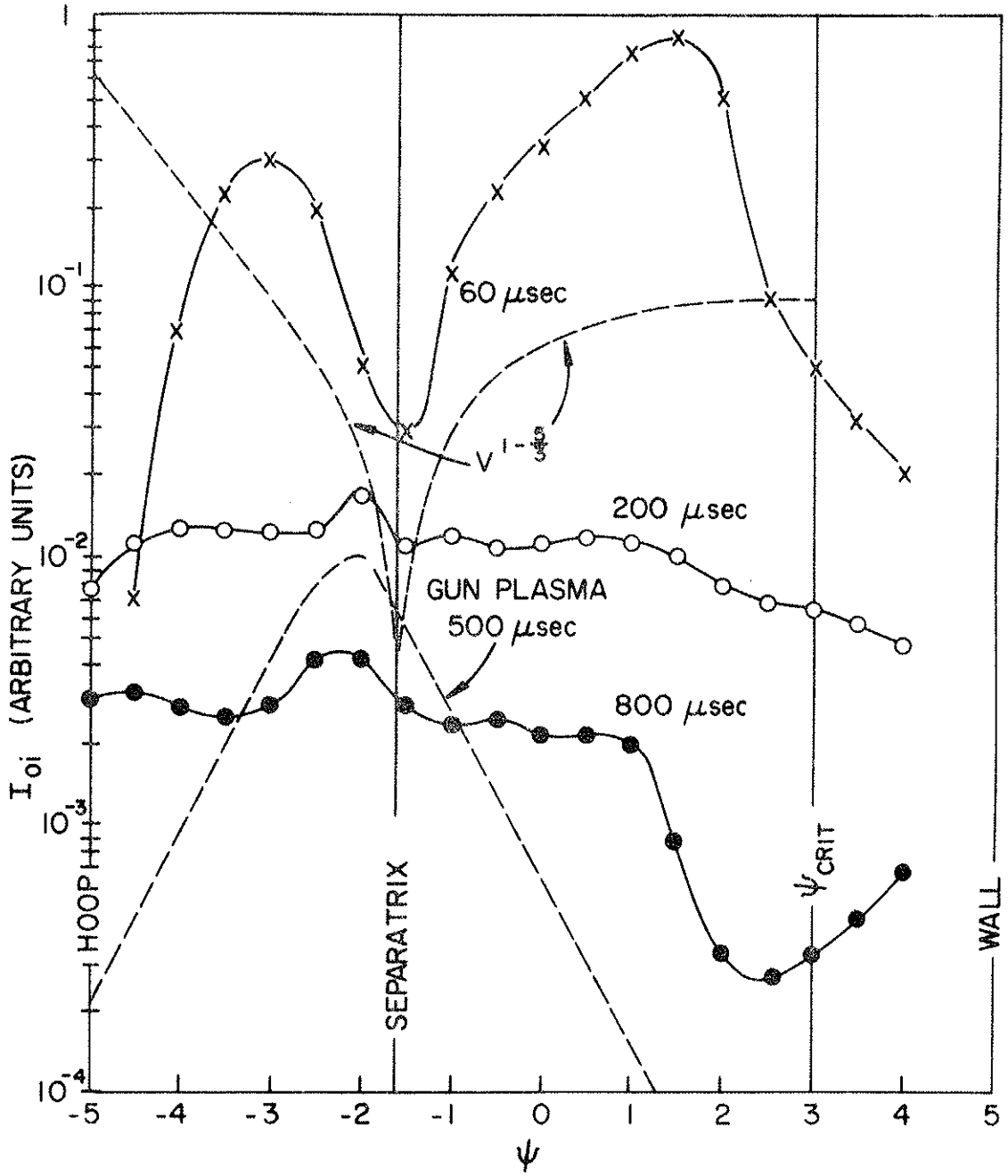
60 μsec
200 μsec
GUN PLASMA
500 μsec
800 μsec
$V^{1-\frac{4}{3}}$
SEPARATRIX
ψ_{CRIT}
WALL
HOOP
I_{oi} (ARBITRARY UNITS)
10^{-1}
10^{-2}
10^{-3}
10^{-4}
-5
-4
-3
-2
-1
0
1
2
3
4
5
ψ

Figure 22. Oscillographs summarizing the gross behavior of the afterglow plasma.

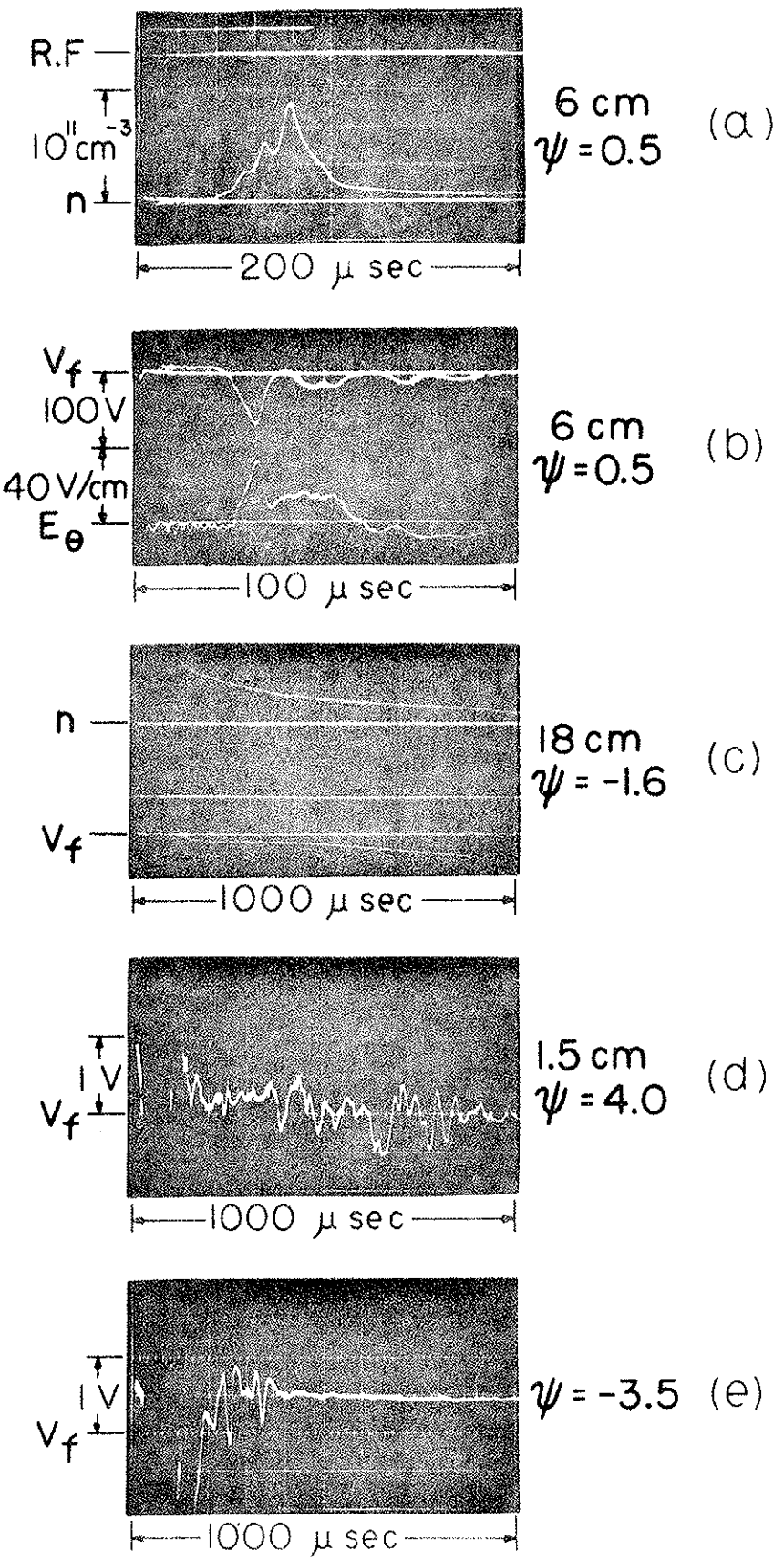
R.F
10^{11} cm^{-3}
n
200 μ sec
6 cm
ψ = 0.5
(a)
V_f
100V
40V/cm
E_θ
100 μ sec
6 cm
ψ = 0.5
(b)
n
V_f
1000 μ sec
18 cm
ψ = -1.6
(c)
1V
V_f
1000 μ sec
1.5 cm
ψ = 4.0
(d)
1V
V_f
1000 μ sec
ψ = -3.5
(e)

resonance region during heating. Figure 22 (c) indicates that, after the heating phase, the ion saturation current and floating potential on the B = 0 axis decay slowly in time with no observable fluctuations. Figure 22 (d) and (e) show that, at the edges of the plasma near the hoops and wall, there are appreciable fluctuations in the floating potential. These phenomena will be discussed in more detail in a later section.

B. Plasma Motion and Particle Loss

By changing the magnetic field strength and microwave frequency, a variety of density distributions can be obtained. One interesting case is produced when resonance occurs at $B_o = 5$ in fig. 2. This contour produces plasma only on the field lines $-5 < \psi < 0$ near the inner hoops. Resonance does not occur on the lines between the separatrix and the outer hoops, so that a scan between the wall and an outer hoop should show the initial density strongly peaked near the separatrix in the region $-1.6 < \psi < 0$.

Figure 23 shows the ion saturation current for such a scan produced by a 144 μsec pulse of X-band microwaves 1.2 msec after the beginning of the magnetic field pulse. The distribution at 1.5 msec is sharply peaked near the separatrix, although even at this early time an appreciable amount of plasma has diffused toward the hoop. This distribution is interesting because it resembles the distribution for the gun injected plasma. By 2.5 msec the density peak has moved significantly toward the hoop. This motion is due in part to the inductive electric field caused by the rising magnetic field. This effect, by itself, would cause a distribution peaked on the separatrix

Figure 23. Ion saturation current distribution in ψ-space for various times after the beginning of the multipole field pulse. The 144 μsec pulse of X-band microwaves begins at 1.2 msec.

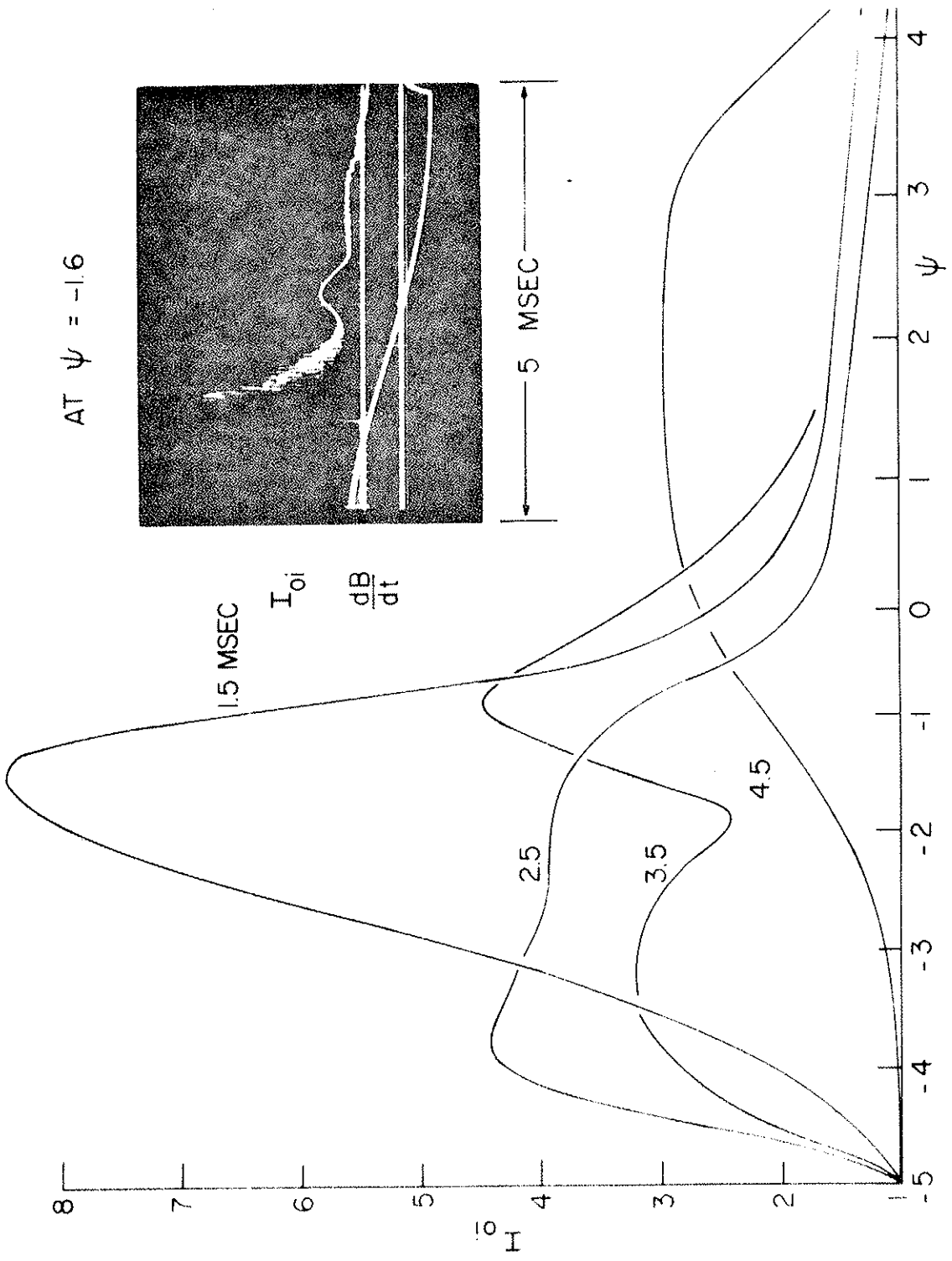
AT ψ = -1.6
5 MSEC
dB/dt
I_oi
1.5 MSEC
2.5
3.5
4.5
I_oi
ψ

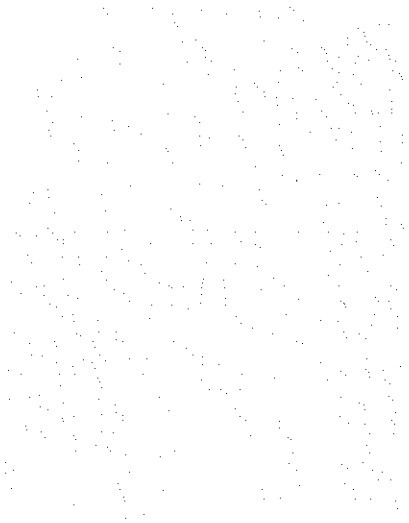

at 1.5 msec to evolve into a distribution peaked at $\Psi = -2.3$ at 2.5 msec. Figure 23 suggests that, in addition to this field line motion, a considerable diffusion is present. By 3.5 msec the field is decreasing sharply leaving a dip on the separatrix where a small number of particles fill a large volume. By 4.5 msec, the plasma is moving rapidly to the walls.

Lencioni[27] has treated theoretically the problem of the evolution of a density profile in the presence of a changing magnetic field for the case in which the field is frozen into the plasma. In the zero gyroradius limit, his results indicate that the density should fall to zero on the separatrix and become infinite on the field line that was the separatrix initially. Experiments[27] on the gun injected plasma indicate a tendency toward this behavior but greatly reduced by the finite ion gyroradius and other effects. It was hoped that the microwave plasma with its small gyroradii ($\Delta\psi < 0.1$) would strongly exhibit the effects of field line motion, but apparently other processes are present that cause diffusion of the plasma across the field.

Although a density distribution initially peaked near the separatrix is expected to be stable against simple interchange instabilities, one might argue that since the plasma is produced in places where the magnetic field strength is comparable to or greater than the magnetic field at the surface of the hoops and walls, it is energetically possible for the plasma to escape from the field. To test the validity of this argument, the plasma produced by the P-band (700 MHz) microwave system was examined. For this case, resonance occurs on a circle

of radius 7.5 cm (B_0 = .25) at a place where $B_{hoop}/B_o \simeq 8$ for the outer hoop. The ion saturation current distribution was measured to determine the evolution of the density profile. Initially the plasma is well confined near the separatrix, but as time goes on a rapid diffusion toward the hoops and wall is observed. The evolution of the profile looks quite similar to the X-band case of fig. 23 indicating that the diffusion is more affected by the shape of the initial distribution than by the location of the resonance zones. Small ($\langle \Delta n \rangle / \langle n \rangle$ ~1-10%), high frequency (~ 1 MHz) fluctuations are observed to accompany this diffusion.

There are three possible sources of plasma loss in a toroidal multipole: 1) recombination, 2) obstacles (including hoop supports), and 3) radial losses (hoop and wall). At the densities in the present experiment, recombination is negligible. Ionization causes the density to grow, and leads therefore to a negative loss. For $kT_e \ll U_i$, as is the case late in the afterglow, ionization can be neglected. The particle loss to the supports was estimated by measuring the ion saturation current to a model support in the same relative position as a real support but electrically insulated from the hoop. The total current to the twelve real supports was taken as twelve times this current. The loss to the walls was measured by biasing all hoops and supports positive with respect to the wall and measuring the ion saturation current to the wall. The flux to the inner hoops was determined by biasing the upper and lower hoops as a floating double probe with mylar sleeves around the supports, and similarly for the outer hoops. These measurements parallel the more detailed tests made by

Meade and Molvik[69] for the gun injected plasma.

Figure 24 shows the relative loss for the various cases. The heating conditions are the same as those for fig. 23. Since the plasma is created near the inner hoops, the initial loss is primarily to the inner hoops. As time goes on, plasma moves toward the outer hoops until the magnetic field starts to decrease, at which time the hoop losses drop sharply, and plasma is transported out to the wall. At very late times (t > 4 msec) the plasma has forgotten the manner in which it was created, and the fluxes to the hoops are approximately proportional to their relative areas. At peak magnetic field (t = 2.25 msec), the walls and supports each contribute about 10% of the total while the remaining 80% is lost to the hoops. These results are similar to those obtained for the gun plasma.[69] Microwave plasmas with different density distributions also give qualitatively similar results.

The plasma lifetime has been measured in three different ways:
1) The number of particles in the machine at time t can be determined by integrating the flux of particles to the hoops, supports, and wall from t to ∞:

$$N(t) = \frac{1}{e} \int_t^{\infty} (I_H(t) + I_S(t) + I_W(t)\ dt.\ )$$

2) The microwave cavity perturbation technique described in Chapter III. B. can be used to measure the total number of electrons in the cavity:

Figure 24. Fractional loss of plasma to hoops, supports, and wall vs. time after the beginning of the multipole field pulse.

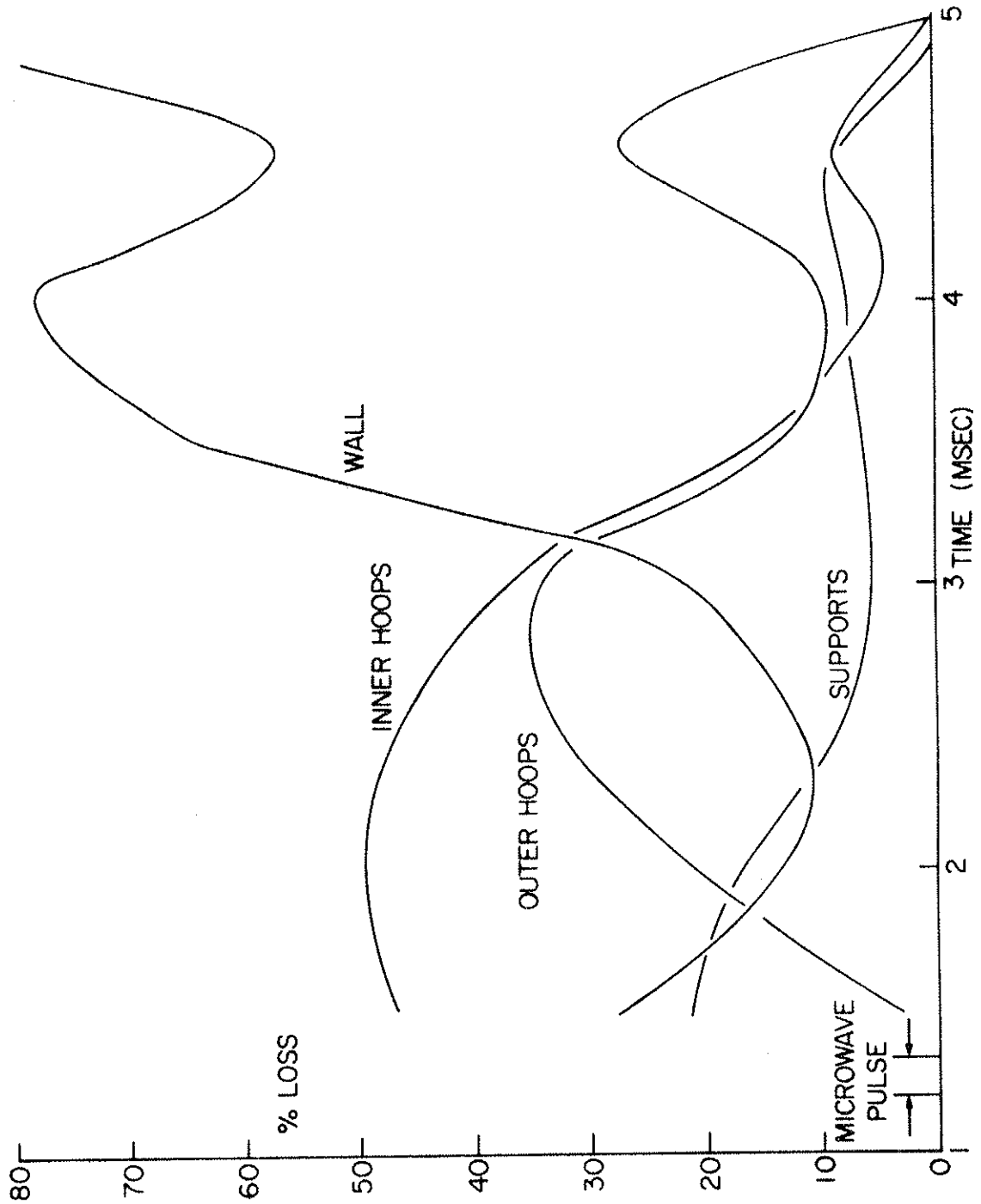
% LOSS
80
70
60
50
40
30
20
10
0
1
2
3
4
5
TIME (MSEC)
WALL
INNER HOOPS
OUTER HOOPS
SUPPORTS
MICROWAVE
PULSE

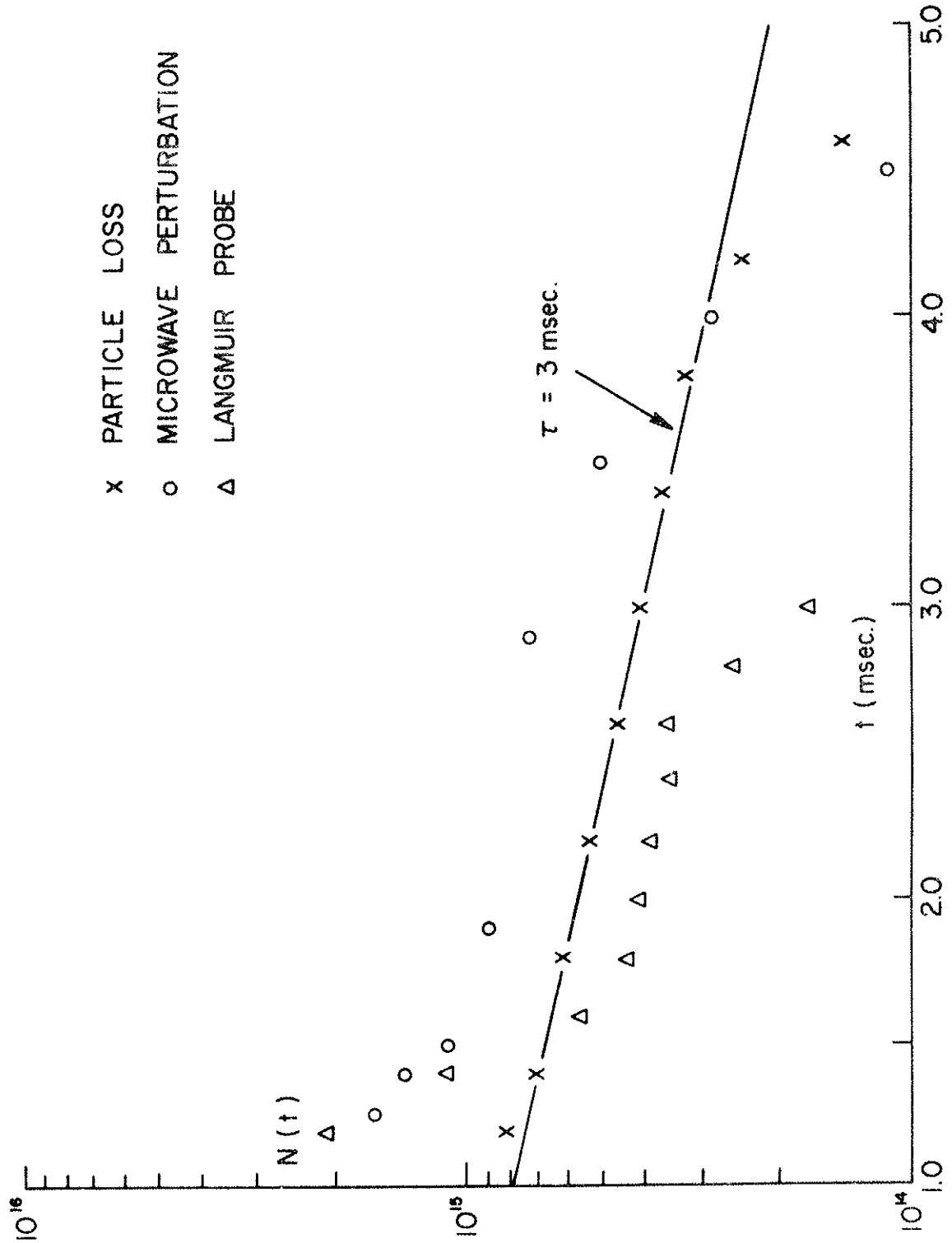
x PARTICLE LOSS
o MICROWAVE PERTURBATION
Δ LANGMUIR PROBE
τ = 3 msec.
N (t)
t (msec.)
10^16
10^15
10^14
1.0
2.0
3.0
4.0
5.0

$$N(t) = \bar{n}\,(t)V = \frac{2\varepsilon_o m\omega^2 V}{e^2}\,\frac{\delta f}{f}\ .$$

3) A Langmuir probe can be used to measure ion saturation current and electron temperature vs ψ and t, and the number of particles calculated from

$$N(t) = eA\sqrt{2\pi M}\int_{-5}^{5}\frac{I_{oi}}{\sqrt{kT_e}}\,(\psi,t)\,V'(\psi)\,d\psi\ .$$

The three techniques were tried for a case resembling that discussed earlier (B_o = 5), except using the S-band system. The results are shown in fig. 25. The methods all give about the same number of particles (~ 10^{15}). The probe data were taken only on the separatrix, and this fact probably accounts for the rapid decay at late times. All methods indicate an initial rapid decay followed by a slower decay near peak field (2.25 msec), and then a rapid decay as the field dies away. The decay rate near peak field gives a lifetime of 3 msec, or about three times longer than the lifetime of the gun plasma as measured by the same methods.

It is interesting to note that the electron temperature at peak field is about a factor of three smaller than for the gun plasma (see next section), and so the results would be consistent with losses that scale like Bohm diffusion, except that the lifetime is several times longer than the Bohm time. The lifetimes do not appear to scale with ion temperature in a manner that would be consistent with thermal flow to the hoop supports, since even if the sheath criterion is taken into account, the microwave plasma lifetime should exceed the

Figure 25. Number of particles in the toroid vs. time as measured by three different methods.

gun plasma lifetime by a factor of $\sqrt{T_i(\text{gun})/T_e(\text{microwave})} \simeq 6$.

C. Electron Cooling

1. Theoretical estimates

Many processes are capable of cooling the electron component of the microwave generated plasma. A cooling rate γ defined by

$$\frac{dT_e}{dt} = - \gamma T_e$$

will be calculated for various processes in order to estimate the rate of temperature decay. The electron distribution function is assumed to remain Maxwellian during the cooling with $T_e >> T_i$.

a) Ionization. It was shown in eq. (23) that ionization causes a temperature decay given by

$$\frac{d}{dt}(kT_e) + \frac{kT_e + 2U_i/3}{\tau_i} = 0$$

or

$$\gamma = (1 + 2U_i/3kT_e)/\tau_i \quad . \tag{29}$$

The graph of τ_i in fig. 9 was used to determine $\gamma(kT_e)$ for electrons in hydrogen gas, and the result is plotted in fig. 26 for a background pressure of 10^{-6} torr. The decay rate increases linearly with pressure.

b) Excitation. Inelastic electron-neutral collissions which do not result in ionization are classed as excitation. The most important such process is excitation from the ground state to the

Figure 26. Calculated decay rate of electron temperature for various cooling mechanisms.

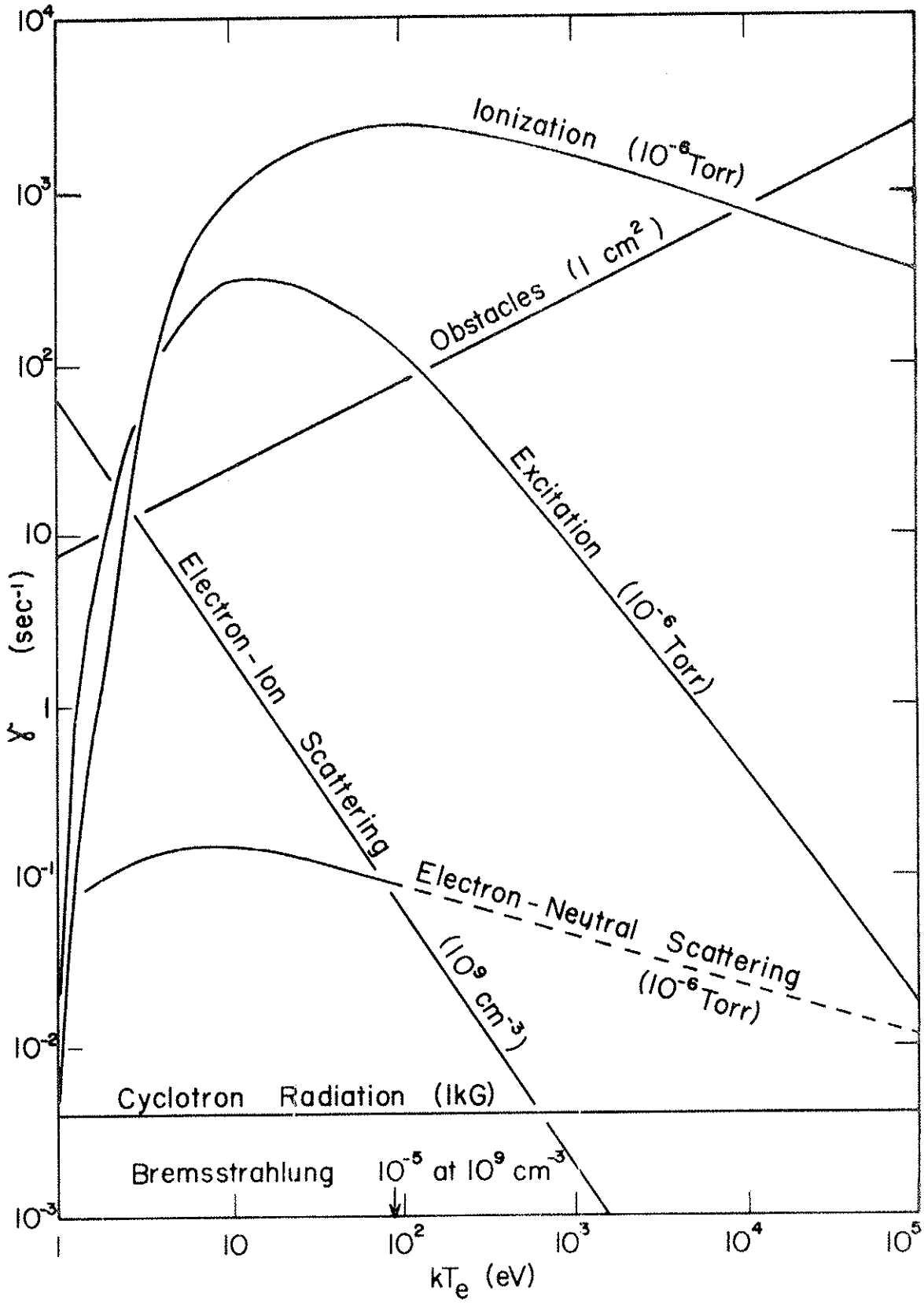
Ionization (10⁻⁶ Torr)
Obstacles (1 cm²)
Excitation (10⁻⁶ Torr)
Electron - Ion Scattering
Electron - Neutral Scattering (10⁻⁶ Torr)
(10⁹ cm⁻³)
Cyclotron Radiation (1kG)
Bremsstrahlung
10⁻⁵ at 10⁹ cm⁻³
γ (sec⁻¹)
kTe (eV)
10⁴
10³
10²
10
1
10⁻¹
10⁻²
10⁻³
1
10
10²
10³
10⁴
10⁵

first excited state. The cooling rate for this process is given by

$$\gamma = \frac{2n_n U_1}{3kT_e} \int_0^\infty \sigma_1(v) v f(v)\, dv \qquad (30)$$

where U_1 is the energy of the first excited state, and $\sigma_1(v)$ is the cross section for excitation to that state. Using published cross section data,[63,70] γ was determined and plotted in fig. 26 for hydrogen at 10^{-6} torr. Above about 10 eV, excitation losses are small compared with ionization. A small fraction of impurities with large excitation cross sections could greatly increase the cooling, however.

c) Electron-neutral elastic scattering. Energy transfer by eleastic scattering can be calculated from a scattering cross section σ_s by

$$\gamma = \frac{mn_n}{M_n} \int_0^\infty \sigma_s(v) v f(v) dv$$

$$\simeq \frac{mn_n}{M_n} \sigma_s(\bar{v})\, \bar{v}. \qquad (31)$$

The latter approximation is valid since $\sigma_s(v)\, v$ depends only weakly on v. The resulting cooling as shown in fig. 26 indicates that this process is not important for $kT_e > 1$ eV.

d) Electron-ion scattering. The energy transfer between hot electrons and cold ions has been calculated by Spitzer.[67] In MKS units, his result is

$$\gamma = \frac{\sqrt{2\pi}\, e^4\, m^{\frac{1}{2}}\, \ell n \Lambda}{6\pi^2 \varepsilon_o M} \qquad \frac{n_i}{(kT_e)^{3/2}} \,. \qquad (32)$$

The result with $\ell n\Lambda = 20$ is plotted in fig. 26 for a typical ion density of 10^9 cm^{-3}.

e) Bremsstrahlung. Electron-ion collissions can produce Bremsstrahlung radiation. The cooling rate determined from formulas of Rose and Clark[71] is

$$\gamma = \frac{e^4 n_i}{18\pi\varepsilon_o^3 c^3 mh}\sqrt{\frac{3}{\pi mkT_e}} \quad . \tag{33}$$

For $n_i = 10^9$ cm^{-3} the cooling is too small to conveniently plot in fig. 26.

f) Cyclotron radiation. In the non-relativistic limit, the cyclotron radiation cooling calculated from formulas of Rose and Clark[72] is

$$\gamma = \frac{2e^4 B^2}{9\pi m^2 \varepsilon_o c^3} \quad . \tag{34}$$

Note that the cooling is independent of electron energy and varies as the square of the magnetic field.

g) Magnetic field expansion. Lencioni[27] has calculated $T_e(\psi,t)$ for a time varying magnetic field under the assumption that the field is frozen into the plasma. Previous measurements (fig. 23) show that this assumption is not well satisfied. If we assume instead that the density distribution remains fixed in space while the field changes, and that the electron motion is adiabatic (i.e.: $W_\perp/B = \text{const}$), the cooling rate is independent of ψ, and for a sinusoidal magnetic field is given by

$$\gamma = -\omega \cot \omega t. \tag{35}$$

Near peak field ($\omega t = \pi/4$) the effect is small, as expected, but an appreciable heating can occur while the field is rising, with a corresponding cooling when the field decays.

h) Obstacles. Obstacles in a plasma cause a cooling since hot particles are preferentially removed from the plasma. Lovberg[73] has shown that the energy loss to an insulator or floating conductor of area A in the plasma is given by

$$\frac{d}{dt}\left(\frac{3}{2} N kT_e\right) = \frac{1}{4} n \bar{v}_i A[e(\Phi_p - \Phi_f) + 2 kT_e]$$

$$\simeq 1.45\, n \bar{v}_i A kT_e.$$

The corresponding particle loss is given by

$$\frac{dN}{dt} = \frac{1}{4} n \bar{v}_i A,$$

so that the cooling rate is

$$\gamma = \frac{1}{kT_e} \cdot \frac{d(kT_e)}{dt} \simeq .72\ n\bar{v}_i A/N \tag{36}$$

Hence for obstacle losses we expect the temperature to decay about three times faster than the density. The cooling rate for an obstacle with an area of 1 cm^2 in the octupole ($V = 3 \times 10^5$ cm^3) is shown in fig. 26.

It is clear from fig. 26 that ionization and obstacles should represent the major sources of electron cooling for typical experimental conditions in the toroidal octupole.

2. Experimental measurements.

An admittance probe (see Chapter III. A.4) was used to measure the electron temperature for both the gun injected and microwave produced plasmas on the B = 0 axis. The results are shown in fig. 27. The gun plasma temperature decay is approximately exponential in time with an initial value of ~ 10 eV and a decay time of ~1 msec. The temperature for the microwave case decays much faster. When the background pressure for the gun plasma is raised to a value equal to that used for the microwaves (5×10^{-5} torr), the decay is much faster than at 10^{-6} torr, suggesting that the fast decay for the microwave plasma is due primarily to the higher pressure. The slight difference between the two high pressure cases is well accounted for by the fact that the gun plasma is produced 700 μsec later than the microwave plasma with respect to the confining magnetic field pulse, and hence some cooling due to magnetic field expansion is expected for the gun plasma.

In order to further study the cooling mechanism, the temperature of the gun plasma 1 msec after injection was measured as a function of background gas pressure. The result is shown in fig. 28. For low pressures, the temperature is relatively constant, but above about 10^{-5} torr the decay rate is quite sensitive to pressure. It is interesting to note that the theoretical estimates of fig. 26 imply that for ~100 cm^2 of obstacles in the plasma (hoop supports and probes), that obstacle losses should dominate at pressures below about 10^{-5} torr, and ionization and excitation should dominate at higher pressures.

Figure 27. Electron temperature for gun and microwave plasma as measured by an admittance probe on the B = 0 axis vs. time after injection.

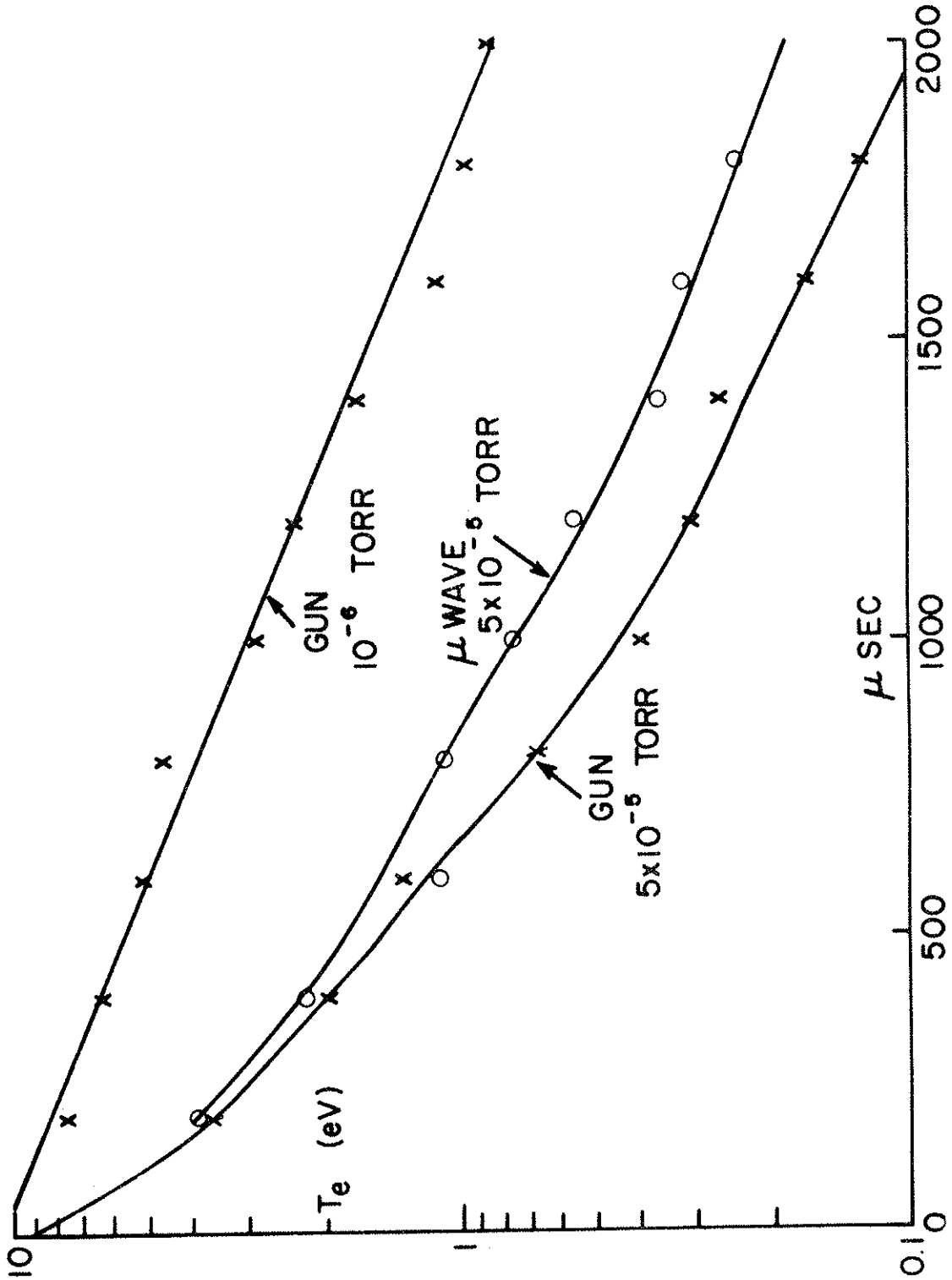
10
1
0.1
T_e (eV)
0
500
1000
1500
2000
μ SEC
GUN
10^{-6} TORR
μ WAVE
5×10^{-5} TORR
GUN
5×10^{-5} TORR

Figure 28. Electron temperature of the gun injected plasma 1 msec after injection vs. background hydrogen gas pressure.

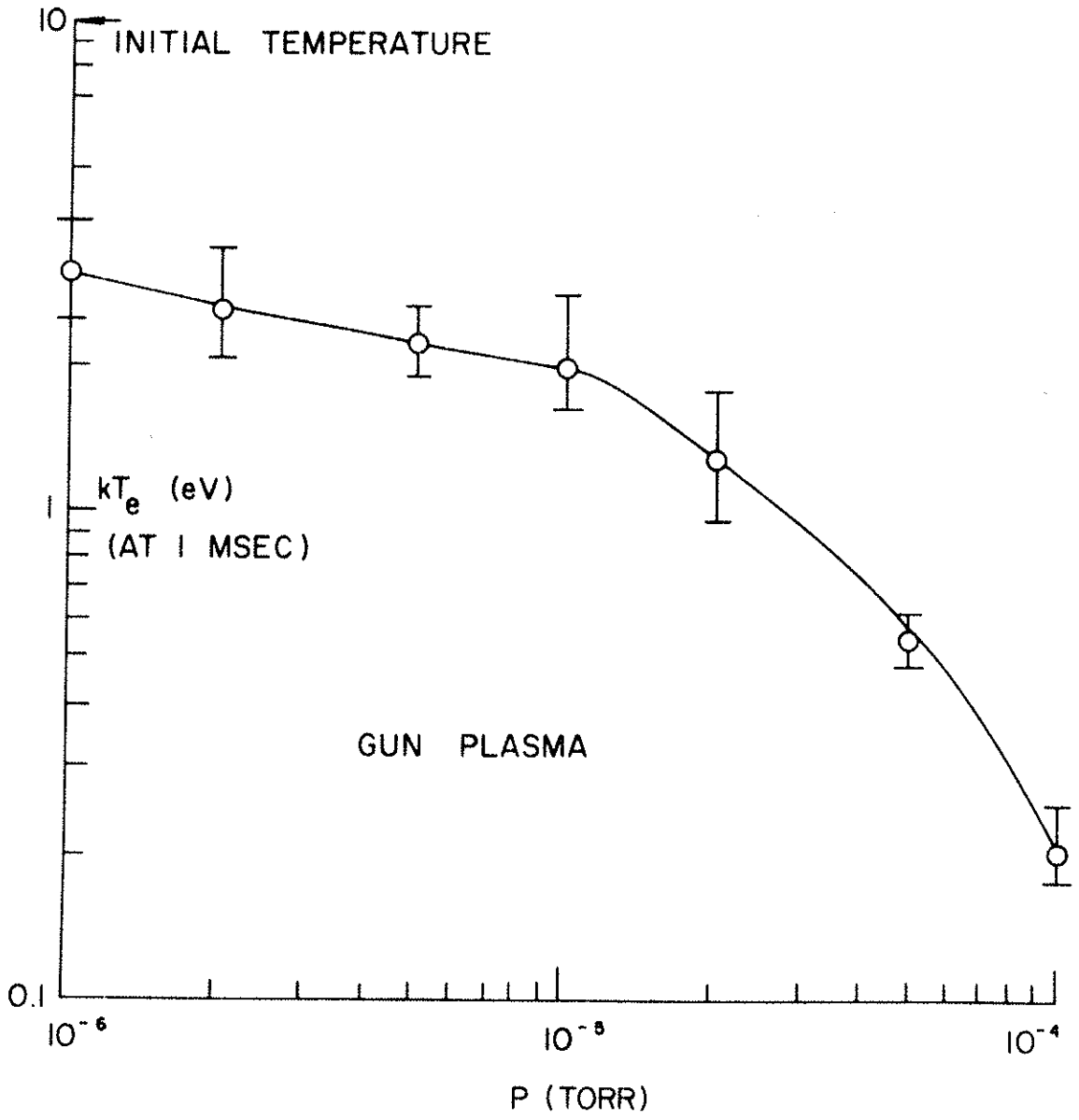
10
INITIAL TEMPERATURE
1
kT_e (eV)
(AT 1 MSEC)
GUN PLASMA
0.1
10^{-6}
10^{-5}
10^{-4}
P (TORR)

However, we should also note that the decay rate for T_e is about the same as the particle decay rate for the gun plasma at low pressure instead of three times faster as expected for simple thermal flow to the obstacles. (See eq. (36).) This observation is probably closely related to the observation that only a small fraction of the plasma is lost to the supports, and that the floating potential generally differs by several volts from the potential of the wall and hoops, indicating that the particle loss cannot be explained by simple thermal flow to the hoop supports.

Admittance probe measurements are subject to considerable error if the distribution departs slightly from a Maxwellian. The electron thermalization time as given by Spitzer[67] is 650 μsec for kT_e = 10 eV and $n = 10^9$ cm^{-3}. For the microwave plasma with $kT_e < 10$ eV and $n > 10^9$ cm^{-3}, the approach to thermal equilibrium should be even faster. Furthermore, measurements using swept single probes and electrostatic energy analyzers show that the distribution is reasonably Maxwellian with a temperature in good agreement with admittance probe results.

D. Fluctuations

1. Between ψ_{crit} and the Wall

Simple MHD theory predicts interchange instability in regions where

$$p'V' = \frac{dp}{d\psi} \frac{d}{d\psi} \oint \frac{d\ell}{B} < 0. \qquad (37)$$

This condition is satisfied between $\psi = \psi_{crit} = 3$ and the wall ($\psi = 5$). Large ($\delta V_f \sim kT_e/e$), $k_{\parallel} = 0$ fluctuations in density and floating potential are observed in this region as shown in fig. 22(d). The oscillations are at a frequency of a few tens of kHz, and the density and potential fluctuations are approximately 180° out of phase implying small diffusion. Figure 29 shows how the amplitude of the density fluctuations varies with distance from the wall in the midplane. The fluctuations amount to about 40% in the unstable region and fall off rapidly inside ψ_{crit}. A similar behavior has previously been observed[74,75] for the gun injected plasma, as shown by the dotted line in fig. 29. When a toroidal magnetic field of 180 G is superimposed on the poloidal field, producing a stellarator-like field with large rotational transform and shear, the amplitude of the fluctuations decreases in the originally unstable region and increases in the originally stable region in a manner similar to that previously observed for the gun plasma.[74] The fluctuations are especially large in the region of zero average shear 4.5 cm from the wall.

2. Fluctuations in regions of inverted density gradient

Interchange instabilities can also occur inside ψ_{crit} when the plasma pressure has a maximum peaked off the separatrix so that eq. (28) is not satisfied. It has already been pointed out that this condition occurs when the plasma is generated, and fig. 22 (b) shows an example of the low frequency fluctuation that results. This fluctuation has an amplitude of about 10 V/cm. Note that $E_\theta > 0$ for the

Figure 29. Amplitude of density fluctuations in the 10-500 kHz range in the midplane near the wall where the plasma is expected to be flute unstable.

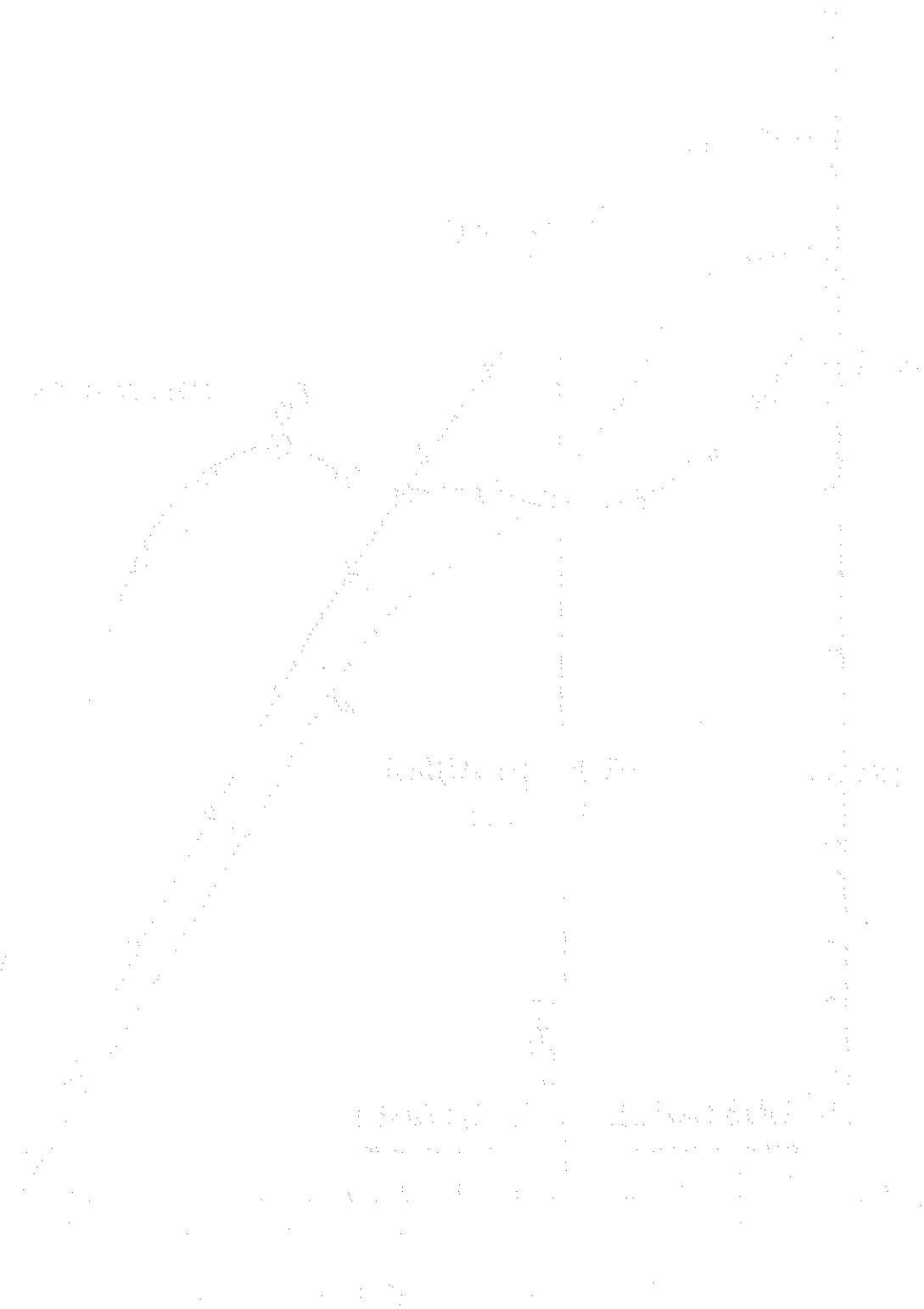

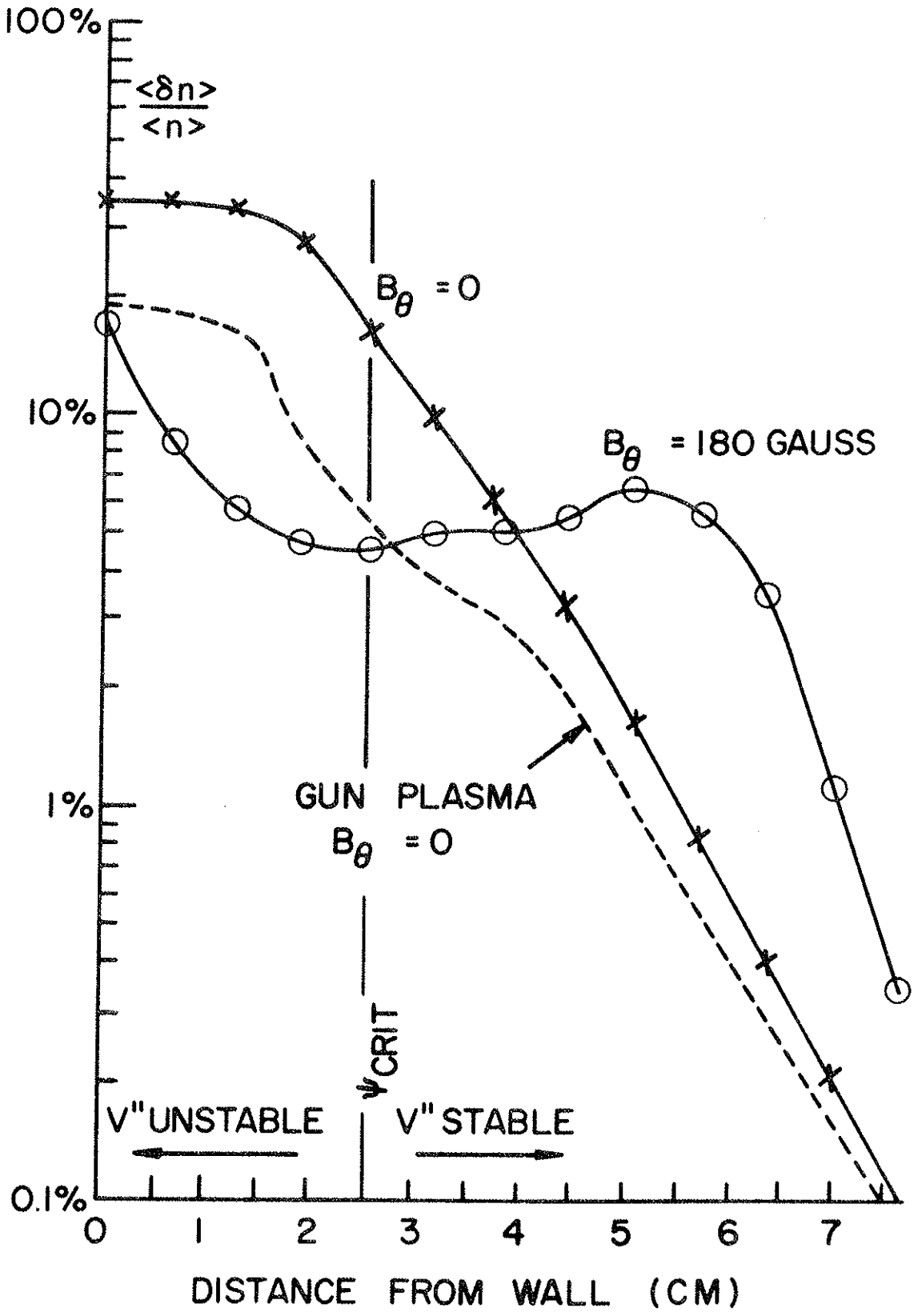
100%
<δn>
<n>
10%
1%
0.1%
B_θ = 0
B_θ = 180 GAUSS
GUN PLASMA
B_θ = 0
ψ_{CRIT}
V" UNSTABLE
V" STABLE
0
1
2
3
4
5
6
7
DISTANCE FROM WALL (CM)

first 60 μsec causing plasma to $\vec{E} \times \vec{B}$ drift toward the wall initially at this azimuth, but as the density builds up (fig. 22(a)) the electric field reverses and the plasma drifts towards the center with a velocity (~ 10^6 cm/sec) that is consistent with the observed collapse of the density profile (fig. 21).

Inverted density gradients can also arise when the magnetic field changes and moves the density peak off the separatrix. The oscilloscope trace in fig. 23 shows an example of the fluctuations that occur on the B = 0 axis under these conditions. The plasma is produced while the field is still rising so that as the density distribution, which is initially peaked on the separatrix, moves toward the hoops, a large fluctuation appears. Near peak magnetic field, the fluctuation disappears, only to reappear later as the field decays and carries plasma out toward the wall. These fluctuations are similar to cases previously observed for the gun plasma, and may account for some of the diffusion observed in the density profiles in fig. 23.

3. Fluctuations in regions of unfavorable curvature

When the density gradient is sufficiently large, fluctuations appear in the MHD stable region where the local field curvature is unfavorable. Figure 30 shows that the amplitude of these fluctuations is maximum where the density gradient is maximum and amounts to about a 10% variation in density. The fluctuations occur only on the side of the peak toward the wall and have nodes in the regions of favorable curvature. This oscillation has a frequency of about 100 kHz in agreement with the theoretical prediction[76-78] of

Figure 30. Profile of density and amplitude of density fluctuations at 500 μsec showing evidence of drift waves localized in the region of unfavorable curvature.

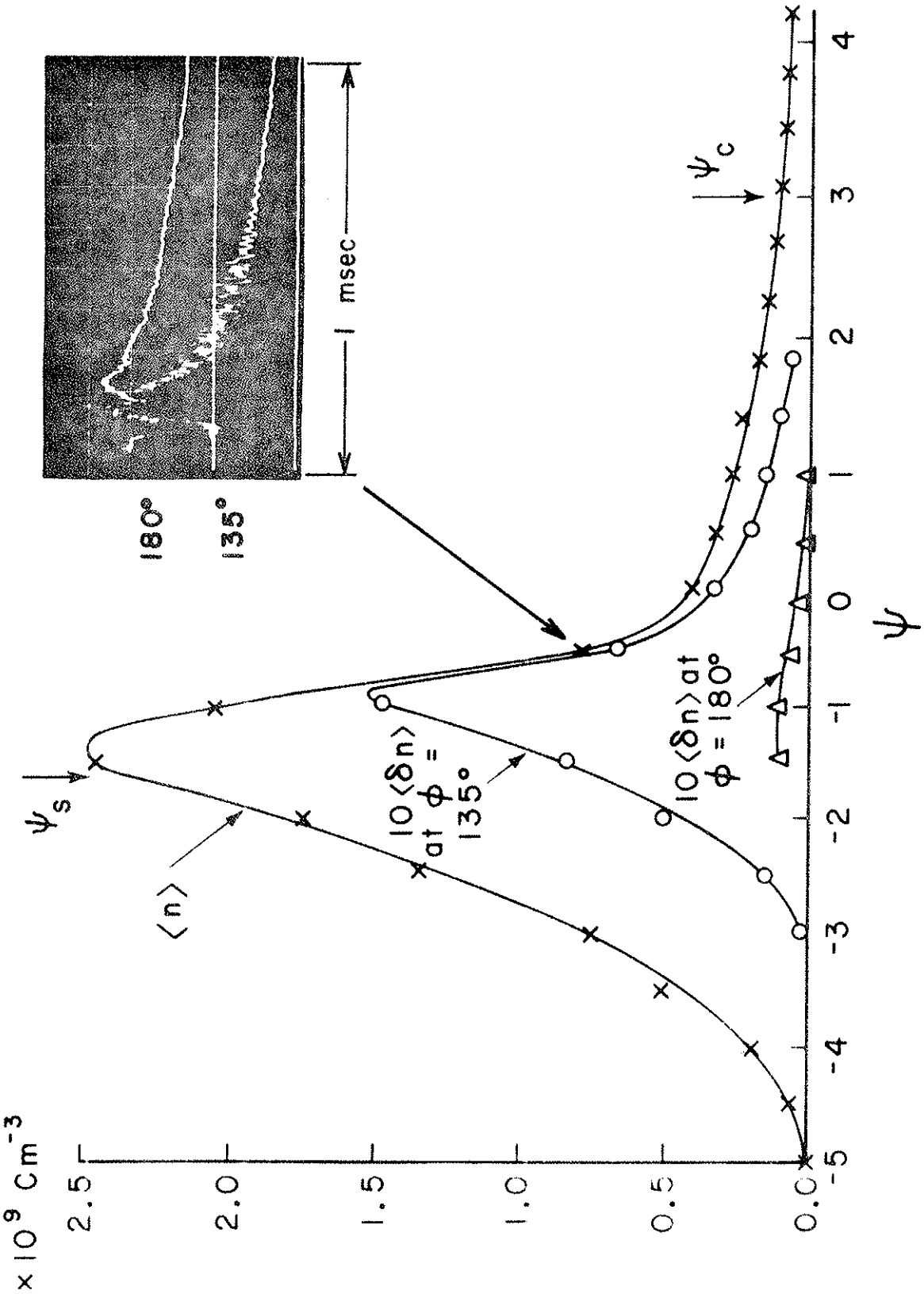
$\times 10^9$ Cm^{-3}
2.5
2.0
1.5
1.0
0.5
0.0
-5
-4
-3
-2
-1
0
1
2
3
4
ψ
ψ_s
ψ_c
$\langle n \rangle$
$10\langle \delta n \rangle$ at $\phi = 135°$
$10\langle \delta n \rangle$ at $\phi = 180°$
180°
135°
1 msec

$$\omega \simeq 0.3\, k_\perp \frac{kT_e}{eB} \frac{\nabla n}{n}$$

and a parallel wavelength one half as long as a closed field line. This drift wave propagates in the direction of the diamagnetic current and has a perpendicular wavelength of 3 cm in agreement with the prediction that

$$k_\perp^2 \rho_i^2 \simeq T_i/T_e \quad .$$

To a close approximation, the density and potential fluctuations are in phase implying no transport in agreement with the fact that the density gradient persists throughout the life of the plasma. The frequency and amplitude of the oscillations decrease in time as the electron temperature decays (see fig. 27). The addition of a toroidal magnetic field of about 100 G does not suppress the fluctuations. The parallel phase velocity of the wave is greater than the ion thermal speed and less than the electron thermal speed:

$$\bar{v}_i < \omega/k_\parallel < \bar{v}_e \quad .$$

This wave is apparently identical to the collisionless ballooning mode observed by Meade and Yoshikawa[78] in a linear quadrupole.

4. Fluctuations between the separatrix and the hoops.

Perhaps the most unsettling observation of the microwave produced plasma is the rapid diffusion toward the hoops, as seen for example in fig. 21. This motion is sometimes accompanied by fluc-

tuationsas in fig. 22 (e). This region has only favorable curvature and should be stable according to any simple theory. It has already been pointed out that the diffusion is present irrespective of the position of the resonance zones, although the appearance of the fluctuations varies drastically. In fact, some cases have been observed in which the diffusion is present without noticeable fluctuations. Since hoop losses constitute the major source of plasma loss in this experiment, as well as for the gun injected plasma, the mechanism which produces this diffusion is worthy of further study. It is possible that azimuthally asymmetric initial density distributions or perturbations such as the hoop supports generate low frequency electric fields which form convective cells enabling the plasma to move out toward the walls and hoops.[79,80]

VII. ION CYCLOTRON RESONANCE HEATING

A. Introduction

Electron cyclotron resonance heating has proved so successful in multipoles that it is tempting to extend the techniques in an attempt to resonantly heat the ions in a plasma. Ion cyclotron resonance heating requires r.f. frequencies that are m/M smaller than is required for electron cyclotron heating. The usual objection to ion cyclotron heating asserts that waves will not penetrate a plasma if the wave frequency is less than the electron plasma frequency, and so for a typical frequency of 1 MHz, the limiting density is about 10^4 cm^{-3}. In fact, it is often possible for low frequency waves to penetrate a considerable distance into a plasma having a much higher density. For example, with no magnetic field, the penetration depth of waves of frequency ω is given by

$$\delta = \frac{c}{\sqrt{\omega_p^2 - \omega^2}} \simeq \frac{c}{\omega_p},$$

where the latter approximation is valid for $\omega << \omega_p$. If we require that 1 MHz waves propagate a distance of 10 cm, we conclude that densities as high as 3×10^9 cm^{-3} would be allowed. In the presence of a magnetic field, it is possible for ion cyclotron waves to propagate through a plasma of arbitrary density[13] provided $\omega < \omega_{ci}$. Hence, it should be possible to excite these waves in a region of strong magnetic field, and let them propagate along the field into a region where $\omega = \omega_{ci}$ (called a "beach") where their energy is absorbed by the ions.

In this chapter, the theoretical model of Chapter IV is extended to the case of ion heating in order to estimate the expected heating rate.

Since the lowest resonant mode of the toroidal cavity is about 300 MHz, the usual method of exciting the cavity would not be effective at 1 MHz. A more feasible method of generating electric fields in the plasma consists of applying a voltage between the hoops and wall. This case is also easy to treat theoretically since there would be no azimuthal electric fields ($E_\theta = 0$). Futhermore, for a typical electron energy of5 eV, an electron travels a distance of about 100 cm during a period of the wave, and so we expect field lines to be equipotentials ($E_\ell = 0$). The potential is then constant on a flux surface, $\Phi = \Phi(\psi)$, leading to a considerable simplification of the theoretical treatment.

B. Calculation of Heating Rate

The power absorbed in the flux shell $d\psi$ can be written in terms of the real perpendicular conductivity $\sigma_\perp$ as

$$\frac{dP}{d\psi} = I \frac{d\phi}{d\psi} = \frac{d\phi}{d\psi} \oint\int \sigma_\perp E_\perp R d\theta d\ell, \tag{38}$$

where $\sigma_\perp$ for the case of $\omega \lesssim \omega_{ci}$ is given by

$$\sigma_\perp = \varepsilon_o \omega_{pi}^2 \nu \left[\frac{\omega^2 + \omega_{ci}^2}{(\omega^2 - \omega_{ci}^2)^2 + 4\omega^2\nu^2} \right] .$$

The ion collision frequency ν is assumed much smaller than ω. The electric field $E_\perp$ can be written as

$$E_\perp = |\nabla\Phi| = \frac{d\Phi}{d\psi}\,|\nabla\psi| = 2\pi RB\,\frac{d\Phi}{d\psi}\,,$$

so that eq. (38) becomes

$$\frac{dP}{d\psi} = 4\pi^2 \left(\frac{d\Phi}{d\psi}\right)^2 \oint \sigma_\perp R^2 B d\ell\,. \tag{39}$$

By writing $\sigma_\perp$ in terms of $B(\ell)$ and expanding $B(\ell)$ in a Taylor series about its resonance value (B_o), the integral in eq. (39) can be evaluated in a manner identical to that used to obtain eq.(12). The result is

$$\frac{dP}{d\psi} = 2\pi^3 ne \left(\frac{d\Phi}{d\psi}\right)^2 \frac{R^2 B_o}{dB/d\ell\big|_{B_o}}\,. \tag{40}$$

The same result could have been obtained directly from eq. (12) by substituting

$$E_\perp = \left(\frac{d\Phi}{d\psi}\right) \nabla\psi\big|_{B_o},$$

pointing out the fact that the heating rate is mass independent and depends only on the strength of the electric field in the resonance region.

Unlike the case of electron heating where the electric field is constant on the average, even at rather high densities, the quantity $d\Phi/d\psi$ is expected to be strongly affected by the plasma. At microwave frequencies, $\overline{E_\perp^2}$ can be easily calculated in terms of the input power and Q of the cavity, but it is difficult to measure $E_\perp$. For $\omega \sim \omega_{ci}$, the electric field can be measured with high impedance probes such as those described in III. A. 1., but the field is more difficult to calculate. Under certain restrictive conditions, an expression for $d\Phi/d\psi$ can be obtained, however.

If we assume that charge cannot flow perpendicular to $\vec{B}$, Poisson's equation can be written for a flux tube as

$$\oint (\nabla \cdot \varepsilon_\perp E_\perp) \frac{d\ell}{B} = 0 \tag{41}$$

where

$$\varepsilon_\perp \simeq \varepsilon_o \left[1 + \frac{\omega_{pi}^2}{\omega_{ci}^2 - \omega^2} \right] .$$

If we assume that the density is sufficiently high that

$$\frac{\omega_{pi}^2}{\omega_{ci}^2 - \omega^2} >> 1$$

(i.e. $n >> 5 \times 10^7$ cm^{-3} at $B = 1$ kG), $\varepsilon_\perp$ can be expressed in terms of $B(\ell)$ and B_o, and substituted into eq. (41) to get the result:

$$\frac{d^2\Phi}{d\psi^2} \oint \frac{R^2 B}{B^2 - B_o^2} d\ell + \frac{d\Phi}{d\psi} \left[\oint \frac{RB}{B^2 - B_o^2} \frac{dR}{d\psi} d\ell + \oint \frac{R^2}{B^2 - B_o^2} \frac{dB}{d\psi} d\ell \right.$$

$$\left. + \frac{1}{n} \frac{dn}{d\psi} \oint \frac{R^2 B}{B^2 - B_o^2} d\ell - 2 \oint \frac{R^2 B^2}{(B^2 - B_o^2)^2} \frac{dB}{d\psi} d\ell \right] = 0. \tag{42}$$

In general, the integrals in eq. (42) would have to be evaluated by computer for a specific magnetic field geometry such as the toroidal octupole. However, we note that for a straight uniform field ($dR/d\psi = dB/d\psi = 0$), eq. (42) reduces to

$$\frac{d^2\Phi}{d\psi^2} + \frac{1}{n} \frac{dn}{d\psi} \frac{d\Phi}{d\psi} = 0,$$

which has the solution $d\Phi/d\psi = \text{const}/n(\psi)$, (43)

or

$$\Phi(\psi) = \frac{\Phi_o \int_{\psi}^{\psi_{max}} d\psi/n(\psi)}{\int_{0}^{\psi_{max}} d\psi/n(\psi)} , \qquad (44)$$

where Φ_o is the total potential applied across the plasma. Equation (43) agrees with our intuition since it describes an infinite parallel plate capacitor filled with an inhomogeneous dielectric such that the condition $\varepsilon E_\perp$ = const (or $E_\perp$ = const/n) is satisfied. Note that the ψ in the above equations has units of webers.

A number of approximations have been made in the preceeding calculations. The condition $\nu << \omega$ is less easily satisfied for ions than for electrons of the same energy. As with electrons, the parallel velocity must satisfy

$$v_{\parallel} << \omega \frac{B_o}{dB/d\ell} ,$$

corresponding to a parallel energy of about 1 keV for typical conditions in the toroidal octupole. The derivation of eq. (42) assumed that the plasma is not in contact with the electrodes that produce the electric field (the hoops and wall). The particle current at the electrodes would greatly reduce the hoop to wall resistance and could lead to a severe plasma loss in the presence of strong r.f. heating pulses.

C. Experimental Measurements

In order to determine the conditions for optimum coupling of r.f. power to the plasma, the impedance between the upper outside hoop and the wall was measured as a function of frequency

with the other hoops floating. In the absence of plasma the capacitance is about 650 pF. When a gun produced plasma with $n \sim 10^9$ cm^{-3} is injected and allowed to decay for 500 μsec, the impedance from hoop to wall can be represented approximately by a 1000 pF capacitance in parallel with a 1000 ohm resistance. This impedance is relatively insensitive to the amplitude of the r.f. voltage.

The hoop was driven with a 1 MHz, 10 volt r.f. signal, and the potential $\Phi(\psi)$ between the hoop ($\psi = -5$) and the wall ($\psi = +5$) was measured with a 10 MΩ floating probe (see III. A. 1.). The result is shown in fig. 31. Note that the electric field $d\Phi/d\psi$ is smallest where the density (as indicated by the ion saturation current, I_{oi}) is large, but that near the boundary of the plasma the field is large. These observations are in qualitative agreement with the prediction of eq. (43). Near the separatrix ($\psi = -1.6$), the field is $d\Phi/d\psi \sim 0.1\ \Phi_o/\psi_{max}$.

Using the low frequency r.f. heating system described in II. C., it is possible to develop an rms voltage of 1 kV between the hoop and wall in the presence of the gun injected plasma. Low impedance probes on the B = 0 axis show that if the r.f. is pulsed on for 100 μsec, the resulting ion saturation current after the heating is decreased by about a factor of three, indicating enhanced loss of plasma during heating. If the r.f. is pulsed on without preionization but with a high background gas pressure ($\gtrsim 5 \times 10^{-5}$ torr), a plasma with $n \sim 10^8$ cm^{-3} is produced.

From eq. (40) and the measured value of $d\Phi/d\psi$ it is possible to predict the average ion heating rate:

Figure 31. Amplitude of the r.f. voltage in the plasma when a 1 MHz r.f. signal is applied between a hoop and the wall. The electric field in the plasma is smallest where the density (as indicated by the ion saturation current, I_{oi}) is large.

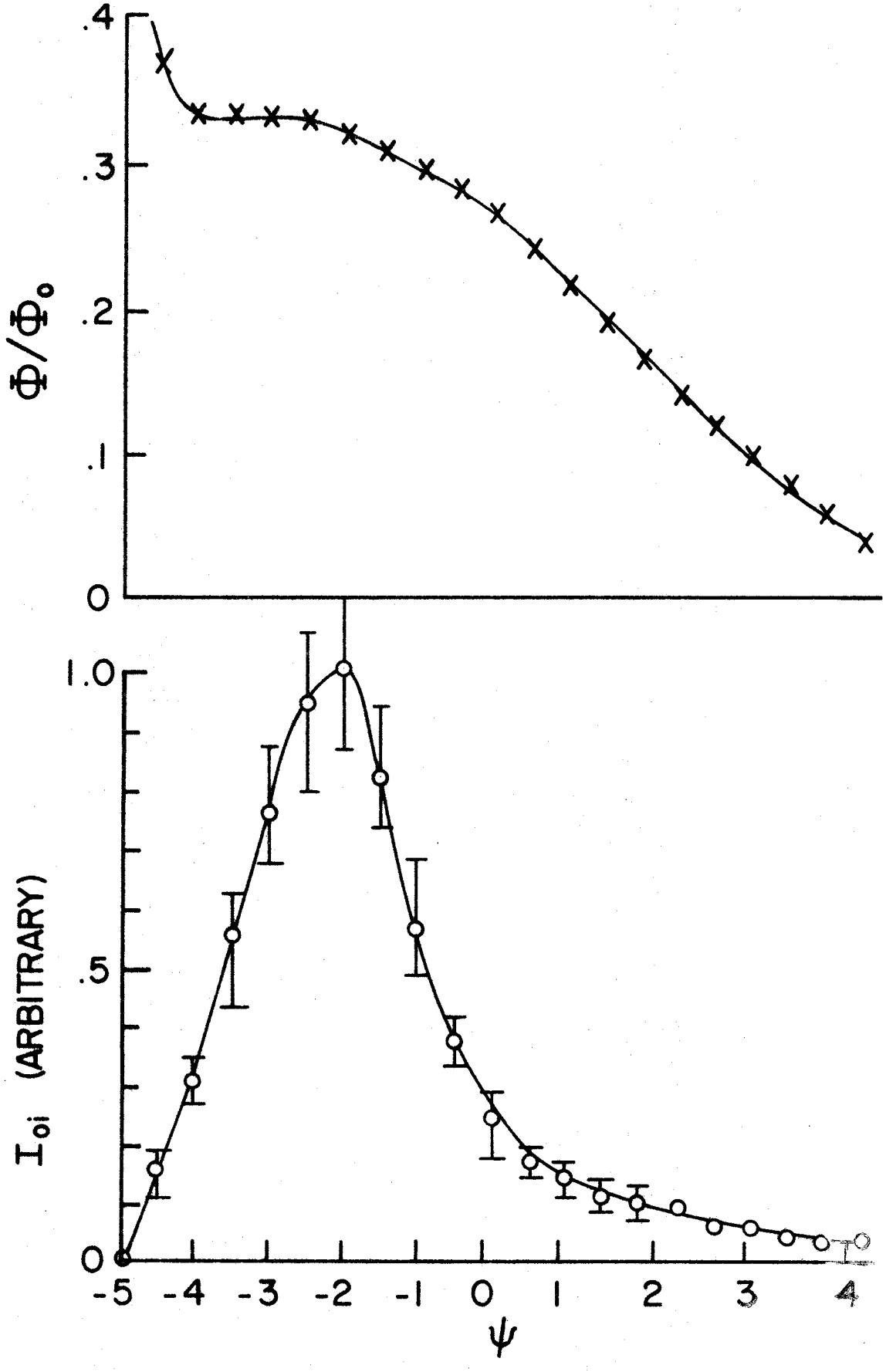
.4
.3
.2
.1
0
Φ/Φ₀
1.0
.5
0
I₀ᵢ (ARBITRARY)
-5
-4
-3
-2
-1
0
1
2
3
4
ψ

$$\frac{d\bar{W}}{dt} = \frac{1}{N}\int \frac{dP}{d\psi}\, d\psi = \frac{2\pi^3 eB_o}{N}\int \left(\frac{d\Phi}{d\psi}\right)^2 \frac{R^2 n(\psi)}{dB/d\ell\Big|_{B_o}}\, d\psi$$

$$\sim 2\pi^3 eB_o R_o^2 \left(\frac{d\Phi}{d\psi}\right)_o^2 \left[\frac{B_o}{V}\frac{dV}{dB}\right]_{B_o} \qquad (45)$$

or about 10^6 eV/sec. Hence for a 100 μsec r.f. pulse, appreciable heating should occur provided the losses are not too serious. Measurements of the ion heating rate are being made by Kuswa and will be reported elsewhere. At higher densities the heating rate should decrease sharply, and more powerful r.f. systems and more efficient means of coupling the power to the plasma would be required.

VIII. CONCLUSIONS

It has been shown that microwave energy can be effectively transferred to the electron component of a plasma confined in a toroidal octupole magnetic field, provided the microwave frequency is chosen so that electron cyclotron resonance occurs somewhere within the field. The heating rate is in qualitative agreement with the results of a simple linear theory of stochastic acceleration. At low background gas pressure, most of the r.f. power goes into increasing the energy of whatever electrons are present. At high background pressure, the energy goes into ionizing the background gas. Quantitative comparisions of theory and experiment are complicated in the first case by obstacle losses and in the second case by the fact that the density in the resonance region rises to such a high value that the electric field is perturbed by the plasma. Nevertheless, the observed spatial distribution of energetic electrons is in good agreement with predictions.

Cold ion plasmas produced by microwave breakdown at high pressure are of interest because they represent a fundamentally different kind of plasma from the usual hot ion, gun injected plasma. Particle loss mechanisms (such as thermal flow to hoop supports which depend strongly on ion temperature have been discredited partly as a result of the observation that microwave produce plasmas do not have significantly longer lifetimes, and a more likely source of particle loss is being sought. Microwave heating provides a means of adjusting the spatial distribution of the plasma, and thereby producing a variety of fluctuations. These

fluctuations do not appear to be an important source of plasma loss, but do provide an opportunity to study basic plasma phenomena.

The theoretical model has been extended to ion cyclotron heating, where it was shown that the ion heating rate should be correspondingly large if suitable means can be found for producing the required low frequency electric fields in the plasma. Both electron and ion cyclotron heating become increasingly difficult at high densities, and more efficient means of coupling the r.f. to the plasma would certainly be required to heat the types of plasmas envisioned in a controlled thermonuclear fusion reactor.

REFERENCES

1. P.C. Thonemann, J. Moffat, D. Roaf, and J.H. Sanders, Proc. Phys. Soc. 61, 483 (1948).
2. J.D. Cobine and D.A. Wilbur, Jour. Appl. Phys., 22, 835 (1951).
3. F. Llewellyn-Jones, Ionization and Breakdown in Gases, (Methuen and Co. LTD, London, 1966).
4. S.C. Brown, Electrical Discharges in Gases, (Wiley, New York, 1966).
5. A.D. MacDonald, Microwave Breakdown in Gases (Wiley, New York, 1966).
6. E.V. Appleton, URSI Proc., Washington (1927).
7. K.G. Budden, Radio Waves in the Ionosphere, (Cambridge Univ. Press, 1961).
8. K. Davies, Ionospheric Radio Propagation (U.S. Government Printing Office, Washington, D.C., 1965).
9. J.M. Kelso, Radio Ray Propagation in the Ionosphere (McGraw Hill Book Co., Inc., New York, 1964).
10. A.S. Bishop, Project Sherwood (Addison-Wesley Publ. Co., Inc., Reading, Mass., 1958).
11. P.L. Auer, H. Hurwitz, and R.D. Miller, Phys. Fluids, 1, 501 (1958).
12. L.R.O. Storey, Phil. Trans. Roy. Soc. London, A 246, 113 (1953).
13. T.H. Stix, The Theory of Plasma Waves, (McGraw-Hill, New York, 1962).
14. R.A. Dandl, A.C. England, W.B. Ard, H.O. Eason, M.C. Becker, and G.M. Haas, Nuclear Fusion, 4, 344 (1964).

15. T.J. Fessenden, M.I.T. PhD Thesis (1965).

16. H. Ikezi, Nagoya University, IPPJ-67 (1968).

17. R.A. Dandl, H.O. Eason, P.H. Edmonds, A.C. England, and N.H. Lazar, Proceedings of the Third International Conference on Plasma Physics and Controlled Nuclear Fusion Research, Novosibirsk, USSR, 1-7 August 1968 (to be published), Paper CN-24/J-6.

18. A.I. Anisimov, V.N. Budnikov, N.I. Vinogradov, V.E. Golant, S.I. Nanobashvili, A.A. Obukhov, L.P. Pakhomov, A.D. Piliya, and V.I. Fedorov, Proceedings of the Third International Conference on Plasma Physics and Controlled Nuclear Fusion Research, Novosibirsk, USSR, 1-7 August 1968 (to be published) Paper CN-24/J-6.

19. B.V. Galaktionov, V.V. D'yachenko, K.M. Novik, and A.D. Piliya, Sov. Phys., Tech. Phys., 13, 838 (1968).

20. J.L. Shohet, Phys. Fluids 11, 1065 (1968).

21. G.E. Guest, in Oak Ridge National Laboratory report ORNL-4150 (1967), page 29.

22. A.J. Lichtenberg, M.J. Schwartz, and D.T. Tuma, Plasma Phys. 11, 101 (1969).

23. T. Kawamura and Y. Terashima in Inst. of Plasma Physics Nagoya University Annual Review (1968).

24. R.A. Dory, D.W. Kerst, D.M. Meade, W.E. Wilson and C.W. Erickson, Phys. Fluids 9, 997 (1966).

25. D.M. Meade, Univ. of Wisc. PhD Thesis (1965).

26. C.W. Erickson, Univ. of Wisc. PhD Thesis (1967).

27. D.E. Lencioni, Univ. of Wisc. PhD Thesis (1969).

28. V. Josephson, Jour. Appl. Phys., 29, 30 (1958).

29. J. Francis Reintjes and Godfrey T. Coate, Principles of Radar, (McGraw-Hill Book Company, Inc., New York, 1952).

30. H.O. Eason, Jr., Proc. of 1966 Symp. on Engr. Problems of Controlled Thermonuclear Research.

31. J.L. Powell and B. Crasemann, Quantum Mechanics, (Addison-Wesley Publ. Co., Inc., Reading, Mass., 1961), page 4.

32. I. Langmuir, in Collected Works of Irving Langmuir (G. Suits, ed.), Vol. 4 and 5, Macmillan (Pergamon), New York, 1961.

33. Yu.M. Kagan and V.I. Perel, Sov. Phys. Uspekhi, 81, 767 (1964).

34. F.F. Chen in Plasma Diagnostic Techniques, R.H. Huddlestone and S.L. Leonard, Eds. (Academic Press Inc., New York, 1965), Chap. 4.

35. B.E. Burke and F.W. Crawford, Am. Jour. of Phys., 32, 942 (1964).

36. J.C. Sprott, Rev. of Sci. Instr., 37, 897 (1966).

37. J.A. Schmidt, Rev. of Sci. Instr., 39, 1297 (1968).

38. E.O. Johnson and L. Malter, Phys. Rev., 80, 58 (1950).

39. R.W. Carlson, T. Okuda, and H.J. Oskam, Physica, 30, 182 (1964).

40. T. Okuda and K. Yamamoto, Jour. Appl. Phys., 31, 158 (1960).

41. S. Aisenberg, Jour. Appl. Phys., 35, 130 (1964).

42. Sin-Li Chen and T. Sekiguchi, Jour. Appl. Phys., 36, 2363 (1965).

43. Z. Zakrzewski, C. Beaudry, and G.G. Cloutier, Rev. of Sci. Instr., 39, 1507 (1968).

44. J.C. Sprott, Rev. of Sci. Instr., 39, 1569 (1968).

45. F.W. Crawford and R. Grard, Jour. Appl. Phys., 37, 180 (1966).

46. C.B. Wharton in Plasma Diagnostic Techniques, R.H. Huddlestone and S.L. Leonard, Eds. (Academic Press Inc., New York, 1965), Chap. 11.

47. M.A. Heald and C.B. Wharton, Plasma Diagnostics with Microwaves (Wiley, New York, 1965).

48. J.C. Slater, Microwave Electronics (D. Van Nostrand Co., Inc., Princeton, N.J., 1950), pages 81-83.

49. T.J. Fessenden and L.D. Smullin, Proceedings of the Seventh International Conference on Phenomena in Ionized Gases, Vol. III (Beograd, 1966).

50. C.W. Erickson, Rev. of Sci. Instr., 37, 1308 (1966).

51. H.P. Eubank and T.D. Wilkerson, Rev. of Sci. Instr., 34, 12 (1963).

52. N.R. Daly, Rev. of Sci. Instr., 31, 264, 720 (1960).

53. G.W. Kuswa, Private Communication.

54. J.H. Adlam and I.C. Taylor, Culham Laboratory Report, CLM-R81 (1968).

55. R.E. Ellis and N.W. Carlson, Rev. of Sci. Instr., 32, 1367 (1961).

56. A.F. Kuckes, Plasma Physics 10, 367 (1968).

57. J.D. Jackson, Classical Electrodynamics (Wiley, New York, 1962), page 602.

58. T. Stix, Phys. Fluids, 7, 1960 (1964).

59. P.A. Sturrock, Phys. Rev., 1, 186 (1966).

60. M. Seidl, Plasma Physics, 6, 597 (1964).

61. I.S. Shklovsky, Cosmic Radio Waves (Harvard Univ. Press, Cambridge, Mass., 1960).

62. E. Fermi, Phys. Rev. 75, 1169 (1949).

63. H.W. Drawin, Fontenay-aux-Roses (Seine) report EUR-CEA-FC-383 (1967).

64. H. Ikegami, I. Hiroyuki, M. Hosokawa, S. Tanaka, and K. Takayama, Phys. Rev. Letters, 19, 778 (1967).

65. C.E. Speck and A. Bers, Mass. Inst. of Tech., Research Lab of Electronics, Quarterly Progress Report No. 91, Page 175 (1968).

66. J.C. Sprott and G. Kuswa, to be published in Bull. Am. Phys. Soc. (Rochester meeting).

67. L. Spitzer, Jr., Physics of Fully Ionized Gases, Interscience, New York (1962).

68. C.L. Longmire and M.N. Rosenbluth, Phys. Rev. 103, 507 (1956).

69. H. Forsen, D. Kerst, D. Lencioni, D. Meade, F. Mills, A. Molvik J. Schmidt, J. Sprott, and K. Symon, Proceedings of the Third International Conference on Plasma Physics and Controlled Nuclear Fusion Research, Novosibirsk, USSR, 1-7 August 1968 (to be published) Paper CN-24/C-1.

70. W.L. Wiese, M.W. Smith, and D.M. Glennon, NSRDS-NB4 National Bureau of Standards, Washington, D.C. (1966).

71. D.J. Rose and M. Clark, Plasmas and Controlled Fusion, M.I.T. Press, Cambridge, Mass., (1961), Page 232 ff.

72. D.J. Rose and M. Clark, Page 232 ff.

73. R.H. Lovberg in Plasma Diagnostic Techniques, R.H. Huddlestone and S.L. Leonard, editors, Academic Press, New York (1965), page 95 ff.

74. D.E. Lencioni, J.W. Poukey, J.A. Schmidt, J.C. Sprott, and C.W. Erickson, Phys. Fluids 11, 1115 (1968).

75. D.M. Meade, Phys. Rev. Letters, 17, 677 (1966).

76. N.A. Krall and M.N. Rosenbluth, Phys. Fluids 8, 1488 (1965).

77. S. Yoshikawa, Bull. Am. Phys. Soc. 12, 630 (1967).

78. D.M. Meade and S. Yoshikawa, Phys. Fluids 10, 2649 (1967).

79. J.A. Schmidt, Univ. of Wisc. PhD Thesis (1969).

80. G.O. Barney and J.C. Sprott, Phys. Fluids 12, 707 (1969).